DEVELOPMENT OF COLLAGEN THIN-FILM DEVICES FOR NANOFILTRATION

A Dissertation

Presented to the Faculty of the Graduate School

of Cornell University

In Partial Fulfillment of the Requirements for the Degree of

Doctor of Philosophy

by

Lori A. Lepak

May 2010

DEVELOPMENT OF COLLAGEN THIN-FILM DEVICES FOR NANOFILTRATION

Lori A. Lepak, Ph. D.

Cornell University 2010

Recent advances in biomedical engineering have created a demand for large-scale production of micro- and nanoscale devices for biological applications. In some applications, trace components of sub-nanoliter volumes of biological fluid mixtures must be identified, isolated, and analyzed. In others, a surface amenable to cell growth at specific positions is required. A porous, biocompatible coating, lithographically patternable by processes compatible with semiconductor processing, is desirable for both applications. Collagen thin films were investigated as a potential coating.

To demonstrate biocompatibility, astrocytes were successfully cultured on collagen films on silicon nitride. Lithographic patternability was proven by generating 25 micron features via a novel direct liftoff technique. Unpatterned free standing collagen films, 50 nm thick and several square centimeters in area, were also created.

For filtration applications, collagen films require a supporting substrate. Several materials were evaluated according to their ease of processing, microfluidic integrability, substrate permeability, and collagen adhesion to the surface while spanning holes in the substrate without tearing. Silicon nitride, polycarbonate (PC), polyethylene terephthalate (PET), and alumina all met the first two criteria. Alumina clearly outperformed the other substrates on the latter two criteria, and thus was selected for further characterizations.

Several physical, chemical, and performance properties were evaluated of the collagen-on-alumina membranes at depositions ranging from one to nine layers. FTIR spectra consistent with the presence of collagen were qualitatively similar at all coverages. As coverage increased, SEM and AFM indicated a gradual change from mainly monomer to fibril-on-monomer film structures. Surface roughness was independent of coverage in monomeric films, and proportional to coverage in fibrillar films. The water contact angle decreased at higher coverages, likely due to increased roughness. Zeta potential decreased at increasing coverage, indicating a reduced positive surface charge, and lower likelihood of fouling.

The transmembrane pure water flux and permeability were measured under typical industrial pressures. Collagen-on-sulfonated alumina films displayed good stability, and permeability inversely proportional to collagen coverage within a commercially useful ultrafiltration range. The measured flux and permeability could be explained in terms of the membrane structure. Collagen-on-alumina membranes are thus likely to prove suitable for biomolecular separations.

BIOGRAPHICAL SKETCH

On August 25, 1975, Lori Ann Lepak became part of the third generation in her family to be born in Auburn, NY. She graduated as valedictorian of the class of 1993 from Auburn High School. A National Merit Scholar, she joined her elder brothers as the first generation in the family to attend a four-year college as she entered Harvard University.

At Harvard, Ms.Lepak embarked upon a broad, interdisciplinary course of study which satisfied all requirements for a non-honors major in chemistry and physics. Her undergraduate research spanned topics as diverse as an X-ray diffraction study of chemical weathering in Hawaiian soils with geology Prof. Heinrich Holland, and an analysis of the alkaloid content of the chimpanzee diet under anthropology Prof. Richard Wrangham. She earned an AB *cum laude* in Chemistry in June 1997. She began her doctoral program at Cornell University in the Department of Chemistry (now Chemisty and Chemical Biology) the following fall. Under Prof. Melissa Hines, she obtained an MS in Physical Chemistry in May 2000. Her research there combined the use of scanning tunneling microscopy (STM) and atomistic computer simulations to explain and predict the morphology of silicon surfaces subjected to wet-chemical etchants.

From August 2000 through October 2001, Ms. Lepak took a leave of absence from her doctoral studies. For much of that time, she worked as a laboratory assistant at the Boyce Thompson Institute, using computer simulations to model the effects of proposed legislative cuts in ozone emission on the growth of forests.

Ms. Lepak resumed her graduate work in November 2001, with Prof. Michael Spencer in Electrical and Computer Engineering. Her research on biomolecular filtration expanded her technical repertoire to include areas ranging from hands-on

nanofabrication to maintenance of live cell cultures. In addition, she enjoyed the privilege of supervising five talented and dedicated students through the Research Experience for Undergraduates (REU) program. All have since been accepted to top graduate programs in their respective fields.

In the summer of 2005, Ms. Lepak discovered her true calling as a teacher when she accepted an adjunct professorship at Elmira College. She oversaw a course combining general and organic chemistry, designed for both nursing students and nonscience majors. It was an intense summer, as she strove to balance labs and lectures, homework assignments and tests for the first time. She made her share of mistakes, but everyone made it through. Over the next year and a half, improving her teaching became the main focus of Ms. Lepak's professional development. As a tutor with the Learning Strategies Center, she worked with small groups including many at-risk students to improve both their chemistry problem-solving and general study skills. This work complemented and enhanced her more traditional instructional role as a teaching assistant for both the organic and general chemistry laboratory courses.

In the spring of 2007, Ms. Lepak returned to full-time doctoral studies, while continuing to privately tutor a handful of students. Her return was interrupted on March 17, when she suffered a vertebral fracture in a horseback-riding accident. During her recovery, with strong support from family and friends, she rediscovered an appreciation for life which in turn rekindled her drive to finish her degree. After devoting the spring of 2008 to research, Ms. Lepak again returned to the classroom in the 2008-9 school year. She greatly enjoyed teaming with Prof. Spencer and labmate Xingqun Jiang to teach a nanofabrication class in the electrical engineering department, while simultaneously returning to her experimental analytical and physical chemistry laboratory roots under Tom McCarrick in the chemistry department. In the summer of 2009, Ms. Lepak again turned her attention to research

and writing. In the fall, even as she once again co-taught introductory nanofabrication with Prof. Spencer, revising and adding several new laboratory experiments, she retained some focus on her ultimate goal of graduating. She presented her oral defense in December, and obtained her doctoral degree in May the following year. Although Dr. Lepak had not yet accepted a permanent position at the time her degree was conferred, she greatly looked forward to the opportunity to build a new career and new life – wherever she might go, whatever she might study, whether in academic or industrial research. But whatever the next step might be, her ultimate goal remained clear: to teach at a small, primarily undergraduate or junior college.

For all those who have believed in me

ACKNOWLEDGMENTS

A comprehensive list of all the people and organizations without whom this work would not exist could easily double the size of this volume.

First and foremost, I offer my thanks to the Nanobiotechnology Center (NBTC) for my stipend and research funding, for the extensive use of their facilities, and especially for the kindness and helpfulness of all their staff. Most of the remainder of the work was performed using instruments at the Cornell Nanoscale Science and Technology Facility (CNF), and would not have been possible without their talented staff. Much of the electron microscopy was performed either at the Cornell Center for Materials Research (CCMR), or at Wadsworth Center (New York State Department of Health; Albany, NY), with the generous help of Mick Thomas and Don Szarowski respectively. Significant portions of the work, more generally, were performed in collaboration with Dr. James Turner and Dr. Hisham Mohammed, both of Wadsworth Center, and Dr. Kimberly Jones and Dr. Malaisamy Ramamoorthy of Howard University. Special thanks also to CNF and NBTC for the motivated and talented Research Experience for Undergraduates (REU) students who performed much of the hands-on experimental work. To these gifted undergraduates who made up the Lepak Group (a wholly owned subsidiary of the Spencer Group) in the summers of 2002-2004; to Diego Rey, Nancy Guillen, Rachel Gabor, Maribella Domenech, and Rachel Yaggie, my future colleagues, I offer my warmest thanks and best wishes.

Bless my committee, Professor Frank DiSalvo and Professor Benjamin Widom, for their unwavering support in my return to school, and their valuable advice

on both professional and personal matters. Advice, support, and an endless supply of M&M's were likewise the hallmarks of my enduring friendship with Tom McCarrick. Tom acted as my mentor and advisor in all but name, from the moment I agreed to serve as his teaching assistant as a first year student, through my return to his teaching fold in what proved to be the final year at Cornell for both of us, culminating in his retirement and my graduation. At this point mere words fail me – are woefully insufficient to express the warmth and depth of gratitude I will always feel toward my advisor, Professor Michael Spencer. Not one page of this work would have been possible without him. He never wavered in his belief in me. From the moment we began working together, he granted me – as he does all of his students – more intellectual freedom than many professors allow even their postdocs. For eight years, Dr. Mike actively solicited my ideas, treated me as a valued member of his team, and showed a deep respect for my humanity – and that of all our colleagues – a quality of leadership as precious as it is rare. He brightened my entire outlook on the world. And to top it all off, he even learned to think about solubility the way a chemist does! It was an honor and privilege to study alongside him.

Nobody could ask for a more collegial group of labmates than I have been blessed with for these seven years. Above all, I thank Xingqun Jiang and Tad Kaburaki for their wealth of ideas about biomolecular filtration and generous sharing of them in discussions. For the earliest experiments involving collagen, I owe a debt as well to Troy Richards. I highly appreciate Ho-Young Cha, Chris Thomas, Huaqiang Wu, Raymond Zhitao Yang, and Shriram Shivaraman both for their friendship, and for exposing me to science ranging from SiC MESFET's to biosensors to SiC crystal growth to GaN powder synthesis to novel SPM tip fabrication to grapheme membranes. It was a pleasure also to have known and worked alongside

Phani, Goutam, Chandra, Choi, Jie, Junxia, and Barry. Finally, I am delighted no end to have worked alongside world-class chemist and trusted friend Tiju Thomas. He has been there for me every step of the way, always quick to offer whatever support I needed – whether a smile or a prayer, a critique of my writing or friendly advice. Tiju is my inspiration – and my aspiration, that I may pay forward his kindness to all my future colleagues and students. Working alongside all of them (and proofreading the English in several of their papers) has exposed me to a broader range of excellent science – and of outstanding people – than are likely to be encountered anywhere else in the world.

Not having had the opportunity previously, I would also like to thank the members of the Professor Melissa Hines group, where I obtained my Master of Science degree. Tracey Newton and Yi-Chau Huang provided no end of moral support and trained me with endless patience how to tame the STM. Thanks also to Rikard Wind, Simon Garcia, and Yu Wang for their valuable discussions of fabrication problems and for their friendship. And to Prof. Hines herself, I owe the acknowledgement that I would not be half the scientist I am today without the organizational skills, self-discipline, and determination she helped ingrain in me.

Outside of the laboratory, it would take forever to list all the friends and family who have believed in me and made my years at Cornell priceless. My mother and brother David especially were always there for me, for any reason, at any hour of the night, whenever I needed to talk. Katrina, the most precious of my five beloved cats, could likewise always be counted on for a reassuring purr over the phone nearly every day of her 17-year life – and for the pure, unconditional love to which mere humans can only aspire. And there were days when Charlie's soft trills – followed by clawing

at the glass on my bedroom window – were what got me out of bed in the morning. He is more than worth his weight in catnip. To all my other friends – be they housemates or Catholic grad groupies, horsewomen or swing dancers, I couldn't have made it without their support.

Finally, ultimately, and above all else, for everyone mentioned above and for all we have shared and accomplished together, I thank God.

TABLE OF CONTENTS

LIST OF FIGURES

LIST OF TABLES

LIST OF ABBREVIATIONS

AFM – atomic force microscopy

ATP – adenosine triphosphate

ATR – attenuated total reflection

BSA – bovine serum albumin

CFM – chemical force microscopy

CPD – critical point drying

CVD – chemical vapor deposition

DNA – deoxyribonucleic acid

ECM – extracellular matrix

FTIR – Fourier transform infrared spectroscopy

FLS – fibrous long spacing collagen

GA – glutaraldehyde

Gly – glycine

HDMS – hexamethyl disilazane

HVEM – high voltage transmission electron microscopy

Hyp – hydroxyproline

IPA – isopropanol

IR – infrared spectroscopy

LB – Langmuir-Blodgett

LPCVD – low pressure chemical vapor deposition

Lys – lysine

MEMS – micro electrical/mechanical systems

MW – molecular weight

MWCO – molecular weight cutoff

PC – polycarbonate

PCR – polymerase chain reaction

PDMS – polydimethylsiloxane

PET – polyethylene terephthalate

PMMA – polymethylmethacrylate

Pro – proline

RNA – ribonucleic acid

RMS – root mean square

SA – sulfonated alumina

SAM – self assembled monolayer

SEM – scanning electron microscopy

SLS – segmental long spacing collagen

TEM – transmission electron microscopy

TER – transendothelial electrical resistance

UV/vis – ultraviolet/visible spectroscopy

WTF – wild type fibril

Chapter 1: Filtration and BioMEMS

1.1 Introduction

The advent of micro- and nanofabrication has enabled major advances in computer technology in the last 50 years. These techniques, which made possible the development of smaller, lower-power, more efficient transistors, now hold the promise of spawning progress in other fields, such as biotechnology. In this rapidly growing field, also known as bioMEMS, hundreds, if not thousands, of research articles and reviews have been published in the past decade.[1-8] The scope of these investigations encompasses both basic and applied research, and a broad range of cell types. In applied biomedical research alone, microfabrication techniques are currently being used to develop retinal [9] and pancreatic [10] implants to treat some forms of blindness and diabetes respectively. For more basic research, microfabrication is often used to create miniaturized hepatic,[11] osteoblast,[12] and endothelial,[13] and other cell mono- and co-culture systems. However, some cell types will not properly grow directly on inorganic substrates. Implantable devices face the additional complication that many inorganic materials provoke inflammatory responses, scarring, or outright toxicity *in vivo*.[14-16] Protecting the functioning of devices, and in many cases promoting the growth of a particular cell type, may require the use of a biocompatible coating such as a protein.

Some biomedical applications may selectively expose live cells to carefully chosen molecules, either on chip or in vivo. Drug delivery targeted to specific tissues is one area of growing interest.[17-19] In other instances, the goal may be to control the size or molecular weight cutoff (MWCO) of particles which are allowed to reach specific cell types, often by filtration through a selectively permeable membrane.[10,

20-23] One specific example would be the separation of large proteins from small molecular cofactors to determine their individual effects on cocultured cell types.[21]

Other biomedical applications do not require the direct interaction of live cells with nanofabricated devices, but may instead involve the serial separation, detection, and analysis of biomolecules on chip. Such chips are known widely in the literature as micro total analysis systems, or μtas.[22-29] Specific examples which have attracted much recent effort include the separation of proteins from each other [30-35] and from DNA,[36-38], frequently as a purification step prior to further analysis. Several components of whole blood, in particular hemoglobin and related metalloproteins, are known inhibitors of the PCR reaction,[39,40] although the exact mechanism of the inhibition remains uncertain.[41] Thus, a preliminary separation of DNA from these inhibitory proteins [37,38] could greatly improve the efficiency of any subsequent PCR on a chip.[42] On-chip separation systems are likely to eventually find a broad array of applications, such as speeding up and more fully automating the testing of sub-microliter forensic samples,[43,44] or performing the high throughput screening of newborns for genetic diseases.[45] Toward these ends, it is desirable to investigate natural, biocompatible materials, capable of forming porous films which can act as filters, as potential coatings for microfabricated biomedical devices.

1.2 Filtration

In general, many strategies are available for the separation of molecules. In bulk processes, the options include centrifugation, distillation, recrystallization, solubility-based extraction, various forms of chromatography, and filtration.[46] Among these techniques, filtration is the easiest to miniaturize for sub-milliliter sample sizes, and to integrate with microfluidics on-chip.[47-51] Filtration generally takes place through a membrane, which can be defined as a selectively permeable

barrier between two bulk phases. Chemical species may be transferred across the barrier in one or both directions. In the simplest case, depicted in figure 1.1, this

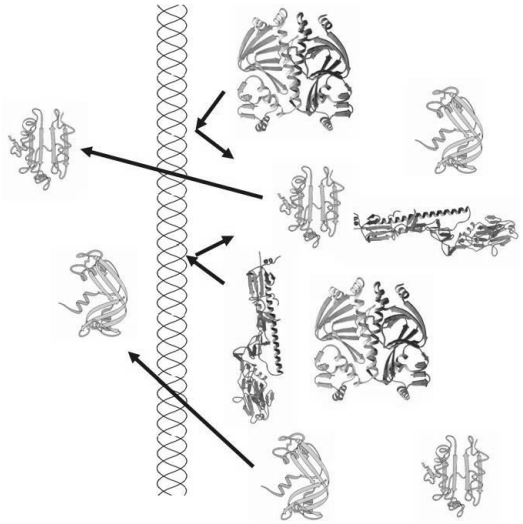

Figure 1.1 Schematic of concentration-driven filtration across a membrane

transfer may be driven purely by passive diffusion along a concentration gradient. In this simple case, rejection may derive solely from the exclusion of solute molecules which are smaller than the pores in the membrane.

Although this is a good approximation to the behavior of some membrane systems, additional effects are often present both in the actuation and the rejection. For example, in many commercial applications, mass transfer is driven primarily by hydraulic pressure.[52] If the solutes are charged, which is usually true of biomolecules, then electric or magnetic fields may be used to actuate the flow.[53,54] Similarly, electrostatic interactions or chemical affinities are often present between the solute and the membrane material. These interactions may be either attractive, leading to adsorption and fouling,[55] or repulsive, causing rejection even when the physical pore size alone would allow the solute to pass.[56,57]

Filtration is often classified according to the size of the particles being filtered. A summary of these filtration size regimes is provided in table 1.1. Filters designed to

Table 1.1 Size Scales of Biologically Relevant Filtration Regimes

Filtration Regime	Particle Size	Biological Examples
microfiltration	100 nm -10 μm	eukaryotic cells, bacteria
ultrafiltration	10-100 nm	bacteria, viruses, colloids
nanofiltration	1-10 nm	proteins, nucleic acids
reverse osmosis	< 1 nm	small molecules, ions

remove particles the size of a typical mammalian cell – a few microns in diameter – fall comfortably within the microfiltration regime. Bacterial cells, perhaps 200 nm wide, lie at the boundary between micro- and ultrafiltration. Ultrafiltration removes viruses, and other particles down to about 10 nm in diameter. Below this, in the nanofiltration range, (1-10 nm), macromolecules such as proteins, DNA, RNA, starches, and other high MW polymers may be separated from each other. At the low end of nanofiltration, even small molecules such as amino acids, single nucleotides, simple sugars, and other cofactors of less than 1000 daltons may be rejected. The smallest pores, less than 1 nm, are found in reverse osmosis membranes. Reverse osmosis is used primarily in environmental applications, to remove dissolved metal cations to soften, desalinate, or even fully deionize, water.

When attempting a specific separation, one must look at the typical sizes of the molecules involved. In the case of biomolecules, most common proteins are roughly spherical, with diameters ranging approximately from 2.5 nm (insulin)[58] to 8.5 nm (albumin).[59] For spherical molecules, MW is often used as a proxy for size because it is easier to measure directly. However, care must be taken when the biomolecule of interest has a more oblong or even linear shape. It should also be noted that rejection behavior is rarely determined by absolute size or MW alone. The solubility and diffusivity of the molecule in the solvent of choice, the size of the solvation shell, and electrostatic interactions between the solute and membrane must all be considered.

Most of these physical and chemical properties could potentially be exploited, either alone or in combination, to achieve a separation in the specific case of hemoglobin and DNA. Hemoglobin is nearly spherical, and about 5.5 nm in diameter.[60] Double-stranded DNA may be many microns long, but is known to have a hydrodynamic radius of 2.4 nm in aqueous solution.[61] Thus, with sufficiently small pores, size exclusion alone may prove sufficient for a separation. In addition, electrostatic charges are likely to prove useful for separating DNA from proteins. At any physiologically reasonable pH, DNA has a negative charge proportional to the fragment length. Hemoglobin has a much higher isoelectric point than DNA, and with it a somewhat tunable charge-to-mass ratio. Thus, an electroosmotic separation of DNA and hemoglobin is likely to be possible at some pH, as has been demonstrated in the separation of proteins with greatly different isoelectric points.[31,32] Should the combination of size and charge effects prove insufficient, differences in chemical affinity between the biomolecule and the membrane may provide yet another basis for separation.[62,63]

Chemical affinity could also be harnessed to enhance size-based separations. For example, each hemoglobin molecule contains four iron atoms which strongly bind to oxygen. Potentially, a molecule with multiple hydroxyl groups could be added to the solution to form complexes with the iron-bearing heme groups, creating composite particles large enough to be rejected by the membrane. The alternate strategy of using hydroxyl groups at the surface of the membrane itself to bind heme is ill advised, as it would likely foul the membrane, perhaps irreversibly,[55,64] reducing both the flux and the useful lifetime of the membrane.

1.3 Filtration: A Theoretical Perspective

Although no rigorous attempts will be made in this work to mathematically model the diffusion of particles through the membrane during filtration, such modeling could, in the long term, prove useful for engineering membranes with properties tailored to specific applications. Consequently, the ease of modeling membrane behavior will be considered as a factor in experimental design. A brief treatment of the main theoretical considerations for modeling filtration is therefore in order.[65-67]

The exact mechanism of filtration varies with the pore structure of the membrane. As can be seen in figure 1.2a, some membranes possess a surface layer which is structurally quite different from the bulk. If the surface 'skin' layer possesses very small pores relative to the bulk, a bottleneck of filtered material will occur at the

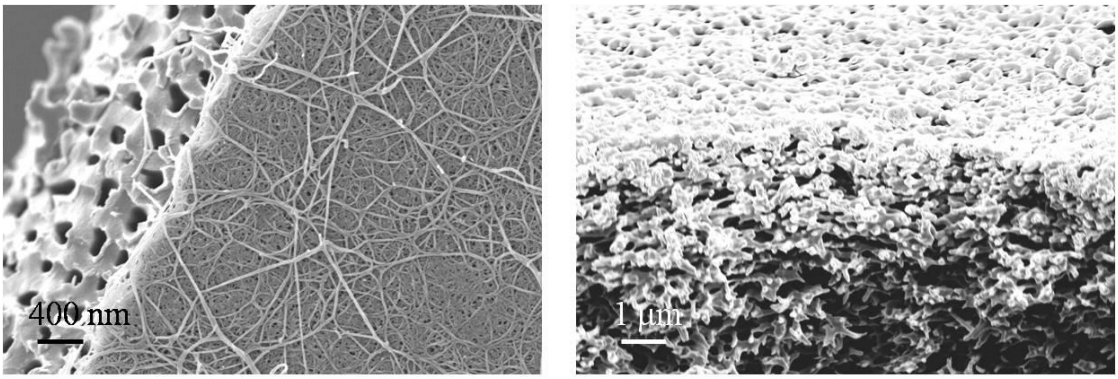

Figure 1.2 Filtration may occur primarily a) at the surface or b) in the bulk surface. In this case, the structural properties of the surface layer will determine the overall properties of the filter. In other membrane systems, as in figure 1.2b, there is nothing special about the membrane structure at the surface; it is merely a continuation of the bulk structure. In this case, the bulk structural properties will be the key to understanding the system, since the molecules subject to filtration will spend most of their time there.

In the simplest, easiest-to-model bulk structure, the channels may be perfectly straight.[68,69] At submicron dimensions, such systems may be modeled as a scaled-down version of water flow through pipes – a laminar flow regime. As can be seen in figure 1.3a, this geometry can be very nearly achieved in some real, directionally-

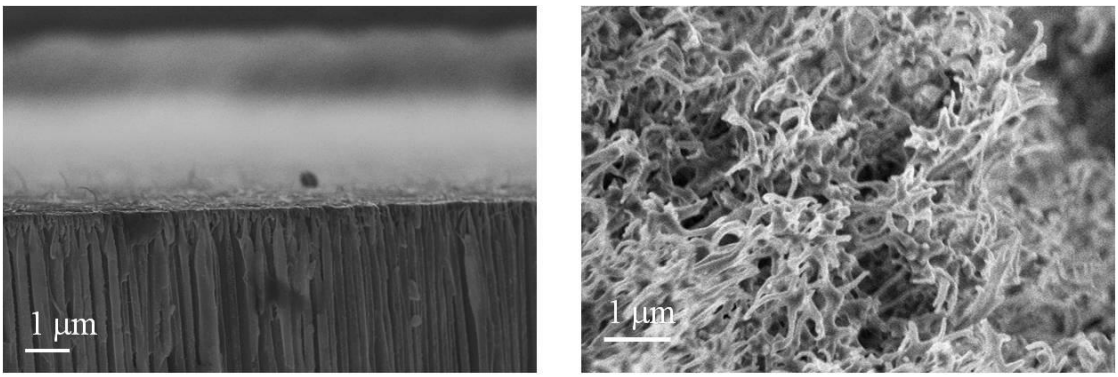

Figure 1.3 Diffusion may follow either a) straight channels or b) tortuous paths etched systems. Membranes made of natural organic materials and formed by other processes, such as precipitation from solution or spin casting, are more likely deposit material in a random 'hairball' packing. This leads to randomly shaped channels with fluids subject to a tortuous path, as in figure 1.3b. In this case, flow is clearly not laminar. One must examine the physical details of the system more closely to select a more appropriate model of filtration.

The high tortuosity of the channels increases both the effective path length of the fluid, and the surface area of the membrane available to interact with the filtrate. As these channels approach molecular dimensions, a large fraction of the solution approaches closely enough to the walls to experience electrostatic interactions.[65] Thus, the charge-dipole and dipole-dipole interactions (if any) among the solute molecules, the solvent, and the membrane itself all must be considered more explicitly. [67,70,71] For example, the effective 'size' of a solute particle may include a monolayer of solvent molecules which surrounds it in the 'bulk' fluid. Conversely,

there is relatively little 'bulk' fluid, and solutes will spend some time with this solvation shell partly replaced by interactions with the surface. Most likely, there will be differences in the relative strengths of the interactions with the solute in the fully solvated compared to surface-bound states. The energetic differences between these two cases will cause solute molecules to partition competitively between the mobile phase (solvent) and the stationary phase (membrane material). The relative affinity of the solute for each phase determines what fraction of time, on average, the molecule spends in each phase. Thus, the rate at which each species traverses the membrane will depend explicitly on polarity as well as size. This situation is analogous to chromatography. Equations derived from chromatographic models [72,73] would thus be most appropriate.

1.4 Experimental Filtration Systems

To experimentally determine whether it is possible for a given membrane to separate two particle species, the relevant physical, chemical, and performance characteristics of the membrane itself must be measured.[74,75] The actual physical pore size and pore density can be observed directly in SEM, both at the surface and in cleaved cross-section. Thus SEM observations may provide clear evidence of whether the surface layer is distinct from the bulk. AFM may provide even higher resolution, quantitative measurements of surface pore size, as well as of membrane surface roughness.[76,77] However, the physical pore size alone cannot account for molecular-level electrostatic interactions between the solutes and the membrane. FTIR and NMR may provide some insights, by identifying the chemical functional groups present at the surface. If ionizable groups are present, zeta potential may be used to quantify the pH-dependent charge at the membrane surface. This surface charge may lead to an 'effective pore size' distinct from the physical pore size, and

dependent upon the charge of the solute particles.[78-82] All this structural information, correlated with membrane preparation conditions, may be fed into a variety of theoretical frameworks and simulations,[83-85] to assist in the process of optimizing the effective membrane pore size and performance for a specific application.[86]

Very often, particular membrane behaviors depend on more than one physical property in complex, interrelated ways. For example, both surface roughness and chemical functionality contribute to the water contact angle, a manifestation of the hydrophobic or hydrophilic behavior of the membrane. The physical 'pore size' measured by SEM relates to several performance properties. Both the flux (volume of fluid passed per unit time) and permeability (flux per unit pressure) tend to increase as pore size increases. Both, however, are also partly dependent on the hydrophilicity. MWCO is also, in general, a function of both pore size and electrostatic interactions between solute and membrane. The bubble point – the pressure at which air bubbles are forced from the pores – also depends explicitly on both pore size and contact angle. Even the tendency to foul, which affects the lifetime of the membrane, depends on a combination of pore size, RMS roughness, and surface functionalization. Thus, the fundamental characterizations of membrane structure become most useful when correlated with actual performance under application-appropriate conditions.[87]

Many of the characterization techniques mentioned above, such as AFM and SEM, are commonly used in other settings in semiconductor processing and will not be discussed in depth here. The focus in the remainder of this section shall be upon performance-based characterizations unique to membrane systems, such as MWCO.

Conceptually, the simplest experimental system for measuring diffusion employs the use of tracers, as diagrammed in figure 1.4. Each tracer is a chromophore which absorbs light over some range of UV or visible wavelengths in the visible or

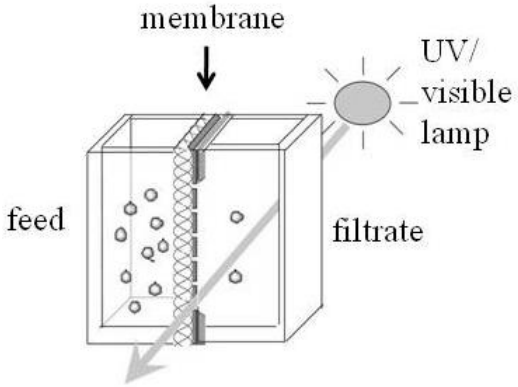

Figure 1.4 Schematic of experimental setup to measure filtration by passive diffusion UV, and can thus be detected by a UV/vis spectrometer. A concentrated feed containing an aqueous solution of one more tracer species is placed on one side of the membrane, while pure water is placed on the other. The tracers are allowed to passively diffuse across the membrane driven solely by the concentration gradient. The absorbance of the filtrate at any point in time can be used to calculate the concentration of chromophores, according to Beer's Law:[88]

$$A = \varepsilon c l,$$

where A= measured absorbance, ε = specific absorbance (tabulated in the literature), l= path length, standardized at 1 cm, and c = concentration of the chromophore. If desired, the change in concentration of a given chromophore as function of time could be used to calculate the diffusion coefficient of each tracer species.

The tracers themselves may be individual highly conjugated dye molecules of low MW (< 1000 daltons),[89-91], proteins or other biomolecules with conjugated groups which absorb UV efficiently,[70,81,90-92] or commercially produced flourescent spheres of known sizes (generally >= 20 nm)[93,94] containing many dye molecules apiece. Experiments may be designed such that several tracer species, each with both a unique size (or MW) and peak absorption wavelength, are simultaneously allowed to diffuse across a given membrane.[95] If smaller tracers are observed to cross the membrane while larger ones are retained, the MWCO can be

approximated.[70,95] In addition, it is often possible to characterize the influence of surface functionality on MWCO. Nanospheres may be chemically functionalized, or appropriate molecular dyes chosen, such that all tracers have either hydrophobic (alkyl), polar (hydroxyl), negatively charged (carboxyl), or positively charged (amine) terminations.[96] By comparing diffusion results for similarly sized species with different chemical terminations, one may detect shifts in the MWCO due to surface chemistry. Molecules corresponding to one chemical class may even visibly adsorb to the membrane more effectively than the others, providing evidence of fouling due to surface charge.[89,97]

This passive diffusion system possesses the advantage that there is little risk of physical damage to the membrane, since no hydraulic pressure is applied. Thus, the experiment can be run with little direct monitoring, apart from the absorbance measurements. However, there are several disadvantages. Most significantly, the flux of chromophores across the membrane will not be constant. Diffusion will be fastest initially, when the concentration difference is highest, and slow down dramatically over time. Hours or days may be required for the system to reach equilibrium. Yet even the initial rate will, in general, be slow relative to a pressure-driven flux system.

Flux experiments can be run in two geometries: either cross-flow (figure 1.5a),

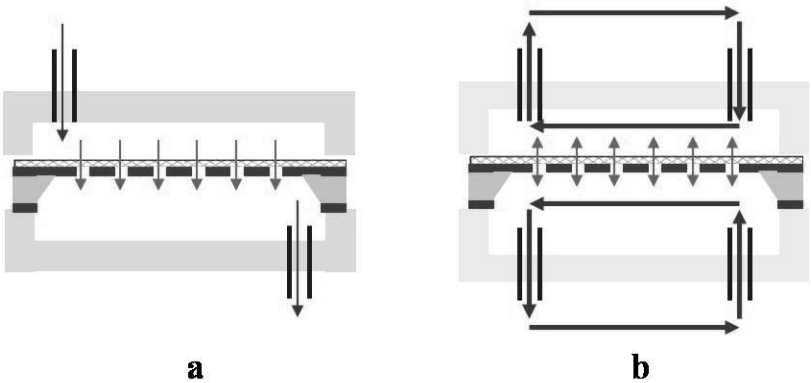

Figure 1.5 Geometric configurations for filtration include a) cross flow and b) tangential flow

or tangential flow (figure 1.5b). In the cross-flow geometry,[98,99] filtrate is driven directly across the membrane, either by hydraulic pressure, electric fields, or both. This actively driven flux is, in general, much greater than in a passive diffusion system. With the feed constantly replenished, the flux is freed from any concentration dependence, and thus may remain stable for a relatively long time. Furthermore, flux may easily be adjusted as a function of applied pressure or electric field. However, particularly at high applied pressures, particles too large to pass through the membrane pores are very likely to become trapped and compacted on the surface. This fouling will inevitably block many pores, diminishing both the flux and the useful lifetime of the membrane. At high enough pressures, the membrane is likely to break.

Damage to the membrane is far less likely to occur in the tangential flow geometry,[100] in which the liquid flows parallel to, rather than directly through, the membrane surface. As in the static cell, passive diffusion along concentration gradients, perhaps in concert with electric fields, drives the transmembrane flux. However, since both the feed and filtrate solutions are constantly replenished by horizontal flow at the membrane surface, the concentration gradient remains high. As a consequence, the flux remains much higher than in a passive system, though lower initially than in a typical direct flow system. By adjusting the flow rates parallel to the membrane on both sides, the flux can be kept nearly constant over time. The fluid flow parallel to the surface also has the potential to resuspend particles which have deposited on the membrane surface. The resulting reduction in fouling helps to maintain an adequate transmembrane flux for a much longer time than is possible in a cross-flow geometry. Thus, tangential flow permits a high, stable throughput with a low likelihood of damage, combining the advantages of the cross flow and passive cells.

1.5 Building the BioMEMS Interface: The Goals of This Work

In this work, we seek to develop a biocompatible coating for bioMEMS devices. Given that such devices will often require a selective placement of this coating, a desirable material should be lithographically patternable in its own right, and integratable with inorganic semiconductor and/or polymeric plastic substrates. With the primary focus on devices for filtration applications, the coating must have pores in a size range well-suited to biomolecular separations. This is likely to require some means of controlling the film thickness, and the pore sizes and structure. It should also be possible to control, or at least characterize, membrane properties such as surface morphology, charge, RMS surface roughness, and hydrophilicity. As far as possible, membrane behaviors such as flux, permeability, fouling, and MWCO should be measured, and controlled as a function of variable parameters such as concentration of membrane material and deposition method. Ideally, a method would be discovered to create nanofiltration membranes and tailor their surface physical and chemical properties for separations of specific biomolecule mixtures, such as DNA from heme, or protein-protein separations.

With an eye on these applications, collagen was selected as the coating for further investigation.[101] In chapter 2, the materials properties of collagen will be explored in depth. These properties lead naturally to the development of a novel, widely applicable lithographic technique for patterning any porous material. Basic biocompatibility of the collagen films will also be demonstrated through cell culturing. Then, in chapter 3, issues surrounding the integration of collagen films onto the substrates most commonly used in the semiconductor and biotechnology industries will be addressed. The development of intergrated films with a suitable porosity for nanofiltration applications provides the framework for this discussion. On the substrate where the integration is most successful, the collagen films will be

characterized in greater detail in chapter 4. The surface physical and chemical properties, as well as some performance properties, of these films will be measured. A theoretical discussion of porosity and pore size control will also be included. Finally, the insights gained from all of these experiments will be linked together in chapter 5, with suggestions for future work.

REFERENCES

[1] Desai, T.A.. Med. Eng. Phys., 22 **(**9), 595-606, 2000

[2] Puleo, C.M., Yeh, H.C., and Wang, T.H.. Tiss. Eng., **13 (12)**, 2839-2854, 2007

[3] James, T., Mannoor, M.S., and Ivanov, D.V.. Sensors, **8 (9)**, 6077-6107, 2008

[4] Loh, O., Vaziri, A., and Espinosa, H.D.S.M.. Exp. Mech., **49 (1)**, 105-124, 2009

[5] Desai, T.A., Hansford, D., and Ferrari, M.. J. Membr. Sci., **159 (1-2)**, 221-231, 1999

[6] Zougagh, M., and Rios, A.. Analyst, **134 (7)**, 1274-1290, 2009

[7] Adiga, S.P., Curtiss, L.A., Elam, J.W., Pellin, M.J., Shih, C.C., Shih, C.M., Lin, S.J., Su, Y.Y., Gittard, S.A., Zhang, J., and Narayan, R.J.. JOM, **60 (3)**, 26-32, 2008

[8] Hediger, S., Sayah, A., Horisberger, J.D., and Gijs, M.A.M. Biosens.Bioelec., **16 (9-12)**, 689-694, 2001

[9] Lu, J.T., Lee, C.J., Bent, S.F., Fishman, H.A., and Sabelman, E.E.. Biomat., **28** (**8)**, 1486-1494, 2007

[10] Desai, T.A., Hansford, D.J., Leoni, L., Essenpreis, M., and Ferrari, M.. Biosensors & Bioelec., **15 (9-10)**, 453-462, 2000

[11] Zhang, Y., Wang, W.J., Feng, Q.L., Cui, F.Z., and Xu, Y.X.. Mat. Sci. Eng. C-Biomimetic And Supramolecular Sys., **26** (**4)**, 657-663, 2006

[12] Muller, R., Abke, J., Schnell, E., Scharnweber, D., Kujat, R., Englert, C., Taheri, D., Nerlich, M., and Angele, P.. Biomat., **27 (22)**, 4059-4068, 2006

[13] Keresztes, Z., Rouxhet, P.G., Remacle, C., Dupont-Gillain, C.. J. Biomed. Mat. Res. Part A **76A (2)**, 223-233, 2006

[14] Sinani ,V.A., Koktysh, D.S., Yun, B.G., Matts, R.L., Pappas, T.C., Motamedi, M., Thomas, S.N., Kotov, N.A.. Nano Letters , **3 (9)**, 1177-1182, 2003

[15] Ainslie, K.M., Tao, S.L., Popat, K.C., and Desai, T.A.. ACS Nano, **2 (5)**, 1076-1084, 2008

[16] Ainslie, K.M., Tao, S.L., Popat, K.C., Daniels, H., Hardev, V., Grimes, C.A., and Desai, T.A.. J. Biomed. Mat. Res. Part A, **91A (3)**, 647-655, 2009

[17] Tao, S.L., and Desai, T.A.. Adv. Drug Delivery Rev., **55 (3)**, 315-328, 2003

[18] Chan, O.C.M., So, K.F., and Chan, B.P.. J. Controlled Release, **129 (2),** 135-143, 2008

[19] Ainslie, K.M., and Desai, T.A. Lab On A Chip, 8 **(**11), 1864-1878, 2008

[20] Desai, T.A., Hansford, D.J., and Ferrari, M.. Biomolec. Eng., **17 (1)**, 23-36, 2000

[21] Graber, D.J, Snyder-Keller, A., Lawrence, D.A., Shain, W., Szarowski, D.H., Al-Kofani, K.A., Roysam, B., and Turner, J.N.. J. Neuroimmunol., submitted.

[22] Fu, J.P., Mao, P., and Han, J.. Trends In Biotech., **26 (6)**, 311-320, 2008

[23] Geng, L.N., Jiang, P., Xu, J.D., Che, B.Q., Qu, F., and Deng, Y.L.. Prog. Chem., **21 (9)**, 1905-1921, 2009

[24] Kutter, J. P.. Trends Anal. Chem., **19 (6)**, 352-363, 2000

[25] Rossier, J., Reymond, F., and Michel, P.E. Electrophoresis, **23 (6)**, 858-867, 2002

[26] Reyes, D.R., Iossifidis, D., Auroux, P.A., and Manz, A.. Anal. Chem., **74 (12)**, 2623-2636, 2002

[27] Auroux, P.A., Iossifidis, D., Reyes, D.R., and Manz, A.. Anal. Chem., **74 (12)**, 2637-2652, 2002

[28] Broyles, B.S., Jacobson, S.C., and Ramsey, J. M.. Anal Chem, **75 (11)**, 2761-2767, 2003

[29] Kalish, H., and Phillips, T.M.. Current Pharm. Anal., **5 (3)**, 208-228, 2009

[30] Lee, J., Soper, S.A., and Murray, K.K.. J. Mass Spec., **44 (5)**, 579-593, 2009

[31] Vaneijndhoven, R.H.C.M., Saksena, S., and Zydney, A.L.. Biotech. Bioeng., **48 (4)**, 406-414, 1995

[32] Ku, J.R., and Stroeve, P.. Langmuir, **20 (5)**, 2030-2032, 2004

[33] Ghosh, R.. J. Chromatogr. A, **952 (1-2)**, 13-27, 2002

[34] Chun, K.Y., and Stroeve, P.. Langmuir, **18 (12)**, 4653-4658, 2002

[35] Saxena, A., Tripathi, B.P., Kumar, M., and Shahi, V.K.. Adv. Coll. Int. Sci., **145 (1-2)**, 1-22, 2009

[36] Footz, T., Wunsam, S., Kulak, S., Crabtree, H.J., Glerum, D.M., and Backhouse, C.J.. Electrophoresis, **22 (18)**, 3868-3875, 2001

[37] Fu, J.P., Schoch, R.B., Stevens, A.L., Tannenbaum, S.R., and Han, J.Y.. Nature Nanotech., **2 (2)**, 121-128, 2007

[38] Ke, X.B., Shao, R.F., Zhu, H.Y., Yuan, Y., Yang, D.J., Ratinac, K.R., and Gao, X.P.. Chemical Communications, **10**, 1264-1266, 2009

[39] Akane, A., Matsubara, K., Nakamura, H., Takahashi, S., and Kimura, K.. J. Forensic Sci. **39 (2),** 362–372, 1994

[40] Al-Soud,W.A. and Radstrom, P.. J. Clin. Microbiol., **39 (2)**, 485–493, 2001

[41] Kermekchiev, M.B., Kirilova, L.I., Vail, E.E., and Barnes, W.M.. Nucleic Acids Res., **37 (5)**, e40, 2009

[42] Zhang, C.S., Xu, J.L., Ma, W.L., and Zheng, W.L.. Biotech. Adv., **24 (3)**, 243-284, 2006

[43] Pumera, M.. Electrophoresis, **27 (1)**, 244-256, 2006

[44] Liu, P., Yeung, S.H.I., Crenshaw, K.A., Crouse, C.A., Scherer, J.R., and Mathies, R.A.. Forensic Sci. Intl.-Genetics, **2 (4)**, 301-309, 2008

[45] Mohamed, H., Pass, K., Caggana, M., and Turner, J.. Clinical Chem., **53 (6)**, A223 E29, 2007

[46] Fessenden, R.J., Fessenden, J.S., and Feist, P.. *Organic Laboratory Techniques*, 3rd edition, Brooks/Cole, Pacific Grove, CA, 2001

[47] Han, J.Y., Fu, J.P., and Schoch, R.B.. Lab On A Chip, **8 (1)**, 23-33, 2008

[48] Atencia, J., and Beebe, D.J.. Nature, **437 (7059)**, 648-655, 2005

[49] Ong, S.E., Zhang, S., Du, H.J., and Fu, Y.Q.. Front. Biosci., **13**, 2757-2773, 2008

[50] Wang, P.C., DeVoe, D.L., and Lee, C.S.. Electrophoresis, **22 (18)**, 3857-3867, 2001

[51] de Jong, J., Lammertink, R.G.H. , and Wessling, M.. Lab On A Chip, **6 (9)**, 1125-1139, 2006

[52] Van der Bruggen, B., Vandecasteele, C., Van Gestel, T., Doyen, W., and Leysen, R.. Env. Prog., **22 (1)**, 46-56, 2003

[53] Kemery, P.J., Steehler, J.K., and Bohn, P.W.. Langmuir, **14 (10)**, 2884-2889, 1998

[54] Bruin, G.J.M. Electrophoresis, **21 (18)**, 3931-3951, 2000

[55] Caillou, S., Boonaert, C.J.P., Dewez, J.L., and Rouxhet, P.G.. J. Biomed. Mat. Res. Part B-App. Biomat., **84B (1)**, 240-248, 2008

[56] Fornasiero, F., Park, H.G., Holt, J.K., Stadermann, M., Grigoropoulos, C.P., Noy, A., and Bakajin, O.. Proc. Nat. Acad. Sci. USA, **105 (45)**, 17250-17255, 2008

[57] Koehler, J.A., Ulbricht, M., and Belfort, G.. Langmuir, **13 (15)**, 4162-4171, 1997

[58] http://www.rcsb.org/pdb/explore/jmol.do?structureId=3I3Z&bionumber=1

[59] http://www.rcsb.org/pdb/explore/jmol.do?structureId=3B9L&bionumber=1

[60] http://www.rcsb.org/pdb/explore/jmol.do?structureId=3D7O&bionumber=1

[61] Mandelkern, M., Elias, J.G., Eden, D., and Crothers, D.M.. J. Molec. Bio., **152 (1)**, 153-161, 1981

[62] Klein, E.. J. Membr. Sci., **179 (1-2)**, 1-27, 2000

[63] Ma, Z.W., Kotaki, M., and Ramakrishna, S.. J. Membr. Sci., **265 (1-2)**, 115-123, 2005

[64] Li, M., He, P., Zhang, Y., and Hu, N.. Biochimica et Biophysica Acta, **1749,** 43–51, 2005

[65] Kaufmann, T.G., and Leonard, E.F.. AIChE J., **14**, 110–117, 1968

[66] Schoch, R.B., Han, J.Y., and Renaud, P.. Rev. Mod. Phys., **80 (3)**, 839-883, 2008

[67] Conlisk, A.T., Datta, S., Fissell, W.H., and Roy, S.. Ann. Biomed. Eng., **37 (4)**, 722-736, 2009

[68] Dalvie, S.K., and Baltus, R.E.. J. Membr. Sci., **71,** 247-255, 1992

[69] Morao, A., Nunes, J.C., Sousa, F., de Amorim, M.T.P., Escobar, I.C., and Queiroz, J.A.. J. Membr. Sci., **336 (1-2)**, 61-70, 2009

[70] Martin-Orue C, Bouhallab S, Garem A.. J. Membr. Sci., **142 (2)**, 225-233, 1998

[71] Ho, A.K., Perera, J.M., Dunstan, D.E., Stevens, G.W., and Nystrom, M.. Aiche J., **45 (7)**, 1434-1450, 1999

[72] Surmeian, M., Slyadnev, M.N., Hisamoto, H., Hibara, A., Uchiyama, K., and Kitamori, T.. Anal. Chem., **74 (9)**, 2014-2020, 2002

[73] Charcosset C.. J. Chem. Tech. Biotech., **71 (2)**, 95-110, 1998

[74] Nakao S.. J. Membr. Sci., **96 (1-2)**, 131-165, 1994

[75] Gumi, T., Valiente, M., Khulbe, K.C., Palet, C., and Matsuura, T.. J. Membr. Sci., **212 (1-2)**, 123-134, 2003

[76] Wyart, Y., Georges, G., Demie, C., Amra, C., and Moulin, P.. J. Membr. Sci., **315 (1-2)**, 82-92, 2008

[77] Singh, S., Khulbe, K.C., Matsuura, T., and Ramamurthy, P.. J. Membr. Sci., **142 (1)**, 111-127, 1998

[78] Sakai, K.. J. Membr. Sci., **96 (1-2)**, 91-130, 1994

[79] Wang, X.L., Tsuru, T., Togoh, M., Nakao, S., and Kimura, S.. J. Chem. Eng. Japan, **28 (2)**, 186-192, 1995

[80] Zhao, C.S., Zhou, X.S., Yue, Y.L.. Desalination, **129 (2)**, 107-123, 2000

[81] Lee S, Park G, Amy G, Hong SK, Moon SH, Lee DH, Cho J.. J. Membr. Sci., **201 (1-2)**, 191-201, 2002

[82] Baltus RE.. J. Membr. Sci., **276 (1-2)**, 101-112, 2006

[83] Otero, J.A., Lena, G., Colina, J.M., Pradanos, P., Tejerina, F., and Hernandez, A.. J. Membr. Sci., **279 (1-2)**, 410-417, 2006

[84] Wang, X.L., Shang, W.J., Wang, D.X., Wu, L., and Tu, C.H.. Desalination, **236 (1-3)**, 316-326, 2009

[85] Otero, J.A., Mazarrasa, O., Villasante, J., Silva, V., Pradanos, P., Calvo, J.I., and Hernandez, A.. J. Membr. Sci., **309 (1-2)**, 17-27, 2008

[86] Ulbricht M.. Polymer, **47 (7)**, 2217-2262, 2006

[87] Bellona, C., Drewes, J.E., Xu, P., and Amy, G.. Water Res., **38 (12)**, 2795-2809, 2004

[88] Christian, G.D., *Analytical Chemistry* 5th edition, John Wiley & Sons, Inc., New York, NY, 398-461, 1994

[89] Mohamed, H., Russo, A. P., Szarowski, D. H., McDonnell, E., Lepak, L. A., Spencer, M. G., Martin, D. L., Caggana, M., and Turner, J. N.. Sep. Sci. Technol., **42,** 25 – 41, 2007

[90] Mohamed, H., Russo, A. P., Szarowski, D. H., McDonnell, E., Lepak, L. A., Spencer, M. G., Martin, D. L., Caggana, M., and Turner, J. N.. J. Chromatogr. A, 18th Intl. Sym. on MicroScale Bioseparations, **1111,** 214-219, 2006

[91] Vlassiouk, I. , Apel, P.Y., Dmitriev, S.N., Healy, K., and Siwy, Z.S... Proc. Natl. Acad. Sci. USA, **106 (50)**, 21039-21044, 2009

[92] Schutte, R.J., Oshodi, S.A., and Reichert, W.M.. Anal. Chem., 76 (20), 6058-6063, 2004

[93] Sung, M.H., Huang, C.P., Weng, Y.H., Lin, Y.T., and Li, K.C.. Sep. Purification Tech., **54 (2)**, 170-177, 2007

[94] Charcosset, C., and Fessi, H.. J. Membr. Sci., **266 (1-2)**, 115-120, 2005

[95] Tam, C.M., and Tremblay, A.Y.. J. Membr. Sci., **57 (2-3)**, 271–287, 1991

[96] http://www.invitrogen.com/site/us/en/home/References/Molecular-Probes-The-Handbook/tables/Summary-of-Molecular-Probes-FluoSpheres-fluorescent-microspheres.html

[97] Huisman, I.H., Pradanos, P., and Hernandez, A.. J. Membr. Sci., **179 (1-2)**, 79-90, 2000

[98] Belfort, G., Davis, R.H., and Zydney, A.L... J. Membr. Sci., **96 (1-2)**, 1-58, 1994

[99] Salgin U, and Salgin S.. Chem.Eng. Tech., **30 (4)**, 487-492, 2007

[100] vanReis, R., Gadam, S., Frautschy, L.N., Orlando, S., Goodrich, E.M., Saksena, S., Kuriyel, R., Simpson, C.M., Pearl, S., and Zydney, A.L.. Biotech. Bioeng., **56 (1)**, 71-82, 1997

[101] Seggiani, M., Lazzeri, L., Cascone, M.G., Barbani, N., Vitolo, S., and Palla, M.. J. Mat. Sci.-Mat.Med., **5 (12)**, 868-871, 1994

Chapter 2: Material Properties of Collagen Thin Films

2.1 Introduction

Silicon, gallium arsenide, and other solid-state inorganic materials have a long history of use in the semiconductor industry. Techniques for processing these materials are well characterized, allowing them to be developed into devices with a wide variety of physical structures, for a large array of MEMS applications.[1,2] Advances in the biological sciences in recent decades have created a demand for large-scale production of micro- and nanoscale devices for biological applications. BioMEMS may include purifying [2-5] and analyzing [5,6] nanoliter or smaller volumes of biological fluid mixtures, and biomedical applications [7-18] including drug delivery,[8-10] cell culturing in vitro,[11,12,15,18] or even implanting functioning biomedical devices in vivo.[13,14] However, the use of the use of semiconductor materials for biological applications is often limited by the inability of cells to grow normally – if at all – on inorganic substrates.[16-19] One possible solution is to coat the surfaces of the microfabricated structures with organic materials which are more amenable to cell growth.[16-21] To accommodate applications where a non-uniform, selective placement of cells is desired, this coating should ideally be lithographically patternable, by processes compatible and integratable with those used to fabricate the underlying MEMS device.[22-29]

To guide the search for a suitable coating, one may look first to Nature itself. In vivo, many types of cells grow on scaffolds made of extracellular matrix (ECM) proteins, such as collagen, elastin, and fibronectin. These may be present in pure form, in composites with each other, or even in collagen-mineral composites as in bone.[12,23-26,29-39] The use of composite materials in laboratory processes introduces variables, such as the relative concentrations of the various components and

their interactions, whose effects are difficult to predict a priori, but which are easily avoided when using pure materials. Therefore, in the interest of developing simple, reproducible, processes for coating semiconductor materials, composites were avoided, in favor of pure collagen. Pure collagen films created in vitro, although chemically similar to those generated in vivo, may possess physical or structural differences, which may in turn affect the biocompatibility of such films.[40-44] Thus, preliminary experiments were performed to provide a proof of concept – that cells are potentially viable when grown upon collagen thin films on semiconductor substrates. Optimizing the films for the growth of particular cell types was beyond the scope of the present work. Likewise, a liftoff technique was developed for lithographically patterning collagen, to demonstrate the general principle that collagen can be coated on devices in a spatially controlled manner. Tailoring these lithographic processes for specific applications is left open for future research.

2.2 Collagen as a material

Collagen is the major structural protein in animals, comprising some 20-25% of the protein in the typical vertebrate body. It is the main organic component of skin, bone, tendon, and eye tissues. As such, its structure has been studied and reviewed extensively.[45-52] The single most common protein in the human body, collagen is non-immunogenic, and even routinely injected for cosmetic purposes.[53] Over 20 kinds of collagen are known to exist in mammals as disaggregated monomers.[49] Several of these varieties (including, most significantly for this work, type I), under certain conditions, will further aggregate into extended rope-like structures known as fibrils, whose exact dimensions vary with the preparation conditions, as shall be discussed briefly below in section 2.3, and at greater length in chapter 4.

At the molecular level, each individual monomer of collagen is made of three polypeptide chains, which twist around each other into a triple helix structure, 3 nm wide and 300 nm long, as depicted schematically in figure 2.1. This nearly unique

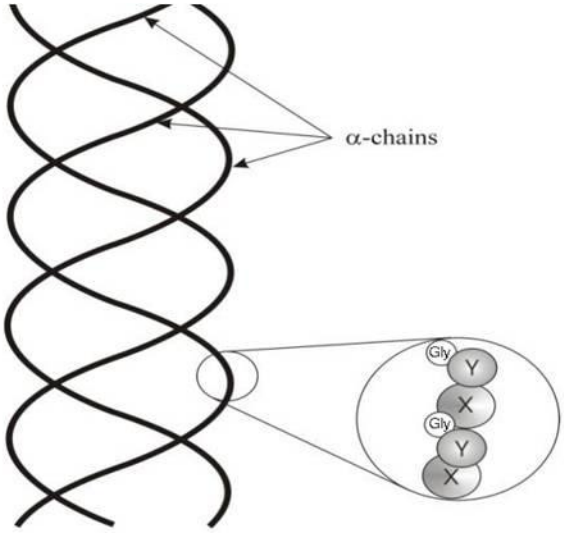

Figure 2.1 Triple helix structure of collagen monomers

quaternary structure is a consequence of the unusual amino acid sequence on all three chains. Except for a small number of residues at each end of the polypeptide, each chain consists largely of glycine-(hydroxy)proline-X triplets (figure 2.2). The amino

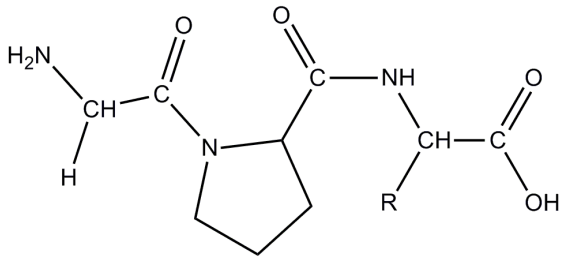

Figure 2.2 Gly-pro-X triplet

acids within each triplet contribute significantly to the overall structural properties of collagen. The structures of the most significant residues are highlighted in figure 2.3. The glycine residue has the smallest side chain of any protein-forming amino acid, a lone hydrogen atom. Glycine must be located on the inside of each helical turn, since

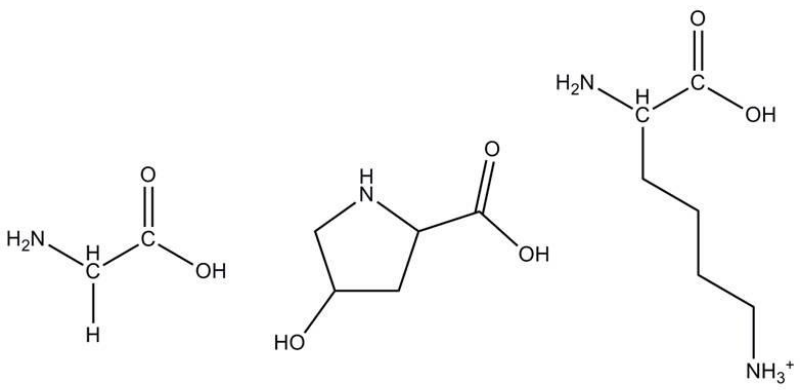

Figure 2.3 Amino acids responsible for the unique chemical properties of collagen

no other side chain will physically fit. Just as steric hinderance dictates the sequence on the inside of the turn, on the outside of the turn, stability of the triple helix is enhanced by structural rigidity. The 5-membered ring incorporated along the peptide chain, which is unique to proline, provides this more effectively than any other amino acid. Therefore, although this requirement is not as strict as for glycine, one or both of the other amino acids in the triplet is usually either proline itself or one of its hydroxylated derivatives, 3- and 4- hydroxyproline.

The relative amounts of proline and its analogs vary slightly across species, tissue type, and collagen type. In mammalian type I collagen, however, about 40-45% of the proline residues are hydroxylated.[54,55] Proline and hydroxyproline together make up over 40% of the triple helix surface,[46,47] meaning that approximately 20% of the surface (non-glycine) residues are hydroxyproline. Collectively, all these hydroxyl groups make collagen hydrophilic. Thus, a collagen coating is likely to successfully mediate interactions between a device and an external aqueous environment. At the same time, one might expect a collagen coating to adhere better to a polar than a nonpolar substrate, since each hydroxyl has the potential to both accept and donate hydrogen bonds to polar groups on any substrate surface. Thus, the presence of hydroxyproline in collagen exerts some influence over substrate choice.

The third residue in each triplet, X, may be any of the 20 amino acids. The sequence of X's is highly variable across species, tissue type, and form of collagen, and is generally responsible for the unique properties of each form of collagen. Lysine residues, although few in number, make an important contribution to two particularly significant chemical properties. First, the lysine side chain contains a basic nitrogen, which is easily protonated. This contributes to an increased isoelectric point, reported by some researchers to be as high as 8 or 9.[56] This implies a slight positive charge on collagen, and with it a repulsion between monomers, in solution at pH 7 and below. Second, the amino groups in the lysine side chains are sterically accessible to and reactive toward aldehydes to form imine bonds. The reaction of lysine residues on two neighboring collagen monomers with a dialdehyde such as glutaraldehyde allows a stable, covalent crosslink to be formed between them. Although complex mixtures of crosslink products are believed to form,[57-59] one of the most common is depicted in figure 2.4. Crosslinking among several monomers in this manner forces them to

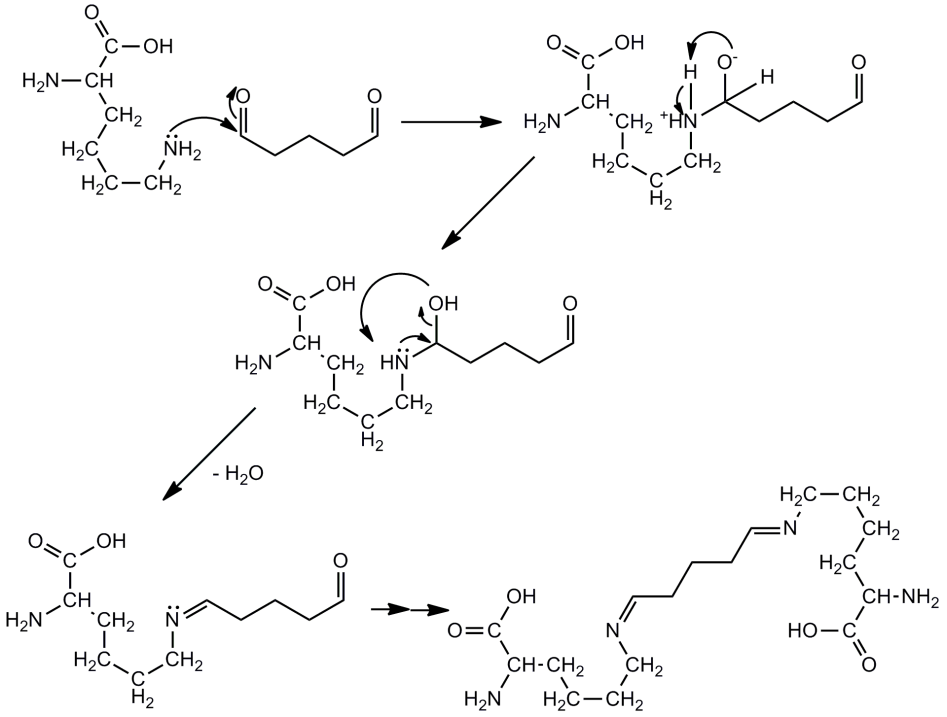

Figure 2.4 Crosslinking of lysine side chains by glutaraldehyde

remain closely aligned, thereby promoting the nucleation of a fibril. It is also possible for monomers which have already been incorporated into neighboring fibrils to crosslink, giving rise to more complex polymeric structures.[35,36]

Before proceeding to a discussion of fibril structure, it should be noted that the structure of collagen monomers can also influenced by temperature and pH. The temperature at which the type I collagen triple helix denatures is somewhat pH dependent, but roughly 35-40^{o}C.[31,50] There is some disagreement in the literature about what the value of the isoelectric point of type I collagen. Reported values range from approximately pH 5.5 [31], to over 9.[34,60] Below the isoelectric pH, one would expect collagen to be positively charged overall. Like charged monomers tend to repel each other, hindering the formation of fibrils. Thus, type I collagen exists primarily in monomeric form in aqueous solution at acidic pHs.[56] As the pH of the solution is raised, acidic side chains on many residues within the collagen are sequentially deprotonated, eliminating positive charges at some positions and creating negative charges at others. As opportunities for repulsive interactions between monomers decrease and for attractive interactions increase, collagen begins to coalesce into fibrils closely resembling their natural form. As the monomers aggregate into physically larger fibrils, the solubility limit is reached and collagen precipitates.

2.3 From Monomers to Fibrils

In vitro, monomers may be induced to aggregate in solution into one of several fibril structures by several different means:[61-88] by raising the pH [65-68]; adding enzymatic [69-71] or chemical crosslinkers [72-78] such as glutaraldehyde,[77-81] or ultraviolet light [82-85]. If fibrils are formed or deposited on a substrate, then the substrate surface chemistry and topography, as well as details of the deposition,

rinsing, and drying process, may all affect fibril structure and distribution as well. [40,80,86-88]

Wild type fibrils are stabilized by crosslinks between a lysine residue near the C-terminal end of one monomer and an enzymatically modified lysine residue near the N-terminal end of a monomer in an adjacent row.[46,47,56] The modified lysine is sequentially hydroxylated, deaminated, and oxidized to an aldehyde, to allow it to form an amide bond to the unmodified lysine. Because of the relative locations of the residues involved, this leads to a staggered offset of monomers between rows.[56] Within a head-to-head row, there is a physical gap (0.6D in wild-type fibrils) between collagen monomers (of length D), leading to a periodic banding pattern (4D in WTF) visible in SEM and AFM.[61,62,89] Fibrils not found outside the laboratory, such as FLS [90], crosslink at different residues and have a longer gap spacing. Another kind of fibril, SLS [89,91], uses ATP as a crosslinker to form short, wide fibrils. Although these and other alternative forms of fibrils exist,[92,93] and could in principle be candidate materials for use in bioMEMS devices, they are not considered further here.

Since type I collagen monomers predominately form the wild type structure in Nature, this structure is most likely to be biocompatible, and thus was selected for further study. Figure 2.5 schematically illustrates the process of wild type fibril formation.[56,94-96] Disaggregated monomers electrostatically repel each other at low pH. As the pH is raised and electrostatic interactions become more favorable, collagen monomers begin to pack parallel and side-to-side with a slight stagger. Computer simulations suggest that a pentamer of monomers, is required to nucleate a stable fibril.[94] Following nucleation, the fibrils grow in a manner similar to crystals. These fibril ‘crystals’ have highly asymmetric sticking coefficients, such that new monomers preferentially add axially rather than equatorially. Mature natural fibrils typically reach 50 nm wide and several microns long. The staggered side-to-side

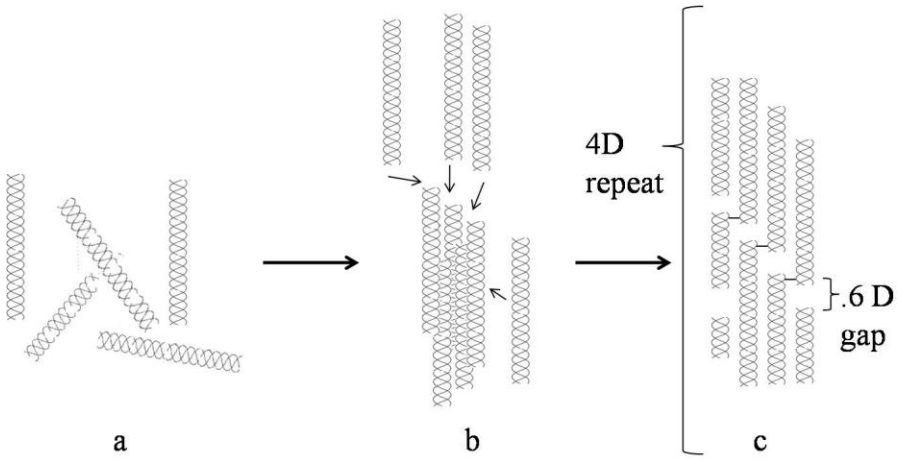

Figure 2.5 Schematic of aggregation of collagen monomers into fibrils a) isolated, positively charged monomers in solution at low pH b) As the pH is raised and charges are neutralized, stable fibril nuclei form from parallel, close-packed, 3.4D staggered monomers. New monomers preferentially add to the fibril axially rather than laterally c) Monomers in mature fibrils are arranged in staggered parallel rows with gaps.

overlap within the fibril nucleus leads to the banding pattern of 75-80 nm observed in the AFM image in figure 2.6. The fibril sizes, 50-140 nm wide and several microns

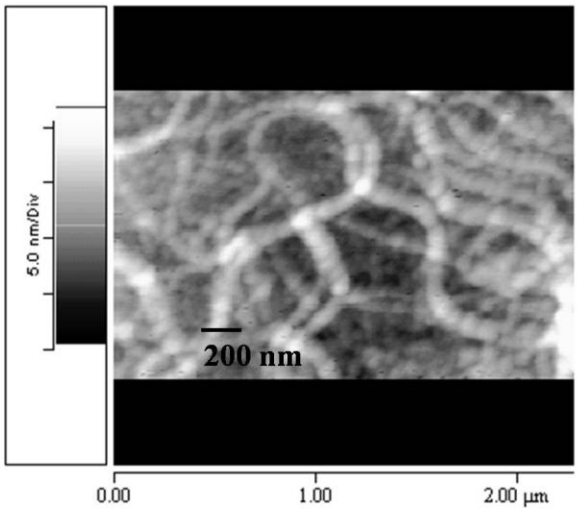

Figure 2.6 AFM image of collagen fibrils

long, are typical for WTF. The fibrils in this sample were generated in solution by raising the pH via dropwise addition of potassium hydroxide, prior to spin casting on silicon.

As can be seen in figure 2.6, although the monomers within a fibril are nearly close-packed, the fibrils themselves do not necessarily close pack to each other. The packing may in fact be random in three dimensions, leading to a collagen 'hairball'. A thin film with 'hairball' packing is likely to have gaps, or pores, which extend through the entire thickness of the film. Fibril structure is likely to have an impact upon the manner of packing, which in turn may influence biocompatibility, film thickness and strength, pore size, and other properties critical to film performance in a given application.

2.4 Collagen: Lithography and Tissue Engineering

Collagen thin films can be deposited on a substrate in several ways,[12,15,86, 92, 97-107] including but not limited to: adsorption from solution,[86,97] evaporation, [98] electrospinning,[12,101] and spin casting.[31,104-107] Spin casting, a technique borrowed from the semiconductor industry,[104] was chosen in this instance, primarily to make the overall process more compatible with device fabrication.

Once a film is created, it is usually necessary to selectively restrict it only to desired parts of the devices. Ideally, this might be achieved through lithographic patterning techniques similar to those already in use in the semiconductor industry. However, to preserve the functioning of most biomolecules, one must avoid the extreme conditions often used in these processes, such as temperatures outside typical physiological ranges, high vacuum, and dehydrating chemicals. In the late 1990's and early 2000's, research and development into techniques for patterning biomaterials flourished.[22-28,108-122] Among these were most of the methods now commonly used for patterning biomaterials, such as microcontact printing [22-24,28, 110,111], dip pen lithography,[112-115] alkanethiol SAMs on lithographically

patterned gold [22-24,27,111,116-118], enzymatic etching [119,120], and parylene dry liftoff. [121]

As with traditional semiconductor lithography, no single patterning technique is appropriate in all circumstances. Several methods with complementary capabilities are often needed to produce a functioning device. Thus, to place in context the utility of direct liftoff, a novel method of biomolecular patterning developed in this work, a brief introduction to each of the other common techniques is in order.

Microcontact printing is a process where a raised-relief 'stamp' is coated with the biomolecule to be patterned, and then pressed into contact with the substrate to transfer the molecules. Biomolecules are applied to an entire wafer surface at once, and several different biomolecules can be applied to a single substrate using different stamps. However, some biomolecule-substrate combinations suffer from adhesion problems, which can only sometimes be overcome by using adhesion promoters.

With microcontact printing, features larger than 100 μm may be easily produced and aligned to patterns on a substrate, even under ordinary laboratory (non-cleanroom) conditions. Given access to standard lithographic equipment, features as small as 500 nm are possible,[122] although this limit is quite sensitive to processing conditions. If patterns are already present on the substrate, alignment of the stamp is typically carried out with a contact aligner, which may introduce registration errors on the order of 1 μm. For this reason, microcontact printing is rarely used to generate submicron features.

At the other end of the feature size scale, dip pen lithography is performed by tracing patterns on the surface with a modified AFM tip. Multiple biomolecular 'inks' may be applied to the same sample – with newer instruments, even simultaneously, [115,123] – although each individual write-head operates serially. Thus, dip pen is most suitable for patterning features with line widths similar to the radius of an AFM

tip – tens to hundreds of nanometers. Larger features require a longer dwelling time for the tip on the substrate. The size and shape of the molecule being patterned, and its relative affinity for the tip and the substrate, will also affect the writing speed. In the specific case of collagen, dip pen lithography is best suited to generating collagen features with line widths between 50 nm and 800 nm.[114]

Other forms of patterning are directly built upon traditional semiconductor fabrication techniques. For example, gold is a lithographically patternable metal, which is known to strongly bind sulfur atoms. Alkanethiols, which possess a sulfur at one end of the molecule and any desired surface termination at the other, will form self-assembled monolayers (SAMs) on gold.[116] Similar self-assembly processes are possible on silicon using chlorosilanes.[16,124] In either case, the surface termination can be controlled to selectively bind the biomolecule of interest.[117,118] Both of these techniques are as independent of size scale as the patterning of the gold or silicon respectively. However, unlike microcontact printing and dip pen lithography, at most two kinds of biomolecule per substrate may be patterned by SAM methods.

In some cases, it is possible to pattern a protein directly, much as any wet-etchable thin film. The protein may be bath applied or even spin cast onto a substrate. Photoresist is then spun atop the protein, and lithographically patterned. In the exposed areas, an enzyme specific to that protein may be used as a 'wet etchant'. This method is highly selective, but somewhat isotropic, leading to sloped undercut profiles.[119] The action of enzymatic etchants may also be far more sensitive than inorganic etchants to processing conditions such as temperature, pH, and ionic strength.[120]

In the semiconductor industry, metals which cannot be wet etched are often patterned via liftoff. Traditional liftoffs often require the use of solvents which are incompatible with biological materials. Solvent-free dry liftoffs for patterning

biomolecules are often possible using parylene. Parylene is a vapor-deposited thin film which may be lithographically patterned, have the biomolecular film applied, and then be physically peeled from a substrate surface.[121] However, to peel easily, the parylene layer must be continuous. Parylene is ill-suited to any pattern requiring the removal of isolated small features, such as holes inside closely spaced gridlines.

Another potential mechanism for liftoff patterning is suggested by the porous structure of spin-cast collagen thin films. With typical pore sizes on the order of 10-20 nm (see section 3.4), these films are permeable to small molecules. Thus, low molecular weight solvents such as ethanol may freely diffuse through the collagen film to access the substrate or another underlying film. If this underlayer is soluble in ethanol, it may become a sacrificial layer, whose dissolution would leave behind a free-standing layer of collagen only tens of nanometers thick.

If the sacrificial underlayer is continuous, then a continuous freestanding film will be created. However, if the underlayer has been lithographically patterned prior to the liftoff, then during spin casting, collagen will coat both the surface of the developed photoresist and exposed regions of the substrate surface. Collagen adheres strongly to hydrophilic surfaces such as the native oxide on a silicon wafer. Thus, in areas inside the pattern, where collagen is in direct contact with the substrate, it might be expected to remain behind when the resist is dissolved, thereby transferring the pattern.

The discussion thus far has not considered which form of collagen might prove most suitable for lithographic patterning. Depending on pH and ionic strength, either monomers or fibrils may exist in solution.[125] As in any photolithographic process, direct liftoff should prove most successful for patterning films of relatively uniform thickness. Thus, to determine whether monomers or fibrils were more amenable to patterning, it was desirable to compare the uniformity of spin cast films of each. The

monomer solution was a commercially available preparation of 0.3% type I bovine skin collagen in an acetate buffer at pH 2. The fibril solution was created from this monomer solution by adding ammonium hydroxide dropwise until the solution began to turn cloudy and viscous, indicating aggregation of the collagen.

A few milliliters of each solution were spin deposited on their respective silicon wafers at 2000 rpm for 1 minute. The results are shown in figure 2.7. The

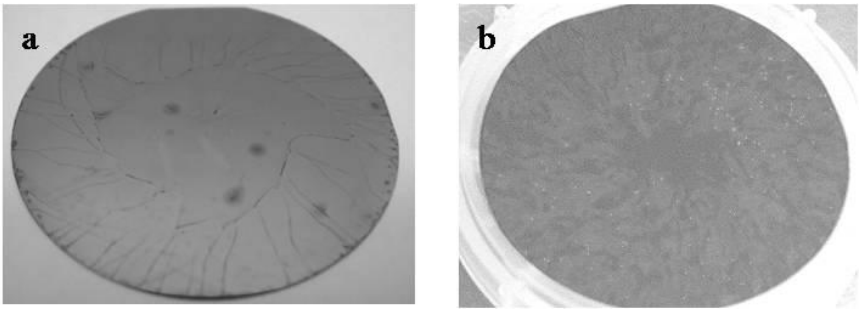

Figure 2.7 Films of collagen spin deposited on silicon a) monomers and b) fibrils

monomer solution generated a film (figure 2.7a) which appeared by eye to be uniform near the center of the wafer. At the edge, the nonuniformity is similar to that observed when too little photoresist is pipetted onto a wafer before spinning; simply using more collagen solution should easily solve this problem. The fibril solution (figure 2.7b), however, generated a visibly nonuniform film, which should be far less amenable to lithography. Thus it was decided to focus solely on monomer solutions for the initial experiments.

2.5 Experimental

2.5.1 Collagen Thin Film Substrates for Cell Cultures

As discussed in the introduction (section 2.1), one major design criterion for collagen films is biocompatibility: the film must be able to sustain live, healthy cell cultures on-chip. Many cell types are routinely cultured on some form of collagen.[126-131] To assess the biocompatibility of these collagen thin films, two

experiments were perfomed in collaboration with Sarina Harris-Ma and Prof. Michael Shuler.[132]

In the first experiment, astrocytes (brain cells) alone were cultured on collagen-coated silicon nitride substrates as diagrammed in figure 2.8. The fabrication of the silicon nitride substrates themselves is discussed in depth in section 3.2, and will not be repeated here. Unfortunately, collagen was observed to adhere poorly to untreated silicon nitride (unpublished data), making it necessary to find a method of

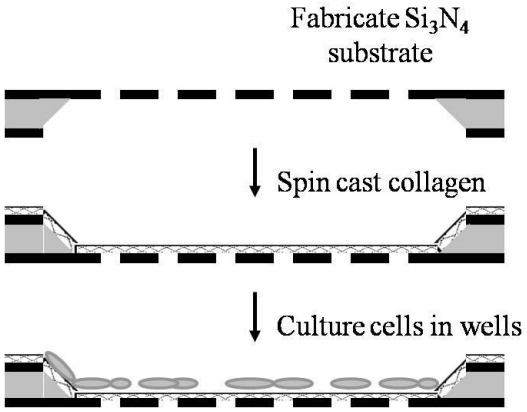

Figure 2.8 Fabrication of substrates for astrocyte cell cultures

improving adhesion. As discussed in section 2.3, glutaraldehyde is known to stabilize crosslinks within fibrils by covalently bonding to collagen monomers. If glutaraldehyde were to bond to silicon nitride as well, it could be used to bond collagen and the substrate surface to each other. To ensure as even a coating of glutaraldehyde on the substrate as possible, a gas phase deposition was performed.[133,134] An open beaker containing an 8% aqueous solution of glutaraldehyde was placed in a sealed chamber at 4^{o}C, to saturate the airspace with glutaraldehyde vapor. The silicon nitride substrates were then placed in the chamber for at least 1 hour. The substrates remained stored in the chamber until immediately prior to the deposition of collagen.

Here, and throughout this entire work, 'one layer' of collagen is defined to be one cycle of pipetting the collagen solution onto the substrate and spinning. Whenever multiple layers were deposited, each layer was cast upon the next immediately, with no rinsing step or time delay in between. In this instance, two layers of a commercially produced solution of 0.3% type I bovine skin collagen (US Biological) were spin cast, at 2500 rpm for 1 min, on the deep-well side of the silicon nitride substrate. After deposition of the final layer, was the sample rinsed in flowing DI water for 3-5 seconds. Following rinsing, the collagen was crosslinked by immersion in a 0.02% solution of glutaraldehyde for 1 h at 4 ^{o}C. Afterward, the substrates were rinsed in DI water at room temperature and allowed to air-dry.

To assess biocompatibility, astrocytes were cultured on the collagen-coated side of the chip. After a few days of growth, the cells were subjected to physiological stress, by removing them from their nutrient solution and exposing them to air for 30 seconds. Photographs were taken of the cells before and after the stress, to asses their reaction. The same stressor was applied to a control group of astrocytes grown on silicon nitride substrates coated with a layer of absorbed 0.1% (1 mg /cm^2) gelatin (which is a partially hydrolyzed form of collagen), rather than spin-cast collagen thin films. Before and after images of these cell cultures were compared as well.

In the second experiment, illustrated in figure 2.9, astrocytes and brain capillary endothelial cells were co-cultured on the opposite sides of the substrate. After depositing the two layers of collagen in the wells, an additional two layers of collagen were spin deposited on the other side of the substrate. The chip was then rinsed, crosslinked, and air dried as in the previous procedure. Astrocytes were cultured inside the wells, and endothelial cells on the opposite side of the membrane, for up to 12 days. Cell viability was evaluated by both optical microscopy and transendothelial electrical resistance (TER).

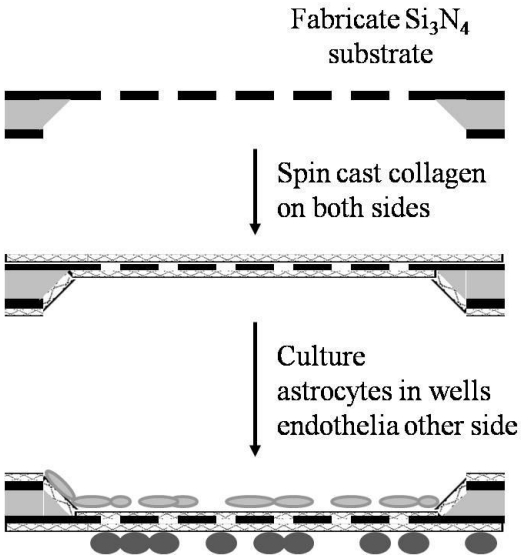

Figure 2.9 Fabrication of substrates for astrocyte and endothelial cell co-cultures

2.5.2 Generating 'thin skin' collagen films

The process for generating a free-standing thin film of monomeric collagen is illustrated in figure 2.10. First, any ethanol-soluble photoresist may be spin-deposited

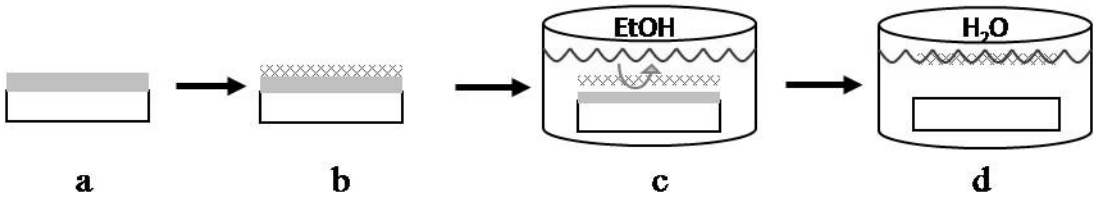

Figure 2.10. Schematic of the collagen thin film generation process. a) photoresist spin cast on silicon wafer b) collagen solution spin cast on photoresist c) ethanol diffuses through pores in collagen film and dissolves photoresist d) wafer is transferred to water bath to float collagen film

upon a silicon substrate using standard cleanroom procedures. In this case, HPR 504 was spun at 4000 rpm for 30 seconds. Then, a single layer of collagen was spin cast directly onto the photoresist at 2000 rpm for 1 minute. At the conclusion of the spinning, the sample was dry. The collagen was not rinsed, crosslinked, or subjected to any other treatments prior to immersion in a beaker of 100% ethanol for 10-20

minutes. The ethanol diffused through the collagen film and dissolved the resist underneath.

Fortunately, the collagen film was slightly less dense than resist-saturated ethanol, and floated on this layer to remain free of direct contact with the substrate. However, collagen is slightly denser than pure ethanol, and thus did not readily float to the surface. To free the collagen, the entire substrate-saturated solvent-collagen film system was slowly lifted from the ethanol beaker without tilting, and transferred to a beaker of water. Collagen is less dense than water, and floated to the surface upon contact. The resist-saturated ethanol rapidly dissolved in the water and was dispersed, leaving the collagen film entirely free.

2.5.3 Lithographic Patterning of Collagen Via Direct Liftoff

The technique described in section 2.5.2 generated a collagen film free of the substrate surface by taking advantage of the film porosity. Alternatively, this porosity can be exploited to leave behind patterned collagen films on a wafer surface. A liftoff technique was developed as diagrammed in figure 2.11. As in the "thin skin" liftoff

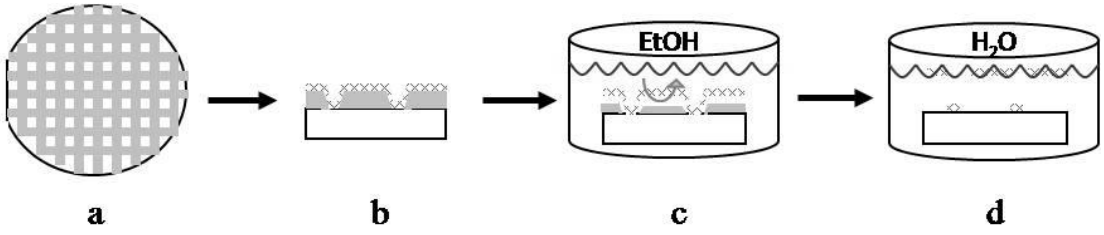

Figure 2.11 Schematic of the collagen liftoff patterning process. a) photoresist spin cast on silicon wafer b) spin cast collagen conformally coats photoresist c) ethanol diffuses through pores in collagen film and dissolves photoresist d) wafer is transferred to water bath to float collagen formerly supported by photoresist; collagen directly in contact with silicon substrate remains. Adapted from [129].

technique, a layer of photoresist was spin deposited on a silicon wafer as described above. This time, the resist was lithographically patterned with a mask containing arrays of square features ranging in size from 1 mm to 2 μm. Following a 10 second

UV exposure through the mask on a contact aligner (Hybrid Technology Group), the pattern was developed via immersion in MIF 300 for 30 seconds. Atop the patterned photoresist, a single layer of collagen was then spin deposited at 2000 rpm for 1 minute. The collagen film was not rinsed or crosslinked, but was briefly allowed to air-dry prior to the liftoff.

As in the 'thin skin' procedure, the wafer was then immersed in absolute ethanol for 10-20 minutes, allowing the solvent to diffuse through the pores in the collagen film and slowly dissolve the underlying resist. Collagen in direct contact with the silicon adhered strongly to the surface, while collagen initially deposited upon photoresist was only loosely held via entanglement with neighboring monomers in the film. As the system was transferred from ethanol to water, gentle agitation helped to tear the nearly-free collagen from the surface-adhered collagen, leaving behind a patterned collagen film on the silicon substrate.

2.6 Results and Discussion

2.6.1 Cells on Collagen Thin Films

One commonly used indication of culture cell viability is the extent of focal adhesions. Healthy culture cells tend to flatten out, and spread over as large an area of their substrate as possible. They adhere strongly to the substrate, often requiring a combination of partial digestion with trypsin and mechanical scraping to forcibly dislodge them from the surface. In contrast, culture cells grown on an inappropriate substrate quickly become unhealthy, 'balling up' into a nearly spherical shape, and making only minimal contact with their substrate surface. Such cells often spontaneously detach into their growth medium. Astrocyte (brain) cells have been observed to have improved focal adhesions when grown on collagen-coated substrates.[127] Partially hydrolyzed collagen, known as gelatin, is commonly used as

a substrate coating for this purpose. Thus, similar or better focal adhesion of astrocytes grown on spin-cast collagen, compared to those grown on gelatin, would be a good indication of biocompatibility.

Cells grown on a biocompatible substrate are more resilient when exposed to a physiological stressor than cells suffering from substrate incompatibility. The extent of this resilience is manifest in the degree of change in the focal adhesion behavior, before and after stress. Prior to the stress of exposure to air, the astrocytes cultured on both spin-cast collagen films (figure 2.12a) and on adsorbed gelatin (figure 2.12c) appeared healthy, with ample focal adhesions. After stress, the cells grown on the thin collagen films remained nearly as spread out as before (figure 2.12b), indicating good resistance. Many of the gelatin-grown cells, by contrast, are either detached entirely

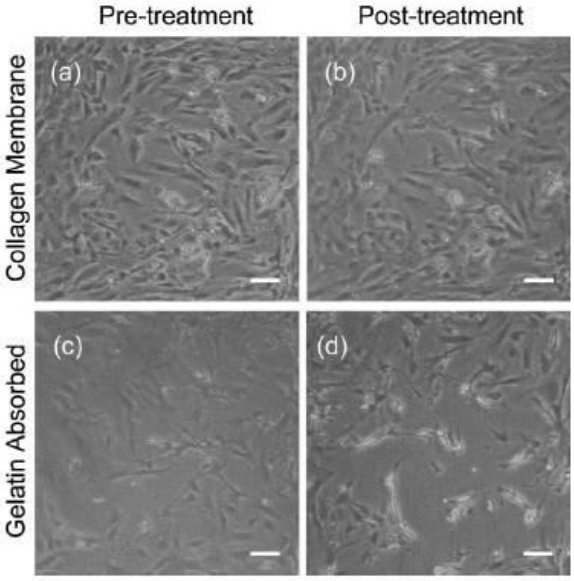

Figure 2.12 Astrocyte cell cultures grown on either a) collagen thin films or c).1% gelatin on unpatterned silicon nitride. Following physiological stress, b) the cells grown on collagen thin films are healthier than d) the cells grown on bulk gelatin. Each scale bar is 100 microns. Reprinted from reference [132].

or rolled up into balls (figure 2.12d), indicating poor health. Thus, the astrocytes cultured on spin-cast collagen films actually fared somewhat better than those grown on standard gelatin substrates.

The astrocyte/endothelial cell coculture experiment was designed not merely as a simple test of biocompatibility, but to evaluate the system as a potential laboratory model for the blood-brain barrier. The details are beyond the scope of the present work; but a few specific points germane to general biocompatibility are presented here. First, endothelial cells grown on the spin-cast collagen films had comparable focal adhesions and fluorescent labeling behavior to cells grown on standard gelatin coated substrates. The ability of these films to support the normal growth of a second cell type raises hopes that collagen thin films may be broadly applicable for promoting the growth of many other cell lines. Second, the coculture experiment on spin-cast collagen lasted two full weeks. Both cell types survived, with their focal adhesions intact, to provide useful data for the entire duration. It is unknown how long the culture could ultimately be sustained if desired. However, it is an encouraging preliminary result for any long-term application, such as an implanted device which must survive for the lifetime of a patient.

Finally, on a few samples, the collagen was inadvertently spun onto only part of the surface intended to support endothelial cell growth. The collagen was visible as a dull white film, in stark contrast to the mirror-reflective bare silicon nitride. Endothelial cell growth was observed only on the collagen-coated regions of the substrates. This suggests that, if a particular application requires that cell growth be restricted to one region of a device, an effective strategy would be to confine the collagen film to the appropriate area, perhaps via lithographic patterning.

2.6.2 Patterned Collagen Films

As proof of principle of the lithographic patternability of collagen thin films, a 2 inch wafer was patterned with an array of squares in a one layer, non-crosslinked collagen film, as can be seen in figure 2.13. The air-dried collagen film appears black.

Although it did not photograph well, the collagen was visibly more hydrophilic than the surrounding silicon. Following a gentle rinse, water drops adhered strongly to the array of collagen squares, but not at all to the uncoated parts of the wafer.

Once the principle was established, it became desirable to quantify what range of feature sizes is easily accessible by this technique. To do this, wafers were

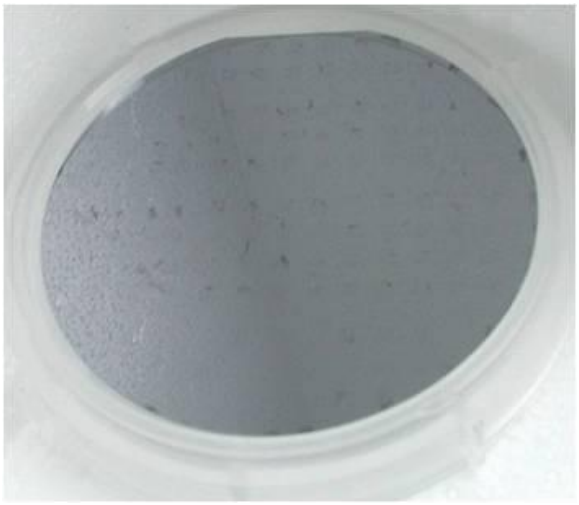

Figure 2.13 Collagen film patterned by direct liftoff against the grey silicon substrate.

patterned with arrays of squares of various sizes, ranging from 1 mm down to 2 μm. Examples of collagen features over the entire size range can be seen in the optical microscope images in figure 2.14. With the direct liftoff, features 100 μm and larger

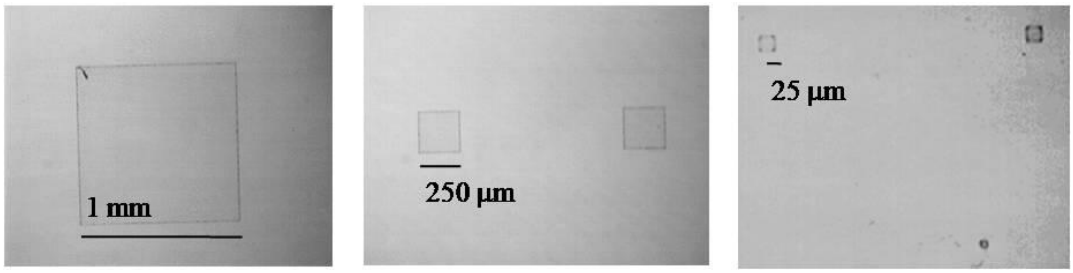

Figure 2.14 Square collagen features produced by liftoff. From reference [135].

were generated in 100% yield. The yield was slightly lower between 25-100 μm. Among the smallest squares observed – measuring 10 μm laterally – less than 5% of the features survived. All squares were well formed, free of both tearing within the

square, and incompletely torn edges folded back over onto the square. In other words, squares either adhered perfectly, or not at all. One possible reason that the largest features adhered the most readily may be that they had many more hydrogen bonds to the surface, simply because they had the largest collagen surface area in contact with the substrate. Acting against this adhesive force, the agitation and subsequent tearing of the collagen acted only at the perimeter of the features. Larger features, with their larger surface-to-perimeter ratio, were therefore more stable. If this explanation is correct, then in principle, increasing the adhesive force by using a more hydrophilic substrate than the native silicon oxide should improve the force balance, and allow smaller features to be formed.

It is possible that hydrogen bonding alone is not the only mechanism of collagen adhesion to the surface. Alcohols are known to form covalent alkoxy-silane bonds on the surface of a silicon substrate; indeed, the site-specific binding rates of IPA to silicon have been quantified.[136] As can be seen in figure 2.15, there are

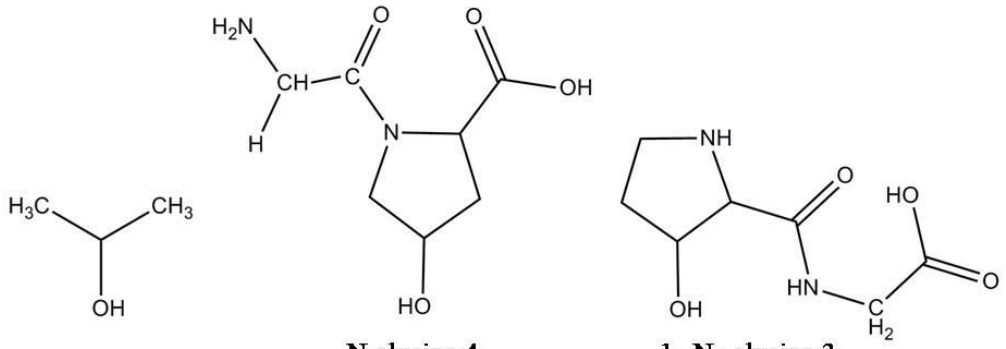

Figure 2.15 Comparison of structures of isopropanol, N-gly-4-hyp, and 1-N-gly-3-hyp great structural similarities between IPA and both 3- and 4- hydroxyproline. Thus, both 3-hyp and 4-hyp could potentially form covalent bonds to silicon. Given the large number of hyp residues per collagen monomer, the first monolayer of monomers may in fact chelate the surface. The hydroxyl group of 4-hyp is less sterically

hindered from the surface than 3-hyp, and might therefore be expected to bond to the surface more readily. Therefore, if covalent chelation is an important contributor to collagen adhesion, then deriving collagen from species and tissue types with a higher 4-hyp/3-hyp ratio should result in stronger bonding, and make the generation of smaller patterned features possible.

Regardless of the mechanism of collagen adhesion, this liftoff patterning process is extremely well suited to create arrays of 100 μm or larger-sized collagen squares separated by bare silicon control regions. As a consequence, this technique may find immediate application for controlling the spatial positioning of collagen-sensitive tissue cultures, such as the endothelial cells discussed in section 2.6.1. Once the technique is refined to reliably produce collagen features on the order of typical cellular sizes (~ 1-10 μm), the effects of the collagen scaffold shape upon the growth patterns of individual collagen-sensitive cells could be investigated. It is well known among tissue engineers that the substrate topography, independent of surface chemistry, can greatly affect cell growth.[126,137-146]

In addition to their potential uses in applied tissue engineering, the patterned films proved useful for more fundamental studies as well. All the surviving collagen features generated by the liftoff technique were of high quality, with extremely sharp edges over their entire perimeter. These extraordinarily sharp edges permitted the use of surface profilometry (figure 2.16) to directly measure thickness of the monomeric collagen film. An air-dried, single spin deposited layer of collagen, not crosslinked, produced films between 30-50 nm thick. Hydrated films could not withstand the high contact force of the profilometer stylus. However, AFM in fluid of rehydrated films later confirmed that wet films had a similar thickness (data not shown). Any shrinkage of the film in the z direction upon dehydration, or swelling upon rehydration, was thus not large enough to observe directly on patterned films.

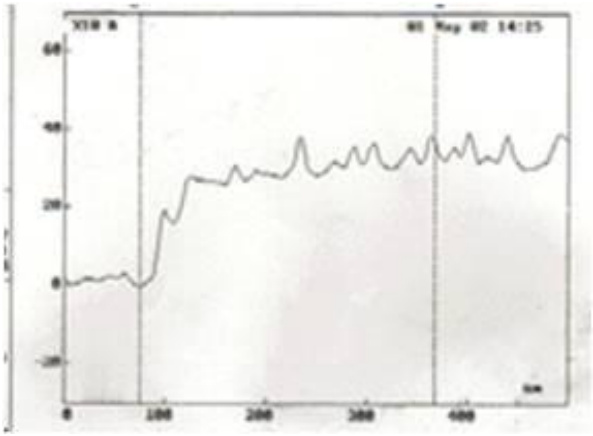

Figure 2.16 Profilometer trace at the edge of a patterned 1 layer collagen film

Literature reports of the magnitude of vertical collagen film shrinkage upon dehydration (and swelling upon hydration) vary widely depending upon the thickness of the film, the extent of crosslinking, and environmental conditions, from as little as 7% [39] to more than two orders of magnitude.[101] The present case appears to be much closer to the lower limit. A variation of 10% -- which in this case would be about 5 nm -- may lie within the measurement error of the profilometer, so vertical shrinkage cannot be definitively ruled out.

There is somewhat stronger evidence that, in general, collagen films shrink in the xy direction during the drying process. The tearing of collagen films upon drying has been observed on many substrates,[86,97,107] and has even been used intentionally for the generation of pores. As shall be seen in chapter 3, collagen films which were air-dried rather than critical point dried frequently tore, a result readily explained by lateral shrinkage upon drying. To quantify the forces which are exerted in the xy plane upon the drying film, one might deposit collagen on a substrate consisting of flexible pillars of a known Young's modulus. As the collagen film shrinks, individual fibrils will exert force upon the pillars, causing them to deflect. From this deflection, the initial applied force can be calculated. Similar experiments

have been successfully performed to quantify the forces involved in cell focal contact adhesion on PDMS.[147]

2.6.3 The Ultimate 'Thin Skin'

In the previous section, a liftoff was used to isolate patterned collagen films on the substrate surface, while the lifted away portions of the collagen film were discarded. The goal of this technique can be easily inverted – to isolate a lifted off, free standing collagen film instead. In this manner, an unpatterned collagen 'thin skin' was successfully lifted off from unpatterned photoresist on a silicon wafer. Made from a single layer of collagen, and not crosslinked, the film covered a surface area comparable to that of the original 2"- diameter substrate. No attempts were made to create larger films, although in principle there should be no difficulty in extending the technique to larger surface areas. The lateral dimensions of the film are limited only by the size of the substrate – with areas on the order of many square centimeters. Lifted off films remained largely intact, with minimal tearing or buckling, as can be seen in color photographs of the collagen film inside the wire ring in figure 2.17.

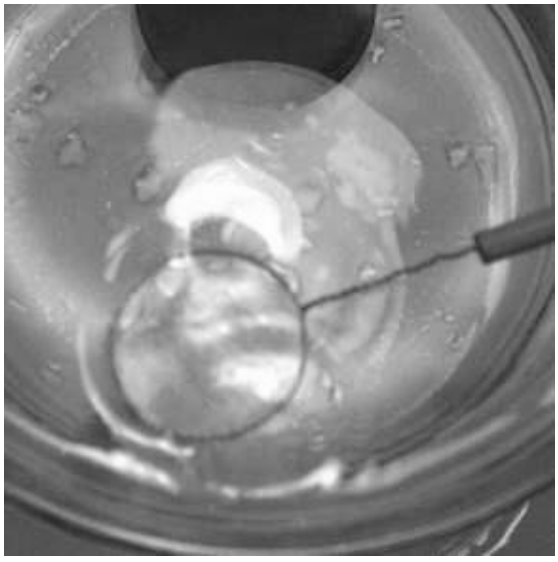

Figure 2.17 One layer collagen film lifted off 2" wafer.

Although very difficult to see in black and white, collagen films were visible either by a pale pink hue, likely due to the presence of residual photoresist, or by a large difference in their refractive index relative to water.

The 'thin skin', being only about 50 nm thick, is too fragile even to be removed from the surface of the water in free-standing form without folding or tearing. For any realistic application, this film must be supported on a solid surface. This could be done by using the wire ring in figure 2.17 as a 'fish hook' to capture the 'thin skin' for further study. In fact, by sliding a substrate beneath the collagen film and lifting it vertically out of the water, the film could potentially be overlaid upon any desired backing. This method of collagen deposition could mitigate some potential difficulties associated with spin casting on a substrate, such as collagen seepage into micron-sized holes, and poor film adhesion to the surface. On surfaces with good collagen adhesion, such as the silicon nitride substrates used for cell culturing, this was deemed unnecessary.

'Fish hook' deposition initially appeared to offer the greatest chance of success for applications requiring a highly porous substrate. Substrates for TEM require a grid of closely spaced holes tens of microns wide, to allow penetration of the electron beam for detailed three-dimensional imaging of the internal structure of a thin film. On a substrate with so little material surface area, an intact collagen film is unlikely to form by spin casting. Unfortunately, even using 'fish hook' deposition, the collagen film did not adhere well to the standard gold-coated TEM grid; it flaked off like paint chips as it dried. It is likely that pretreating the gold grid with an alkanethiol SAM to have a more hydrophilic termination could improve collagen adhesion. However, one potential difficulty remains. Substrate surface termination has been observed to affect the fibrillar structure of a collagen film during formation.[148] Although this is unlikely to affect a dry collagen film, exposure to aqueous solution may allow the non-

crosslinked monomers to redissolve and become mobile. If the monomers are able to dissolve and redeposit, this could permit structural rearrangements within the film. Ultimately, the investigations of 'fish hook' deposition were abandoned when the silicon nitride substrates, used for the cell culturing experiments in section 2.6.1, proved suitable for the TEM studies as well. These results shall be presented in chapter 3.

Although liftoff and 'fish hook' deposition was initially developed for basic research into the internal collagen film structure, these techniques could prove quite useful in applied research as well. One example can be seen by revisiting the coculture of astrocytes and endothelial cells discussed in section 2.6.1. Although the prior discussion emphasized the results related to biocompatibility, the primary goal of the experiment was to attempt to model the blood-brain barrier by observing the physical contact (if any) between cells on opposite sides of the film. Such physical contact would require one or both cell types to extend processes through the film, in the general direction of the substrate. On a non-transparent substrate, this would be quite difficult to observe. As an alternative, the cells could be cultured on a freestanding 'thin skin' collagen film, which is not only transparent, but thin enough to allow even TEM to assess cell penetration into and through the collagen layer. The detailed knowledge of the growth interactions between the cells and the lithographically processed collagen film obtained in this manner could find broad applications in tissue engineering.[11,137,139,140]

For any biological applications, two potential drawbacks of the 'thin skin' liftoff procedure must be noted. First, although many photoresists are considered to be biocompatible,[149,150] in the sense of being processable under solvent-free, low temperature conditions, the effects upon culture cell growth of residual photoresist bound to the collagen may still be difficult to predict a priori. Second, the use of

absolute ethanol to dissolve the photoresist risks denaturing the collagen monomers. Although this would not necessarily impair the effectiveness of the film as a culture substrate, it is likely to affect the film structure,[151] making its effect upon cell growth more difficult to predict. At a minimum, ethanol would be expected to strongly dehydrate the film, potentially increasing the extent of tearing. Both of these potential problems could be neatly sidestepped by developing an alternative, aqueous-based chemistry for the sacrificial layer.

Although water solubility is desired, care must be taken that the sacrificial material does not dissolve in the aqueous collagen buffer itself during the deposition. The most general answer would be to pre-saturate the collagen solution with the sacrificial material to prevent further net dissolution. However, adding this material to the collagen solution itself may risk either denaturing the monomers themselves, or incorporating the sacrificial material into a composite collagen film. Another possible solution is to find a material which is insoluble at the pH of the collagen buffer (~pH 3), but soluble at a neutral or slightly basic pH where collagen is insoluble. An organic acid would be the most likely candidate. Unfortunately, preliminary experiments involving the water-soluble benzoic acid failed.

Benzoic acid proved problematic because it deposited in a polycrystalline film of centimeters-long, millimeter-wide needles, with the grain boundaries rough enough to create breaks in the collagen film. An amorphous sacrificial material would produce the smoothest possible surface, but water soluble solids are usually crystalline. More realistically, atomic scale smoothness could be approximated by a polycrystalline material with grain sizes in all dimensions smaller than a typical nanofibril. Conversely, a smooth surface could also arise from a single crystal of sacrificial material large enough to contain the entire collagen film on a single facet. Each of these scenarios is unlikely, but not altogether impossible.

Together, the solubility and roughness barriers do make the development of an aqueous sacrificial chemistry unlikely. However, if one were found, the gains in biocompatibility and mildness of chemical processing conditions could be great. Several biocompatible materials, such as monosaccharides and salts, suggest themselves as possible candidates for sacrificial layers. The best results to date were achieved using saturated solutions of fructose, but even these resulted in cohesive liftoff areas of no more than 2 mm^2. It is uncertain whether the formation of rough crystal grains, or dissolution of the fructose in the collagen solution, or both, were primarily to blame.

As the adhesion and sacrificial layer problems illustrate, many potential avenues remain for optimizing the lithographic patterning of collagen films. However, the principle of patternability has now been established. Attention may now be turned to the primary goal of the overall project: integrating and developing the collagen thin films for filtration applications.

2.7 Conclusions

Two of the major criteria for ideal collagen thin films were assessed in this chapter: biocompatibility and lithographic patternability. Both astrocyte and brain endothelial cells were successfully cultured on two layer, glutaraldehyde-crosslinked collagen films spin deposited on silicon nitride. Although the film preparation conditions could most likely be further optimized for the growth of these cells, or tailored for additional cell types, this experiment provided proof of principle for biocompatibility.

Second, a novel method of lithographically patterning collagen thin films was developed. In direct liftoff, an alcohol solvent penetrates the pores in the collagen film to access and dissolve an underlying sacrificial layer. This technique provides a

straightforward and relatively chemically benign method of patterning collagen features larger than approximately 50 μm. The further optimization of parameters such as the choice of sacrificial layer and spin casting conditions for the collagen film is yet to be done, but the principle has been established as sound. Finally, the liftoff of an intact collagen film, several square centimeters in area but only tens of nanometers thick, was accomplished. This raises the experimental possibility that a collagen film could be generated on a sacrificial layer, lifted off intact, and redeposited on any arbitrary substrate. Taken together, these findings demonstrate the promise of collagen thin films, acting as an interface between biomaterials and engineered semiconductor devices in bioMEMS applications.

REFERENCES:

[1] Dean, R.N., and Luque, A.. IEEE Trans. Indust. Elec., **56 (4)**, 913-925, 2009

[2] Lee, L.J.. J. Chin. Inst. Chem. Eng., **34 (1)**, 25-46, 2003

[3] Geng, L.N., Jiang, P., Xu, J.D., Che, B.Q., Qu, F., and Deng, Y.L.. Prog. Chem., **21 (9)**, 1905-1921, 2009

[4] Fu, J.P., Mao, P., and Han, J.. Trends In Biotech., **26 (6)**, 311-320, 2008

[5] Zhang, C.S., Xu, J.L., Ma, W.L., and Zheng, W.L.. Biotech. Adv., **24 (3)**, 243-284, 2006

[6] Zougagh, M., and Rios, A.. Analyst, **134 (7)**, 1274-1290, 2009

[7] James, T., Mannoor, M.S., and Ivanov, D.V.. Sensors, **8 (9)**, 6077-6107, 2008

[8] Adiga, S.P., Curtiss, L.A., Elam, J.W., Pellin, M.J., Shih, C.C., Shih, C.M., Lin, S.J., Su, Y.Y., Gittard, S.A., Zhang, J., and Narayan, R.J.. JOM, **60 (3)**, 26-32, 2008

[9] Ainslie, K.M., and Desai, T.A. Lab On A Chip, 8 **(**11), 1864-1878, 2008

[10] Leoni L, Boiarski A, and Desai TA.. Biomed. Microdev., **4 (2)**, 131-139, 2002

[11] Ni M, Tong WH, Choudhury D, , Rahim NAA, Iliescu C , and Yu H.. Intl. J. Molec. Sci., **10 (12)**, 5411-5441, 2009

[12] Chen, J.-P., Chang, G.-Y., and Chen, J.-K.. Coll. Surf. A, **313-314**, 183-188, 2008

[13] Desai, T.A., Hansford, D.J., Leoni, L., Essenpreis, M., and Ferrari, M.. Biosensors & Bioelec., **15 (9-10)**, 453-462, 2000

[14] Leoni L, and Desai TA Source: IEEE Trans. Biomed. Eng., **48 (11)**, 1335-1341, 2001

[15] Morra, M., Cassinelli, C., Cascardo, G., Cahalan, P., Cahalan, L., Fini, M., and Giardino, R.. Biomat., **24**, 4639–4654, 2003

[16] Muller, R., Abke, J., Schnell, E., Macionczyk, F., Gbureck, U., Mehrl, R., Ruszczak, Z., Kujat, R., Englert, C., Nerlich, M., and Angele, P.. Biomat., **26 (34)**, 6962-6972, 2005

[17] Rossler, S., Scharnweber, D., and Worch, H.. J. Mat. Sci. Lett., **18 (7)**, 577-579, 1999

[18] Norman, J.J., and Desai, T.A.. Tissue Eng., **11 (3-4)**, 378-386, 2005

[19] Sinani, V.A., Koktysh, D.S., Yun, B.G., Matts, R.L., Pappas, T.C., Motamedi, M., Thomas, S.N., and Kotov, N.A.. Nano Lett., **3**, 1177–1182, 2003

[20] Muller, R., Abke, J., Schnell, E., Scharnweber, D., Kujat, R., Englert, C., Taheri, D., Nerlich, M., and Angele, P.. Biomat., **27 (22)**, 4059-4068, 2006

[21] Ignatius, M.J., Sawhney, N., Gupta, A., Thibadeau, B.M., Monteiro, O.R., and Brown, I.G.. J. Biomed. Mat. Res., **40** (**2)**, 264-274, 1998

[22] Rozkiewicz, D.I., Kraan, Y., Werten, M.W.T., de Wolf, F.A., Subramaniam, V., Ravoo, B.J., and Reinhoudt, D.N.. Chem.-A Euro. J., **12 (24)**, 6290-6297, 2006

[23] Mrksich, M., Dike, L.E., Tien, J., Ingber, D.E., and Whitesides, G.M.. Exp. Cell Res., **235**, 305-313, 1997

[24] Mrksich, M., Chen, C.S., Xia, Y.N., Dike, L.E., Ingber, D.E., and Whitesides, G.M.. Proc. Nat. Acad. Sci.USA, **93 (20)**, 10775-10778, 1996

[25] Dewez, J.L., Lhoest, J.B., Detrait, E., Berger, V., Dupont-Gillain, C.C., Vincent, L.M., Schneider, Y.J., Bertrand, P., and Rouxhet, P.G.. Biomat., **19 (16)**, 1441-1445, 1998

[26] Dike, L.E., Chen, C.S., Mrksich, M., Tien, J., Whitesides, G.M., and Ingber, D.E.. In Vitro Cell. & Dev. Bio.-Animal, **35 (8)**, 441-448, 1999

[27] Ostuni, E., Yan, L., and Whitesides, G.M.. Coll. Surf. B-Biointerfaces, **15**, 3-30, 1999

[28] Kane, R.S., Takayama, S., Ostuni, E., Ingber, D.E., and Whitesides, G.M.. Biomat., **20**, 2363-2376, 1999.

[29] Alaerts, J.A., De Cupere, V.M., Moser, S., de Aguilar, P.V.B., and Rouxhet, P.G.. Biomat., **22 (12)**, 1635-1642, 2001

[30] Dupont-Gillain, C.C., Alaerts, J.A., Dewez, J.L., and Rouxhet, P.G.. Bio-Med. Mat. Eng. **14 (3)**, 281-291, 2004

[31] Barbani, N., Lazzeri, L., Cristallini, C., Cascone, M.G., Polacco, G., and Pizzirani, G.. J. Appl. Polym. Sci., **72**, 971-976, 1999

[32] Seggiani, M., Lazzeri, L., Cascone, M.G., Barbani, N., Vitolo, S., and Palla, M.. J. Mat. Sci.-Mat.Med., **5 (12)**, 868-871, 1994

[33] Hanagata, N., Takemura, T., Monkawa, A., Ikoma, T., and Tanaka, J.. J. Biomed. Mat. Res. Part A, **83A (2)**, 362-371, 2007

[34] Coombes, A.G., Verderio, E., Shaw, B., Li, X., Griffin, M., and Downes, S.. Biomat., **23**, 2113–2118, 2002

[35] Itoh, S., Kikuchi, M., Takakuda, K., Koyama, Y., Matsumoto, H.N., Ichinose, S., Tanaka, J., Kawauchi, T., and Shinomiya, K.. J. Biomed. Mat. Res., 54 **(**3), 445-453, 2001

[36] Kikuchi, M., Itoh, S., Ichinose, S., Shinomiya, K., and Tanaka, J.. Biomat., 22 **(**13), 1705-1711, 2001

[37] Kikuchi, M., Ikoma, T., Itoh, S., Matsumoto, H.N., Koyama, Y., Takakuda, K., Shinomiya, K., and Tanaka, J.. Comp. Sci. Tech., 64 **(**6), 819-825, 2004

[38] Thomas, V., Dean, D.R., Jose, M.V., Mathew, B., Chowdhury, S., and Vohra, Y.K.. Biomacromol., **8 (2)**, 631-637, 2007

[39] Sistiabudi, R., and Ivanisevic, A.. J. Phys. Chem. C, **111 (31)**, 11676-11681, 2007

[40] Rossler, S., Scharnweber, D., Wolf, C., and Worch, H.. J.Adhesion Sci. Tech., **14** (**3)**, 453-465, 2000

[41] Fassett, J.T., Tobolt, D., Nelsen, C.J., Albrecht, J.H, and Hansen, L.K.. J. Biol. Chem., **278 (34)**, 31691–31700, 2003

[42] Hanagata, N., Takemura, T., Monkawa, A., Ikoma, T., and Tanaka, J.. Biochem. Biophys. Res. Comm., 344 **(**4), 1234-1240, 2006

[43] Koyama, H., Raines, E.W., Bornfeldt, K.E., Roberts, J.M., and Ross, R.. Cell, **87 (6)**, 1069–1078, 1996

[44] Henriet, P., Zhong, Z.D., Brooks, P.C., Weinberg, K.I., and DeClerck, Y.A.. Proc. Natl. Acad. Sci. USA, **97 (18)**, 10026–10031, 2000

[45] Nimni, M.. *Collagen*, CRC Press, Boca Raton, CA, 1988

[46] Kadler, K. Protein Profile, **1 (5)**, 519-638, 1994

[47] Kadler, K. Protein Profile, **2 (5)**, 491-619, 1995

[48] Okuyama, K.. Conn. Tiss. Res., **49 (5)**, 299-310, 2008

[49] Gelse, K., Poschl, E., and Aigner, T.. Adv. Drug Delivery Rev., **55** (**12)**, 1531-1546, 2003

[50] Komsa-Penkova, R., Koynova, R., Kostov, G., and Tenchov, B.G.. Biochim. Biophys. Acta-Protein Struct. Molec. Enz., **1297 (2)**, 171-181, 1996

[51] Petruska, J.A.,and Hodge, A.J.,. Proc. Natl Acad. Sci. USA **51**, 871-876, 1964

[52] Bozec, L., and Horton, M.. Biophys. J., **88** (**6)**, 4223-4231, 2005

[53] Lee, C.H., Singla, A., and Lee, Y.. Int. J. Pharm., **221**, 1–22, 2001

[54] Rosenbloom, J., Bhatnagar, R.S., and Prockop, D.J.. Biochim. Biophys. Acta, **149 (1)**, 259-&, 1967

[55] Kivirikko, K.I., and Prockop, D.J.. Biochem. J., **102 (2)**, 432-+, 1967

[56] Veis, A and George, A., 'Fundamentals of interstitial collagen self-assembly'. In: Yurchenco, P.D., Birk, D.E. and Mecham, R.P., Eds,. *Extracellular Matrix Assembly*, Academic Press, New York, 15-46, 1994

[57] Cheung, D.T., Nimni, M.E.. Conn. Tiss. Res., **10 (2)**, 187-199, 1982

[58] Damink, L.H.H.O., Dijkstra, P.J, Vanluyn, M.J.A., Vanwachem, P.B., Nieuwenhuis, P., and Feijen, J.. J. Mat. Sci.-Mat. Med., 6 **(**8), 460-472, 1995

[59] Fuguet, E., van Platerink, C., and Janssen, H.-G.. Anal. Chim. Acta, **604**, 45–53, 2007

[60] Freudenberg, U., Behrens, S.H., Welzel, P.B., Muller, M., Grimmer, M., Salchert, K., Taeger, T., Schmidt, K., Pompe, W., and Werner C.. Biophys. J., **92**, 2108–2119, 2007

[61] Trelstad, R., Hayashi, K., and Gross, J.,. Proc. Natl. Acad. Sci. USA, **73**, 4027–4031, 1976

[62] Kadler, K.E., Holmes, D.F., Trotter, J.A., and Chapman, J.A.. Biochem. J., **316**, 1–11, 1996

[63] Goh, M.C., Paige, M.F., Gale, M.A., Yadegari, I., Edirisinghe, M., and Strzelczyk, J.. Physica A **239,** 95-102, 1997

[64] Strasser, S., Zink, A., Heckl, W.M., and Thalhammer, S.. J. Biomech. Eng.-Trans. ASME, **128** (**5)**, 792-796, 2006

[65] Koster, S., Leach, J.B. Struth, B., Pfohl, T., and Wong, J.Y.. Langmuir, **23**, 357–359, 2007

[66] Li YP, Asadi A, Monroe MR, and Douglas EP.. Mat. Sci. Eng. C-Biomimetic And Supramolecular Systems, **29 (5)**, 1643-1649, 2009

[67] Guo, C. and Kaufman, L. J.. Biomat., **28**, 1105–1114, 2007

[68] Cheng, X.G., Gurkan, U.A., Dehen, C.J., Tate, M.P., Hillhouse, H.W., Simpson, G.J., and Akkus, O.. Biomat., **29 (22)**, 3278-3288, 2008

[69] Chen RN, Ho HO, Sheu MT., Biomat., **26** (**20),** 4229-4235, 2005

[70] Holmes, D.F., Watson, R.B., Chapman, J.A., Kadler, K.E.. J.Molec. Bio., **261 (2)**, 93-97, 1996

[71] Ciardelli, G., Gentile, P., Chiono, V., Mattioli-Belmonte, M., Vozzi, G., Barbani, N., and Giusti, P.. J. Biomed. Mat. Res. Part A, **92A (1)**, 137-151, 2010

[72] Watanabe, K., Nakagawa, J., Ebihara, T., and Okamoto, Y.. Polymer, **38,** 5155–5159, 1975

[73] Watanabe, K., Nakagawa, J., Ebihara, T., and Okamoto, Y.. Polymer, **37**, 1285–1288, 1996

[74] Wollensak, G., and Spoerl, E.. J. Cataract And Refractive Surgery, **30 (3)**, 689-695, 2004

[75] Angele, P., Abke, J., Kujat, R., Faltermeier, H., Schumann, D., Nerlich, M., Kinner, B., Englert, C., Ruszczak, Z., Mehrl, R., and Mueller, R.. Biomat., **25 (14),** 2831-2841, 2004

[76] Rault, I., Frei, V., Herbage, D., AbdulMalak, N., and Huc, A.. J. Mat. Sci.-Mat. Med., **7 (4)**, 215-221, 1996

[77] Saito, H., Murabayashi, S., Mitamura, Y., Taguchi, T.. J. Mat. Sci. –Mat. Med., **19** (**3),** 1297-1305, 2008

[78] Charulatha V, and Rajaram A. Biomat. **24** (**5)**, 759-767, 2003

[79] Spoerl, E., Wollensak, G., Reber, F., and Pillunat, L.. Ophthalmic Res., **36** (**2),** 71-77, 2004

[80] Douglas, T., and Haugen, H.J.. J. Mat. Sci. – Mat. Med., **19 (7)**, 2713-2719, 2008

[81] Lastowka, A., Maffia, G.J., and Brown, E.M.. J. Amer. Leather Chem. Assn., **100** (**5)**, 196-202, 2005

[82] Wollensak, G., Spoerl, E., and Seiler, T.. Am. J. Ophth., **135 (5)**, 620-627, 2003

[83] Chan, B.P., and So, K.F.. J. Biomed. Mat. Res. Part A **75A** (**3)**, 689-701, 2005

[84] Chan, B.P., Hui, T.Y., Chan, O.C.M., So, K.F., Lu, W., Cheung, K.M.C., Salomatina, E., and Yaroslavsky, A.. Tiss. Eng., **13** (**1)**, 73-85, 2007

[85] Chan, O.C.M., So, K.F., and Chan, B.P.. J. Controlled Release, **129 (2),** 135-143, 2008

[86] Jacquemart, I., Pamula, E., De Cupere, V.M., Rouxhet, P,, Dupont-Gillain, C.C.. J. Coll. Interface Sci., **278** (**1)**, 63-70, 2004

[87] Denis, F. A., Pallandre, A., Nysten, B., Jonas, A.M., and Dupont-Gillain,. C.. Small, **1**, 984–991, 2005

[88] Gurdak, E., Rouxhet, P.G., and Dupont-Gillain, C.C.. Coll. Surf. B-Biointerfaces, **52** (**1)**, 76-88, 2006

[89] Silver, F.H. and Trelstad, R.L.. J. Bio. Chem., **255 (19)**, 9427-9433, 1980

[90] Paige, M.F., Rainey, J.K., and Goh, M.C.. Micron, **32**, 341–353, 2001

[91] Paige, M. F., and Goh, M. C.. Micron, **32,** 355-361, 2001

[92] Jiang, F.Z., Horber, H., Howard, J., and Muller, D.J.. J. Struc. Bio., **148 (3)**, 268-278, 2004

[93] Xu, S.H., Yamanaka, J., Miyata, I., and Yonese, M.. Coll. Polymer Sci., **285** (**8),** 899-906, 2007

[94] Prockop, D.J, and Hulmes, D.J.S.. 'Assembly of Collagen Fibrils de Novo from Soluble Percursors'. In: Yurchenco, P.D., Birk, D.E. and Mecham, R.P., Eds,. *Extracellular Matrix Assembly*, Academic Press, New York, 47-90, 1994

[95] Ottani, V., Martini, D., Franchi, M., Ruggeri, A., and Raspanti, M.. Micron, **33 (7-8)**, 587-596, 2002

[96] Christiansen, D.L., Huang, E.K., and Silver, F.H.. Matrix Bio., **19 (5),** 409-420, 2000

[97] Dupont-Gillain, C.C., Jacquemart, I.. Surf. Sci., **539** (**1-3),** 145-154, 2003

[98] Scharnweber, D., Born, R., Flade, K., Roessler, S., Stoelzel, M., and Worch, H.. **Biomat., 25 (12), 2371-2380, 2004**

[99] Sun, M., Stetco, A. and Merschrod S., E.F.. Langmuir**, 24**, 5418-5421, 2008

[100] Huelin, S.D., Baker, H.R., Poduska, K.M, and Merschrod S.,E.F.. Macromolecules, **40**, 8440-8444, 2007

[101] Baker, H.R., Merschrod, E.F., and Poduska, K.M.. Langmuir **24**, 2970-2972, 2008

[102] Jayasinghe S.N., and Edirisinghe, M.J.. J. Mat. Sci. Lett. **22** (**22)**, 1617-1619, 2003

[103] Zhang, J., Senger, B., Vautier, D., Picart, C., Schaaf, P., Voegel, J.-C., and Lavalle, P.. Biomat., **26,** 3353-3361, 2005

[104] Lawrence, C.J.. Phys. Fluids A, **31**, 2786-2795, 1988

[105] Mertig, M., Thiele, U., Bradt, J., Leibiger, G., Pompe, W., and Wendrock, H.. Surface Interface Anal., **25**, 514, 1997

[106] Thiele, U., Mertig, M., and Pompe, W.. Phys. Rev. Lett., **80 (13)**, 2869-2872, 1998

[107] Mertig M, Thiele U, Bradt J, Klemm D, Pompe W. App. Phys. A-Mat. Sci. & Processing, **66**, S565-S568, Part 1 Suppl. S, 1998

[108] Christman KL, Enriquez-Rios VD, Maynard HD, Soft Matter, **2 (11)**, 928-939, 2006

[109] Mendes, P.M., Yeung, C.L., and Preece, J.A.. Nanoscale Res. Let., **2 (8)**, 373-384, 2007

[110] Kumar, A., Biebuyck, H.A., and Whitesides, G.M.. Langmuir, **10 (5)**, 1498-1511, 1994

[111] Monroe, M.R., Li, Y.P., Ajinkya, S.B., Gower, L.B., and Douglas, E.R.. Mat. Sci. Eng. C- Mat. Bio. App., **29 (8)**, 2365-2369, 2009

[112] Piner, R.D., Zhu, J., Xu, F., Hong, S.H., and Mirkin, C.A.. Science, **283 (5402)**, 661-663, 1999

[113] Lee, K.B., Park, S.J., Mirkin, C.A., Smith, J.C., Mrksich, M.. Science, **295 (5560)**, 1702–1705, 2002.

[114] Wilson, D.L., Martin, R., Hong, S., Cronin-Golomb, M., Mirkin, C.A., and Kaplan, D.L.. Proc. Nat. Acad. Sci. USA, **98 (24)**, 13660-13664, 2001

[115] Zhang, M., Bullen, D., Chung, S.W., Hong, S., Ryu, K.S., Fan, Z.F., Mirkin, C.A., and Liu, C.. Nanotech., **13 (2)**, 212-217, 2002

[116] Bain, C.D., Troughton, E.B., Tao, Y.T., Evall, J., Whitesides, G.M., and Nuzzo, R.G.. J. Am. Chem. Soc., **111 (1)**, 321-335, 1989

[117] Bain, C.D., Evall, J., and Whitesides, G.M.. J. Am. Chem. Soc., **111 (18)**, 7155-7164, 1989

[118] Prime, K.L., and Whitesides, G.M.. Science, **252 (5010)**, 1164‑1167, 1991

[119] H.R.Bhangale, *Investigation of Filtration Properties of Collagen on Silicon Wafer* (Cornell University, 2001)

[120] Peng, Q.J., Guo, Y.K., Zhu, J.H., Zeng, Y.S., and Liu, S.J. J. Mod. Opt., **50 (11)**, 1725-1734, 2003

[121] Orth, R.N., Kameoka, J., Zipfel, W.R., Ilic, B., Webb, W.W., Clark, T.G. and Craighead, H.G.. Biophys. J., **85(5)**, 3066-3073, 2003

[122] Qin, D., Xia, Y.N., and Whitesides, G.M.. Nature Protocols, **5 (3)**, 491-502, 2010

[123] Hong, S. and Mirkin, C.A.. Science, **88**, 1808-1811, 2000

[124] Monkawa, A., Ikoma, T., Yunoki, S., Ohta, K., and Tanaka, J.. J. Nanosci. Nanotech., **7 (3)**, 833-838, 2007

[125] Dupont-Gillain, C.C., Jacquemart, I., Rouxhet, P.G.. Coll. Surf. B-Biointerfaces **43 (3-4)**, 179-186, 2005

[126] Bunyaratavej, P., and Wang, H.-L.. J. Periodontol., **72**, 215-229, 2001

[127] Gottfried, C., Cechin, S. R., Gonzalez, M. A., Vaccaro, T. S., and Rodnight, R.. Neuroscience, **121**, 553, 2003

[128] Ichii, T., Koyama, H., Tanaka, S., Kim, S., Shioi, A., Okuno, Y., Raines, E.W., Iwao, H., Otani, S., and Nishizawa, Y.. Circ. Res., **88 (5)**, 460–467, 2001

[129] Elliott, J.T., Halter, M., Plant, A.L., Woodward, J.T., Langenbach, K.J., and Tona, A.. Biointerphases, **3 (2)**, 19-28, 2008

[130] Elliott, J.T., Tona, A., Woodward, J., Jones, P., and Plant, A.. Langmuir, **19 (5)**, 1506–1514, 2003

[131] Elliott, J.T., Woodward, J., Langenbach, K.J., Tona, A., Jones, P.L., Plant, A.L.. Matrix Biol., **24 (7)**, 489–502, 2005

[132] Ma, S.H., Lepak, L.A., Hussain, R.J., Shain, W., and Shuler, M.L.. Lab on a Chip, **5** (**1**), 74-85, 2005

[133] Barbani, N., Giusti, P., Lazzeri, L., Polacco, G., and Pizzirani, G.. J. Biomat. Sci.-Polymer Ed. **7** (**6)**, 461-469, 1995

[134] Barbani, N., Cascone, M.G., Giusti, P., Lazzeri, L., Polacco, G., and Pizzirani, G.. J. Biomat. Sci.-Polymer Ed., **7** (**6),** 471-484, 1995

[135] Lepak, L.A., Richards, T., Guillen, N., Caggana, M., Turner, J.N. and Spencer, M.G.. Proc. Mater. Res. Soc., **752,** 321-326, 2002

[136] Newton, T.A., Huang, Y-C., Lepak, L.A., and Hines, M.A.. J. Chem. Phys., **111 (20)**, 9125-9128, 1999

[137] Norman, J.J., and Desai, T.A.. Tissue Eng., 11 **(**3-4), 378-386, 2005

[138] Stevenson PM, Donald AM.. Langmuir, 25 **(**1), 367-376, 2009

[139] Evans, H.J., Sweet, J.K., Price, R.L., Yost, M., and Goodwin, R.L.. Am. J. Physiol., **285**, H570–H578, 2003

[140] Lee, P., Lin, R., Moon, J., and Lee, L.P.. Biomed. Microdevices, **8**, 35–41, **2006**

[141] Craighead, H.G., James, C.D., and Turner, A.M.P.. Current Opinion In Solid State & Mat. Sci., **5 (2-3)**, 177-184, 2001

[142] Chen, G.P., Ushida, T., and Tateishi, T.. Macromolecular Biosci., **2 (2)**, 67-77, 2002

[143] Thomas, V., Dean, D.R., and Vohra, Y.K.. Current Nanosci., **2 (3)**, 155-177, 2006

[144] Ricci, J.L., Grew, J.C., and Alexander, H.. J. Biomed. Mat. Res. Part A, **85A (2)**, 313-325, 2008

[145] Grew, J.C., Ricci, J.L., and Alexander, H.. J. Biomed. Mat. Res. Part A, **85A (2)**, 326-335, 2008

[146] Hanson, J.N., Motala, M.J., Heien, M.L., Gillette, M., Sweedler, J., and Nuzzo, R.G. Lab On A Chip, **9 (1)**, 122-131, 2009

[147] Balaban, N.Q., Schwarz, U.S., Riveline, D., Goichberg, P., Tzur, G., Sabanay, I., Mahalu, D., Safran, S., Bershadsky, A., Addadi, L., and Geiger, B.. Nature Cell Bio., **3 (5)**, 466-472, 2001

[148] Elliott, J.T., Woodward, J.T., Umarjia,A., Meib,Y., and Tonac, A. Biomat. **28,** 576-585, 2007

[149] Ganesan, R., Yoo, S.Y., Choi, J.H., Lee, S.Y., and Kim, J.B.. J. Mat. Chem., **18 (6)**, 703-709, 2008

[150] Douvas, A., Argitis, P., Diakoumakos, C.D., Misiakos, K., Dimotikali, D., and Kakabakos, S.E.. J. Vac. Sci. Tech. B, **19 (6)**, 2820-2824, 2001

[151] Bratescu, M.A., Saito, N., and Takai, O.. Jap. J.Appl. Phys. Part 1-Regular Papers Brief Communications & Review Papers, **45 (10B)**, 8352-8357, 2006

Chapter 3: Collagen Thin Films Supported on Substrates

3.1 Collagen and Supporting Substrates

Ultimately, collagen films are of interest in the present work primarily because of the potential for their porous structure to permit the selective diffusion of molecules. However, collagen films, whether made of monomers or fibrils, have typical thicknesses on the order of 50-200 nm (see section 2.6.2). Thus, they are far too mechanically fragile to be used in filtration experiments without some form of supporting substrate. In the literature, collagen films have been studied on a wide variety of inorganic [1-10], polymeric [11-24], and even Langmuir-Blodgett (LB) film [6,25,26] substrates. For filtration applications, the most desirable substrate would possess the following properties:

1) It must be either commercially available, or able to be fabricated by standard semiconductor processing techniques. In any case, the processing demands must be reasonable in terms of time and cost.
2) It must be possible to interface the substrate with micro- (or even macro-) fluidic devices to perform actual diffusion or flow experiments.
3) Collagen must adhere to the surface strongly enough not to tear or peel off, especially when confronted with the mechanical stresses of drying and rehydration. However, it must not adhere so strongly that it strictly follows the contours of the surface and fails to span pores in the substrate.
4) It must possess a high permeability in its own right, so that the properties of the collagen film itself, rather than those of the substrate, control the behavior of the combined system, such as flux and molecular weight cutoff (MWCO).

Several candidate materials which met the first two criteria were identified: etched silicon nitride, polycarbonate, polyethylene terephthalate, and etched alumina. Each was tested for satisfaction of the third criterion, with the results presented in the remainder of this chapter. When appropriate, the behavior of the system was evaluated according to the fourth criterion; these results will be presented in chapter 4.

3.2 Fabrication of Suspended Silicon Nitride Film Substrates

Given that the integration of collagen films into silicon-based MEMS devices is a desirable goal,[27-29] the development of a silicon based substrate was preferred for initial tests. A means of modifying the solid, single-crystal silicon was required to create holes in the substrate through which a filtrate could pass. One such technique is depicted schematically in figure 3.1. In this procedure, developed by Kuiper et al,[30]

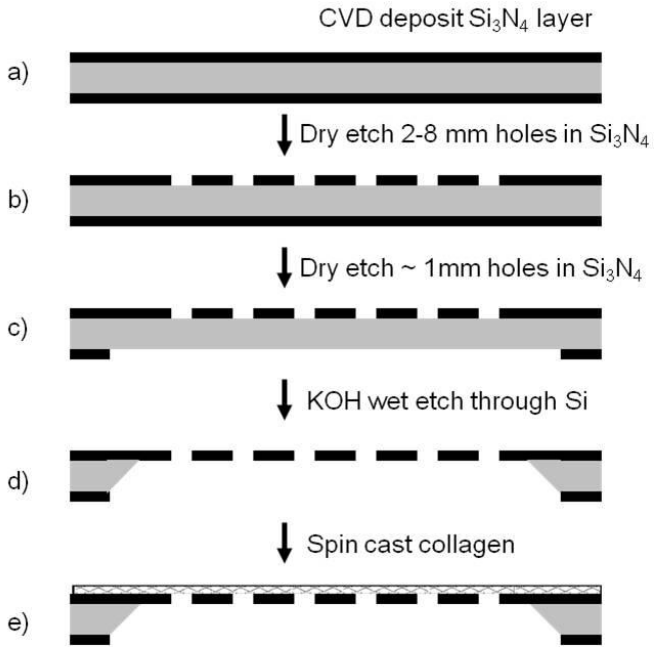

Figure 3.1 Schematic of fabrication procedure for nitride support substrates for collagen films.

an etched silicon nitride thin film is suspended over through-etched regions of a silicon wafer.

Standard thickness 3 or 4 inch diameter silicon wafers were used in all silicon nitride substrate experiments. First, an approximately 200 nm thick, low-stress non-stoichiometric film of silicon nitride was grown on the wafer by low-pressure chemical vapor deposition (800^{o}C, 16 sccm NH_3, 95 sccm SiH_4, 90 minutes). This thickness was suitable for the range of porosities in the present experiment. Arrays with much greater hole densities – up to 25% porosity – were attempted, but nitride films thicker than 1 μm were required to remain unbroken, with such a large fraction of the film volume removed. At this thickness, even the 'low stress' inherent in the deposition began to manifest itself, with large cracks visible even in the optical microscope on most samples. Due to the great expense of the long deposition times required to generate the thick film substrates, the high-porosity process was abandoned. Thin (200 μm) nitride films were used as substrates for all collagen-on-nitride characterizations discussed in the present work.

For the photolithography, wafers were primed with P-20 HDMS solution, which was spin deposited at 4000 rpm for 30 seconds. Immediately, Shipley 1818 photoresist was spin-deposited on the polished side at 4000 rpm, 30 seconds spinning. The wafer was baked on a 90^{o}C hot plate for 1 minute to remove volatile solvents. The wafer was exposed for 3 seconds on an EV620 contact aligner to broadband UV through a borosilicate glass/chrome photomask patterned with arrays of square holes. Following exposure, the wafers were developed in MIF 300 developer for 1 minute. To transfer the pattern to the nitride layer, the wafers were plasma etched (29.4 sccm CF_4, 150 W) for 10 minutes (200 nm nitride) or 45 minutes (1 μm nitride) to ensure that the etch extended into the silicon substrate. The resist was removed by rinsing with acetone and either methanol or isopropanol.

The wafer was inverted and identical priming and resist spinning procedures were performed on the back side. The EV 620 was used in back side alignment mode to pattern large, nearly 1 mm rectangles centered directly opposite the array of small holes on the front side. Identical development and dry etch procedures were used to transfer the pattern to the back side. The resist was removed from the wafer as before. Then wafers were etched in boiling 40% KOH until the entire thickness of the wafer was etched through. The procedure had a visual endpoint, in which the nitride windows became transparent at the conclusion of the etch; but it generally took 6-7 hours. A typical 3 inch wafer at the end of the fabrication process is shown in figure 3.2a. Figure 3.2b is an optical microscope image of a single nitride window, in this case patterned with an array of 4 μm holes. For all windows, all holes within a given window were the same size, and each window contained the same number of holes. The sizes of the holes were either 2, 4, 6, or 8 μm on neighboring windows, to create devices with overall porosities of 0.07%, 0.29%, 0.65%, and 1.15%, respectively.

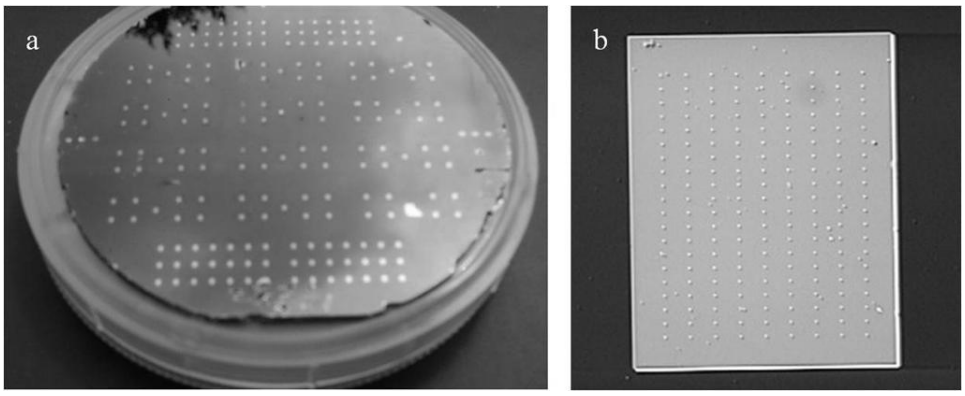

Figure 3.2 Patterned silicon nitride windows etched through silicon wafer. a) a complete layout of silicon nitride windows patterned on a 3 inch wafer. b) one nitride window, patterned with an array of through-etched 4 μm holes

3.3 Deposition of Collagen on Silicon Nitride

At this point, the substrate was nearly ready for the deposition of collagen. On many substrates, however, some form of surface treatment is desirable to facilitate

protein adhesion.[31-41] To improve collagen adhesion on silicon nitride, the wafers were primed with glutaraldehyde vapor.[42,43] The wafers were placed in a dessicator where the drierite crystals had been replaced by liquid 8% aqueous glutaraldehyde for at least 1 hour, refrigerated. A commercially available solution of 0.3% wt. collagen in an acetate buffer (U.S.Biological) was allowed to warm to room temperature before spin casting. The collagen solution was pipetted onto the window-containing area of the wafer, followed by spinning at 2500 rpm, 1 minute. Throughout the remainder of this work, one spin deposition cycle is defined to be one layer of collagen. Consecutive layers were deposited without any rinsing or drying steps in between. For the silicon nitride substrates, films of between 1 and 4 layers were used for subsequent characterizations. After the final spin, wafers were rinsed in deionized water, and immediately placed in a 0.02% glutaraldehyde solution and returned to the refrigerator for 90 minutes to cross-link the collagen monomers.[44] The wafers were rinsed in flowing DI water and allowed to air dry in the fume hood prior to use.

3.4 Collagen Film Internal Structure

For some thin film applications, such as cell culture, the surface structure is the major determinant of system performance.[45,46] For others, such as filtration, both the bulk and surface film properties may contribute significantly to device behavior. In such cases, an understanding of the interior structure of the film is essential. Toward this end, the interior structure of the collagen film was characterized using high-vacuum electron microscopy (HVEM), a procedure similar to transmission electron microscopy (TEM).[47] HVEM allows electrons to be accelerated to relativistic speeds, and thus have much greater penetration than in conventional TEM. Commercial silicon nitride substrates for TEM are only available up to 200 nm thick, [48] since thicker films would require cleaving or sectioning to allow electron beam

penetration. With HVEM, films several hundred nanometers thick can be imaged non-destructively in their entirety.

Four layers of collagen solution were spin-deposited on silicon nitride substrates and cross-linked following the procedures described in section 3.3. The film samples were then shipped to our collaborators in the Turner group at Wadsworth Center [49] for staining and HVEM imaging. The samples were stained with osmium tetroxide prior to imaging, so that the heavy metal could act as a far more efficient scattering center for electrons than the light atoms (C, N, O, and H) which make up the protein. Samples were imaged at a point where the collagen spanned a hole in the nitride substrate. A typical image is shown in figure 3.3.

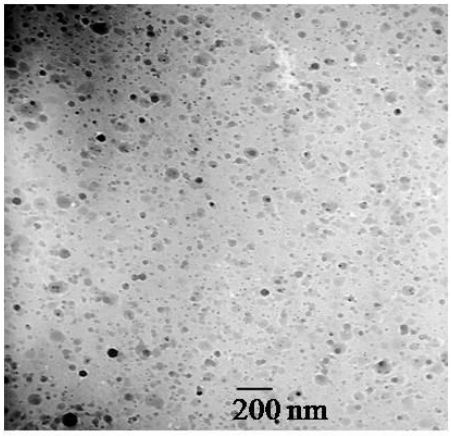

Figure 3.3 Structure of 200 nm thick collagen thin film, imaged via HVEM. Reproduced from reference [50].

Osmium scatters the incident electron beam, preventing the electrons from reaching the detector. Therefore, regions of the image will appear dark in proportion to osmium uptake. Gaps in the film selectively take up the osmium more strongly than the collagen itself, so dark areas correspond to pores. A pore extending through all four layers would appear darkest, through three of the four layers slightly lighter, and so forth, with regions of unbroken collagen between all four layers appearing lightest. Several levels of grayscale were in fact observed, consistent with a "Swiss cheese" or "hairball packed" structure of the collagen film. This can be easily

explained by the spin deposition process. As successive aliquots of collagen solution are pipetted onto a collagen layer that is already present on the surface, spinning causes collagen monomers to crash out of solution wherever, and in whatever orientation, they randomly happen to be. By chance, some fraction of pores in the previous layer will be fully or partially covered by new monomers, while others will not.

By imaging at several incident electron beam angles, the thickness of the 4 layer film was determined to be approximately 200 nm. This implied that on average, a 50 nm of collagen was deposited on the silicon nitride per spin. This thickness was consistent with the profilometry measurements of single spin layers of collagen on silicon (see figure 2.16). Unfortunately, this could not be verified directly by HVEM imaging of a single layer of collagen on silicon nitride.

As can be seen from the scale bar, the lateral dimensions of the darkest pores averaged approximately 20 nm, only slightly larger than the radius of a typical protein. This raises the hope that an additional layer or two of collagen might be sufficient to reduce the pore size to a range ideal for biomolecular filtration. Furthermore, the distribution of pore sizes appeared to be quite narrow. This is likely to translate into a relatively sharp MWCO, which is highly desirable for separating molecules of similar sizes.

3.5 Collagen Film Surface Structure on Silicon Nitride

Over the small areas (~ 2 μm squares) imaged by HVEM, the bulk structure of the 4 layer collagen film tentatively appeared suitable for filtration. This HVEM characterization did, however, suffer from two inherent limits. First, the film could only be imaged over length scales of a few microns. Any larger scale defects in the film might remain unobserved purely by chance, if they occupied only a small fraction

of the total surface area – yet even a single 2 μm hole not spanned by collagen could provide larger molecules a pathway to bypass the collagen filter, broadening the MW distribution of the filtrate. Second, the great strength of HVEM – its ability to probe the bulk structure of the film – necessarily implies that the surface only contributes a tiny fraction of the total signal. If the surface did have significantly smaller pores than the bulk, as is in fact known to be the case in the cellulose acetate membrane system investigated by Russo [51] and Mohammed [52], the properties of the surface layer could entirely determine the filtration behavior of the system, irrespective of bulk structure.

SEM provided a solution to both of these difficulties. After preliminary experiments in which damage from the electron beam was observed in real-time when scanning uncoated samples, all samples were sputter coated with a thin (~ 5nm) layer of either Au or Au/Pd alloy prior to imaging. A Zeiss/LEO SEM, operated at a low accelerating voltage (~ 4keV) to further minimize damage, was used to image sample surfaces at a range of magnifications.

Even a cursory glance at the one layer collagen film reveals why it proved impossible to obtain an HVEM image at this coverage. As can be seen in figure 3.4a,

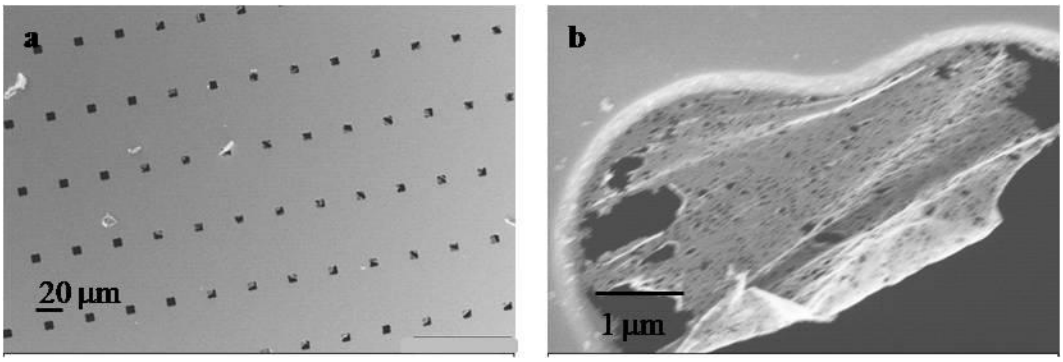

Figure 3.4 SEM images of one layer of collagen on silicon nitride

nearly all of the holes in the nitride were spanned by badly torn collagen films – or none at all. With no straightforward procedure to pre-align the electron beam to a

hole with a relatively intact collagen film, the odds of aligning to one at random were extremely low. The large number of micron-sized gaps in the film, visible in both figure 3.4 a and b, would also provide filtrate molecules ample opportunity to bypass the collagen layer, making it ineffective as a filter.

In spite of its limitations, the one layer film did provide some theoretical insights. First, it was unclear at this point whether a collagen film suspended over a hole in silicon nitride would, even under identical spinning conditions, adopt an equal thickness to a film supported on a silicon wafer, which had previously measured. The abundance of torn films made it relatively easy to image a film in cross-section to determine its thickness. The result is shown in figure 3.5. A single layer of collagen

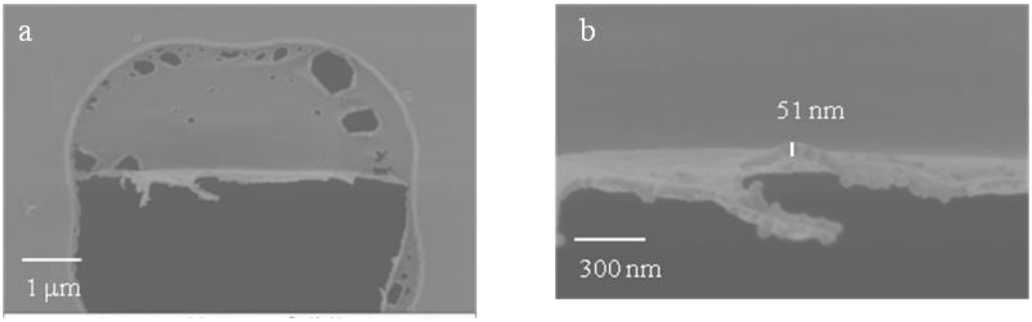

Figure 3.5 SEM of cross-section of one layer of collagen on silicon nitride

was found to be 51 nm thick. This is nearly identical to the profilometry measurement of the single layer film on silicon (figure 2.16) suggesting that when comparing silicon and silicon nitride, the substrate had little effect upon the initial film thickness. Furthermore, this thickness is one-quarter that of the 4 layer film imaged in HVEM. This indicates that the collagen in the first layer, spun directly onto the nitride, adopts the same thickness as subsequent layers, which are deposited onto collagen. Again, this indicated that the substrate has little effect upon film thickness in this system.

A second insight provided by these images proved no less remarkable. The films appeared to be generally quite flat and featureless, with no evidence of fibril formation to any significant extent. This implied that the film consisted of

monomers– that, in fact, a spin-cast solution of 300 nm long, 3nm diameter monomers was able to generate a 50 nm thick film which in many places spanned 6 μm holes in the nitride as in figures 3.4 b and 3.5a – holes as long as 20 monomers laid end to end! This raised hopes that thicker collagen films might prove mechanically stronger, perhaps to the point of spanning the holes in the nitride without tearing.

The two layer collagen film did indeed appear to be far more stable. Unlike the 1 layer film in figure 3.4a, where few nitride holes were spanned by collagen, most of the holes appear to be nearly completely covered by the 2 layer film (figure 3.6a).

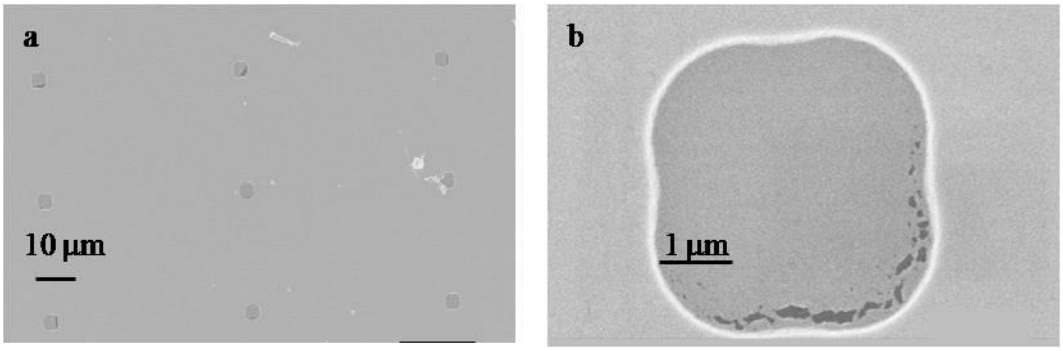

Figure 3.6 SEM images of two layers of collagen on silicon nitride

At a higher magnification (figure 3.6b), it becomes apparent that the collagen film remains nearly intact as it spans the 4 μm holes in the nitride. However, the film is slightly torn near the edge of the hole, with some gaps in the film up to a few hundred nanometers in length. Unfortunately, the situation does not consistently improve upon the deposition of a third layer (figure 3.7). The holes with the highest quality films are

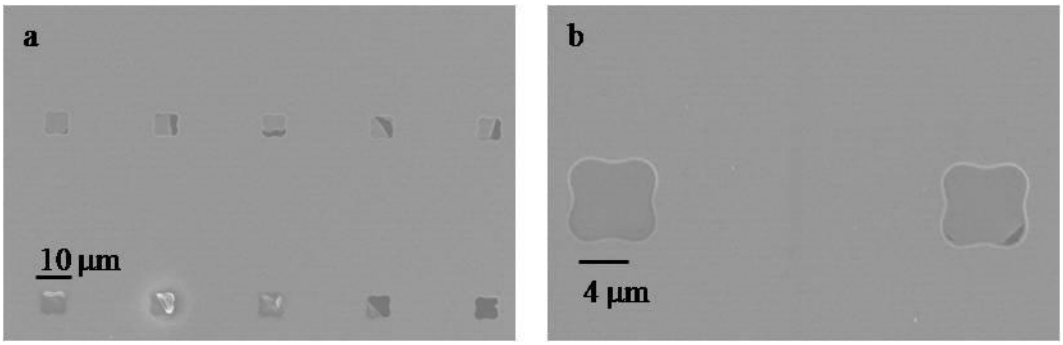

Figure 3.7 SEM images of three layers of collagen on silicon nitride

indeed free of tears (figure 3.7b, left) However, viewed over larger length scales, a larger fraction of the surface area spanning the 4 μm holes appears to be torn in the 3 layer films than in the 2 layer films. This puzzling result has not been definitively explained. The most likely explanation is that, apart from the singular fragility of the 1 layer film, there may in fact be no correlation between film thickness and either the likelihood of tearing or the average size of tears. In any case, regardless of collagen coverage, the tears occupied a large enough fraction of the surface area on all samples that they were not expected to have a sufficiently sharp MWCO to be useful. Clearly, a new approach – either an alternate substrate, a change in the preparation procedure, or both – was needed to eliminate tearing, and to generate a film useful for filtration. But the silicon nitride system suffered from another major drawback, which argued in favor of seeking an entirely new kind of substrate.

3.6 Packaging Nitride Substrates in PDMS

Assuming that the difficulties of producing a stable collagen film spanning the holes in the nitride could be overcome, it would become necessary to develop a system for delivering a fluid to the membrane for filtration, and removing both filtrate and retentate afterward. Ever since its development by the Whitesides group in 1998,[53] PDMS has been the material of choice for on-chip microfluidic systems. PDMS has several advantages for a rapid prototyping system. It is a liquid polymer which can be poured over a mold, then heat-cured to hold its shape. Once cured, it becomes an elastomer which can be peeled off the mold and attached to the device chip. The elastomer is soft enough to self-seal around an injection hole, allowing fluids to be introduced via syringe. Finally, PDMS is transparent, allowing fluid flow to be easily visualized upon introduction of a dye into the fluid.

The PDMS used in the present work to interface with both sides of the nitride substrates is shown in figure 3.8. The reservoir in contact with the membrane is 125

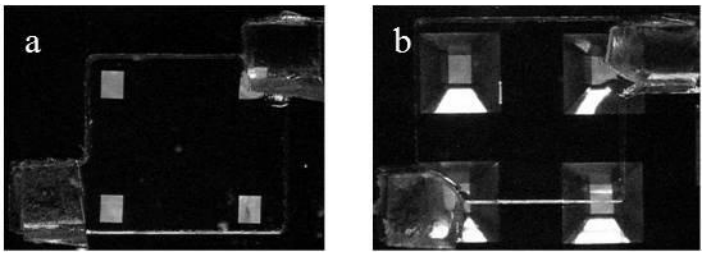

Figure 3.8 PDMS package on silicon nitride substrates. a) front side view and b) back side view

microns high, and 5 mm on a side. The large squares at the lower left and upper right corners of the reservoirs are the injection and outlet ports. They are located outside the window area to prevent damage to the nitride windows by hydraulic pressure from the injection itself.

The general procedure for PDMS processing is outlined in figure 3.9.

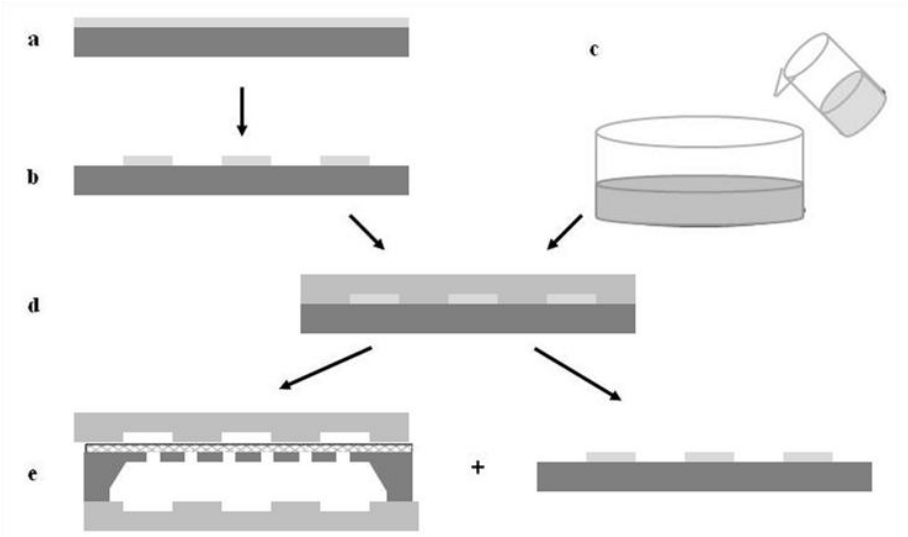

Figure 3.9 Schematic of standard PDMS processing for microfluidic device integration a) SU8 photoresist is spin cast on a silicon wafer and b) SU8 is lithographically patterned to create a master mold. c) PDMS base and crosslinker are mixed d) Liquid PDMS is poured over the mold and heat cured. d) PDMS elastomer is peeled from the master and attached to the device, freeing the master for reuse

Although the mold can be generated in many possible ways – for example, in preliminary experiments in the present work, PDMS was poured over scrap metal

blocks salvaged from the machine shop – to make microfluidic channels which are easily alignable to features on-chip, nanofabrication is the most reliable, reproducible method. Nanofabricated molds are typically made using the negative-tone photoresist SU8. Depending on the processing conditions, SU8 can form films anywhere from tens to hundreds of microns thick. SU8 50 was spun onto a silicon wafer at 1200 rpm for 30 seconds. Prior to UV exposure, the wafer was baked at 90^{o}C for 30 minutes. Using a patterned overhead projector transparency as a photomask, the wafer was exposed to a UV lamp for 90 seconds. A post exposure bake of 2 minutes at 90^{o}C was performed to complete the chemical reactions necessary for negative behavior in the photoresist. The wafer was developed in SU-8 developer (Microchem) for 15 minutes. The sample was then rinsed in isopropanol, and immersed in fresh developer for an additional minute to ensure that the process was complete. The mold was rinsed again in first isopropanol and then water, to clean it prior to PDMS processing.

Once the mold was created, the PDMS itself was prepared in a separate beaker. A viscous base, Sylgard 184 (Dow Corning) was mixed with a crosslinking solution (Sylgard 184 curing agent, Dow Corning) – in most experiments, in the 10:1 w:w ratio recommended by the manufacturer. The resulting highly viscous mixture was degassed under vacuum twice – once after the initial mixing, and again after pouring over the mold prior to curing. The samples were cured in an oven at 60^{o}C for 90 minutes. After curing, the PDMS elastomer was peeled from the mold. The mold could then be reused indefinitely. The PDMS was cut with a razor blade to the appropriate size to cover the desired portions of the wafer. Although, in general, PDMS fluidics can be aligned to a device wafer in a contact aligner if desired, in the present instance the PDMS was aligned to the devices by eye. Adhering the fluidic layer to the device was all that remained.

Typically, for PDMS to permanently bond to a device wafer, both the PDMS and the wafer must be cleaned in an oxygen plasma. The plasma serves not only to remove organic contaminants, but to activate the surface with electrical charges. After cleaning, both pieces are immediately immersed in water to hydroxylate both surfaces, and they are immediately pressed together to allow hydrogen bonds to form between the two surfaces. Materials bonded in this manner may retain a watertight seal together indefinitely.[53] Unfortunately, this procedure cannot be used for the collagen-on-nitride devices. Oxygen plasma is routinely used in the semiconductor industry precisely because it is highly effective for ashing organic materials such as photoresist. Organic materials such as collagen are equally vulnerable.

Given that collagen itself is already hydroxylated over a large percentage of its surface, it was hoped that the device wafer might already be sufficiently activated for adhesion. The PDMS itself was subjected to oxygen plasma as usual; but with only one surface activated, the packaging never truly stuck to the device wafer. Another possible means of adhesion lay with varying the composition of the PDMS elastomer itself. The ratio of base to crosslinker in the original mix determines both the ultimate hardness and adhesiveness of the PDMS. More crosslinker made the product mechanically harder and easier to peel off the mold, but ultimately more difficult to adhere to the device wafer. Less crosslinker made the PDMS both stick to the device wafer more readily, and flow to self-seal at injection sites more easily. However, this also made the PDMS far less mechanically robust, difficult to release from the mold without tearing, and at very low levels of crosslinking, unable even to hold its shape. The manufacturer's suggested ratio did indeed appear to be the best compromise between stickiness and stability; however, it was not sticky enough to form a watertight seal to either collagen or silicon nitride.

Having exhausted these options, the only obvious option remaining was to physically clamp the PDMS in place, as shown in figure 3.10. Unfortunately, several

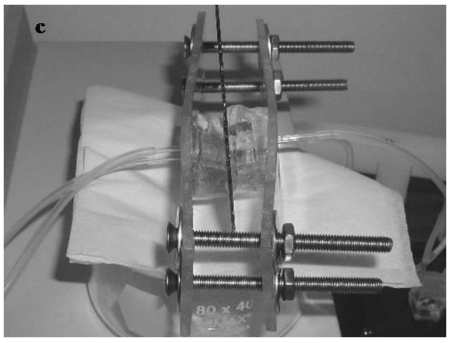

Figure 3.10 PDMS clamped to substrate during filtration test, to combat poor adhesion

difficulties remained with this procedure. Uneven clamping inevitably led to leaks, most often between the substrate and the PDMS, but occasionally at the injection and outlet sites. Leaks between the PDMS and the syringe were sealed with vacuum grease, but using large amounts of grease could get quite messy. Leaks at the substrate surface were usually solvable by tightening the clamps, but occasionally, the force required to make the seal watertight actually broke the wafer. Leaks could also, in principle, be minimized by reducing the fluid pressure.

To obtain the lowest experimentally achievable fluid pressure, peristaltic pumps (*VWR Scientific*, variable flow *mini pump)* were used to circulate fluid in the tangential geometry described in chapter 1 (figure 1.5). Peristaltic pumping requires that the fluid being pumped be incompressible. This implies that the system must have airtight seals at all junctions. Failing this, the pumps themselves were prone to collecting air bubbles within the tubes, stopping the pumping. The system thus required constant, close monitoring throughout the experiment, as pumping could cease without warning at any moment. Even when the pumping itself proceeded perfectly, the silicone tubes themselves readily adsorbed dye molecules. These tubes

were nearly impossible to clean, yet very expensive to replace. Clearly, a more practical experimental setup for the filtration tests was required.

3.7 Commercial Substrates – Polycarbonate and Polyethylene terephthalate

Suspended silicon nitride film substrates did provide a proof of concept for the integrability of collagen thin films into a silicon based on-chip system. However, there were several problems – foremost among them, the extremely cumbersome implementation of the packaging for flow testing. Even if this difficulty were to be overcome, the low porosity of the nitride films could be expected to greatly limit flow rates across the membrane, and result in long experimental times being required to complete MWCO tests. Higher porosity nitride films, in principle, are possible to fabricate, but the costs of process development (particularly mask development and long furnace depositions of the nitride) were prohibitive. All these factors made the silicon-on-nitride process ill-suited to rapidly characterize diffusion across large numbers of collagen test films. To save time and money, commercially produced membranes of other porous materials – initially polycarbonate (PC) and polyethylene terphthalate (PET), and later alumina – were investigated as potential substrates.

PC and PET have much in common chemically. As can be seen in figure 3.11,

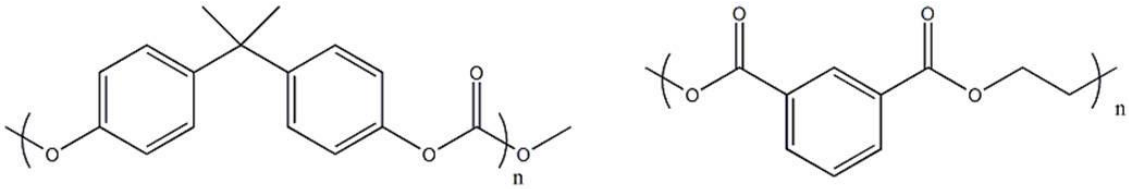

PC **PET**

Figure 3.11 Structures of PC and PET monomers

both materials contain ester groups which can promote the adhesion of collagen by acting as hydrogen bonding partners for the hydroxyproline residues. Both also contain some hydrophobic groups which may interact with the nonpolar groups on

collagen – 2 aromatic rings per monomer in the case of PC, and 1 aromatic ring on PET. The additional hydrophobic group per monomer makes PC slightly more hydrophobic than PET. It was thus possible that the adhesion characteristics of collagen would differ between the two substrates. Collagen is known to adhere at least somewhat to both PC and PET;[12-14] indeed, PET cell culture inserts coated with collagen are available commercially.[54] For either PC or PET to serve as an optimal porous support, however, the collagen need not simply adhere to the surface, but adhere weakly enough to form a suspended film over the .5 - 5 μm wide track-etched holes, rather than penetrate into the substrate bulk and coat the walls of the holes. It was unknown which – if either – substrate was more likely to behave this way; thus, both kinds of membranes were tested in parallel.

In both cases, the ease of integration into a test system for diffusion experiments drove the decision to try PC and PET as supporting membranes. Both are widely commercially available for use in cell culture inserts, which are shown in figure 3.12. A track-etched polymer membrane [55,56] constitutes the bottom of a

Figure 3.12 Commercially available PC (left) and PET (right) cell culture inserts

cup which can hold about 1 mL of a dye-containing liquid. This insert can then sit in a reservoir of pure deionized water, allowing passive diffusion to take place between the two fluid reservoirs with no need for active pumping, as diagrammed in figure 3.13. By eliminating both the possibility of pump failure, and the limitation to a single

device-under-test due to pump availability, it became possible to test multiple membranes simultaneously while leaving them unattended. Elimination of the bottleneck in the testing step also allowed multiple membranes to be prepared at once,

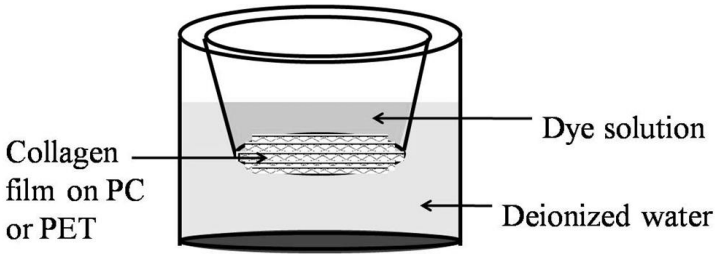

Figure 3.13 Schematic of passive diffusion through collagen film integrated on cell culture insert

free of uncertainty about the stability of films during storage. Batch processing of the collagen films also greatly improved the uniformity of the preparation conditions. Taken together, the use of cell culture inserts solved many of the problems associated with the silicon nitride system.

As described above for nitride substrates, both PC and PET substrates were primed with glutaraldehyde vapor for at least 1 hour prior to spinning. The collagen solution was allowed to warm to room temperature prior to spinning. Between one and four layers of collagen were then spin-deposited at 2000 rpm for one minute, with no rinsing in between layers. In the initial experiments, after the last layer, the film was rinsed with deionized water. Some films were examined immediately; others were first crosslinked in 0.02% glutaraldehyde at 4^{o}C for 1.5 hours and rinsed again. Whether crosslinked or not, these films were then allowed to air-dry in the hood at ambient temperature and humidity. The films were now ready for characterization.

3.8 SEM Surface Structure of PC, PET, and Collagen Films

Since a primary concern with the collagen-on-nitride system had been the integrity of the collagen films when spanning holes in the substrate, SEM imaging was

given the top priority, to determine if collagen on either PC or PET perfomed any better. The experimental procedures for SEM imaging were similar to those previously used to image the nitride substrates. All samples were sputter coated with an Au/Pd alloy to minimize both charge buildup and actual damage from the electron beam. In addition, low accelerating voltages (~2 keV) were used to image the samples.

Both substrates, prior to the deposition of collagen, appear in figure 3.14.

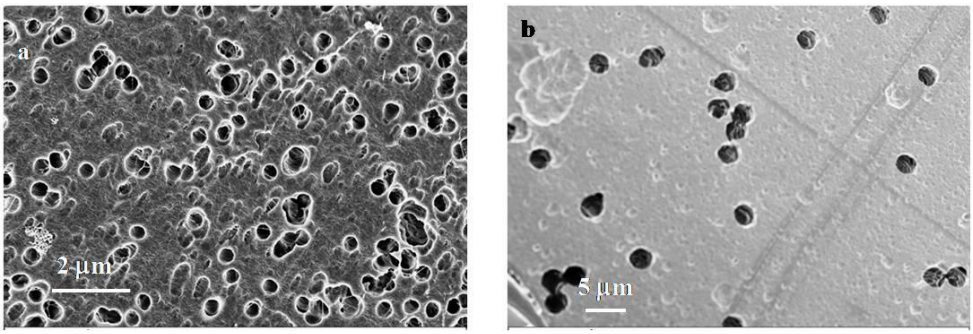

Figure 3.14 SEM images of a) PC and b) PET membranes prior to collagen deposition

Unlike the nanofabricated silicon nitride system, the track etched holes in both PC and PET are both irregularly shaped and randomly positioned. Some of the holes overlap, requiring the collagen film to span lengths nearly double or triple the nominal hole size, for ideal coverage.[57] Conversely, large areas of the membrane surface may be devoid of holes. Thus, percent porosity can only be defined as an average over length scales of a millimeter or more. It should be carefully noted that the scales of the two images are quite different. PC (figure 3.14a) has a high density of small holes (nominally 400 nm); PET has fewer, but larger holes (nominally 3 μm). This translates into nominal porosities of 5.65% for PET [58] and 12.56% for PC.[59] Thus the two substrates differ significantly in both porosity and chemistry.

Finally, it should be noted that on both substrates, the holes often have irregular sidewall profiles, and are oriented at a range of angles to the membrane surfaces. While this may not impact the ability of collagen to cover the holes, it

ultimately complicates any theoretical analysis of fluid flow through the membrane.[60-62] At this point, however, finding a substrate which collagen would stick to and span holes in, was a prerequisite for even an experimental determination of the filtration behavior, much less a theoretical description.

Experimentally, all collagen-containing films produced in the manner described in section 3.7 – whether on PC or PET, from one to five layers, crosslinked or not – failed to produce a collagen film which spanned holes in the substrate when imaged by SEM. Some typical failed films, in this case 4 layers on PC, are shown in figure 3.15. Only upon very close examination of figure 3.15a is any collagen visible

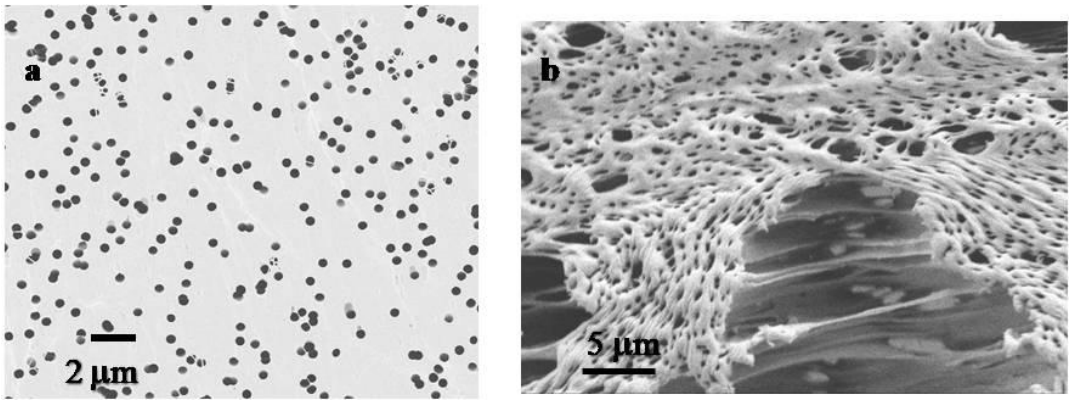

Figure 3.15 SEM of collagen on PC without CPD. a) Poor spanning of pores, although b) collagen appears to adhere to the surface.

at all. At most, 10% of the holes appear to be partly spanned by two or three fibrils apiece. Few, if any, holes are spanned by anything remotely resembling an intact film. Upon closer examination, in figure 3.15b, collagen fibrils do appear to be present on the surface. However, the fibrils follow the contours of the surface closely, and largely fail to span the holes in the PC substrate. This tendency was also observed on PET (data not shown).

Thus, the choice of substrate had not proven as effective at solving the tearing problem as it had the integration problem. Reexamining the procedure for preparing the collagen film itself seemed to be the only possible solution.

3.9 CPD and Collagen Films on PC and PET

Collagen gels are known to undergo substantial swelling in response to hydration [2,7,8,63-65]. Conversely, one might expect collagen films to undergo significant shrinkage during dehydration and drying. As the film dries, the remaining water droplets on the surface shrink, causing their surface tension to be exerted over ever smaller areas of the collagen. In the limit that the drop size approaches zero, the force per unit area increases until it becomes great enough to tear the film at its weakest points. Tearing has indeed been observed during the drying of collagen films supported on solid substrates [2,19,65]. If a film, at most 200 nm thick, had originally spanned a hole, it might tear disproportionately in the unsupported areas and recede to the solid portions of the substrate surface. This analysis suggests that to eliminate tearing, one must eliminate surface tension during dying. A more gradual dehydration, such as critical point drying the collagen films rather than allowing them to air dry, might prove sufficiently gentle to preserve the hole-spanning portions of the film. Thus, a new procedure for crosslinking and gradual dehydration followed by critical point drying (CPD) was developed, as shown in figure 3.16.

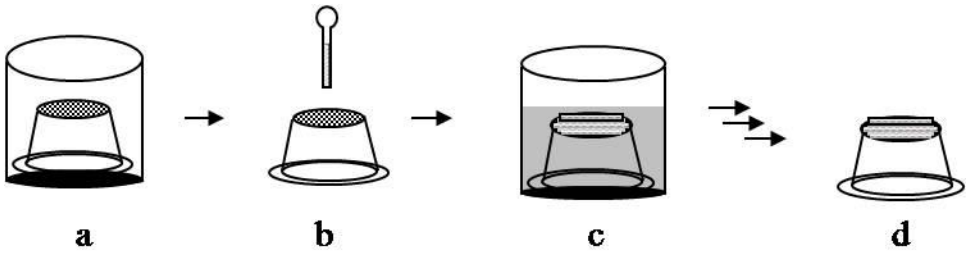

Figure 3.16 Preparation of collagen films on PC and PET substrates a) Porous cell culture insert vapor primed in sealed chamber with glutaraldehyde vapor b) Saturated collagen solution spun onto porous surface c) Crosslink collagen in 4% glutaraldehyde in acetate buffer d) Gradual dehydration in a series of dilute buffers to pure ethanol

Immediately after spinning, the often still-wet collagen films were placed in a room temperature solution of equal parts 8% aqueous glutaraldehyde/ 0.1M acetate

buffer at pH 4 for 10 minutes to allow the collagen to crosslink. Then the sample was placed transferred to 100% buffer solution for 10 minutes. At this pH, the collagen remains stable in fibrillar form. To minimize deformation of the collagen by gradually reducing the ionic strength of the solution, the samples sat for 10 minutes each in the following series of dilutions in deionized water: 90% buffer, 70% buffer, 50% buffer, 25% buffer, 10% buffer, pure deionized water. At this point, any free ions should have been removed. The gradual dehydration into pure ethanol could then begin. The samples spent 10 minutes in each of the following ethanol dilutions in deionized water: a second 100% deionized water bath, 10% ethanol, 25% ethanol, 50% ethanol, 70% ethanol, 90% ethanol, 100% ethanol. When multiple samples were under preparation simultaneously, the first samples to be completed were transferred to their own separate 100% ethanol Petri dish and kept under solution until all samples were ready for CPD.

The CPD itself was performed under the standard recipe for the NBTC tool (Baltec CPD-408): The chamber was purged three times with gaseous CO_2 up to a pressure of 10 bar at 25^{o}C, followed by 33 cycles of rinsing in liquid CO_2 at up to 50 bar at 25^{o}C, and finally a single supercritical cycle at 80 bar CO_2 and 35^{o}C.

3.10 SEM of CPD Collagen Films on PC and PET

Once critical point drying was incorporated into the procedure, both the PC and PET systems were reexamined by SEM. Stable, hole-spanning collagen films were successfully produced on both substrates. In fact, three layer films spun onto PC (figure 3.17a) spanned the holes in the substrate so well, that it was difficult to detect where the holes had originally been! Whether directly supported on PC or spanning holes, the collagen film appeared to be a very uniform mass of fibrils, intertwined in a "hairball" or "heap of spaghetti" fashion (figure 3.17b). Typical fibril diameters

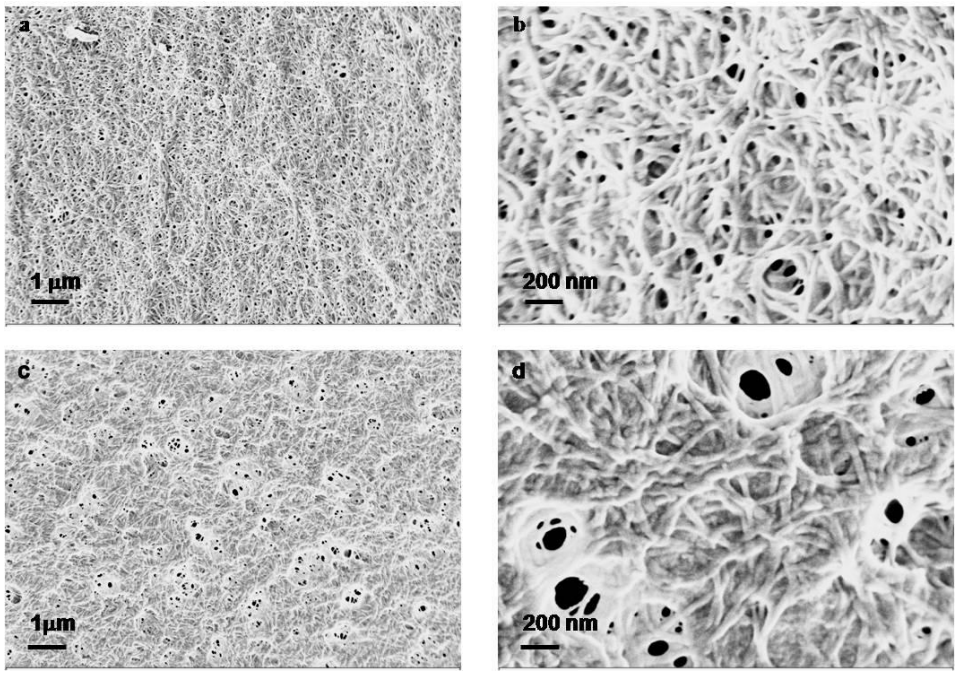

Figure 3.17 SEM images of collagen spin deposited on PC substrates a) and b) 3 layers of collagen c) and d) 5 layers of collagen.

appeared to be quite uniform, at about 30-40 nm. The visible pores in the composite film also appeared to have a narrow size distribution, averaging about 20 nm.

The situation becomes somewhat puzzling when examining a 5 layer collagen film prepared under similar conditions (figure 3.17c). Supported regions of the film have a generally similar morphology to the 3 layer film. The fibrils within the film also appear to have similar dimensions and to pack in a similar manner. There is one striking difference, however. The holes in the initial substrate are spanned less effectively by the 5 layer film than the 3 layer film! In figure 3.17c, it is obvious where the holes in the PC substrate initially were. The electron beam preferentially deposits static charges on the collagen film where it sits atop the insulating substrate, making the supported portions of the collagen film appear darker. Among the unsupported regions of the collagen, which appear to be nearly white, pores much larger than those in the 3 layer film are visible. Upon closer examination (figure 3.17d), some of the pores appear to be as large as 200 nm in diameter – ten times the

size of typical pores in the 3 layer film! Such large pores would present little barrier to small molecules with a hydrodynamic radius of less than 10 nm. Thus, the 5 layer film would be unlikely to have a sharp MWCO in the desired MW range. It is puzzling how a collagen film could span the holes in the substrate less effectively when more collagen is available. Perhaps at a higher coverage there are subtle differences in the fibril structure itself, such as slightly larger fibril diameters, which may incorporate the surplus collagen. Alternately, a slightly closer packing of most of the fibrils would, by default, force the remaining pores to cluster. Such differences might not be readily observable at these magnifications without a detailed statistical analysis of the feature sizes in the images.

Interestingly, on PC, the pores in the collagen film tended to be near the center of the holes in the substrate, unlike the silicon nitride system, where the films tore primarily at the edges. This suggests that, in contrast to silicon nitride, the pores likely did not originate from tearing during the drying process. A possible alternate explanation lies hidden among the observations of the non-CPD samples in section 3.8. In those experiments, collagen adhered strongly enough to PC to follow the contours of the surface without spanning the holes. Perhaps even when subject to CPD, the initial layer of collagen fibrils coats the surface essentially conformally. Subsequent layers of fibrils span the holes in PC primarily by spanning other collagen fibrils at the holes edges, and then themselves being spanned -- much as bricks might be stacked with a slight offset to form an arch or a dome. A similar process is observed in the growth of multilayer collagen membranes on LB films.[6] If insufficient collagen is available to 'cap the dome', one would expect the pores to remain near the center of the holes, as is observed.

On PET (figure 3.18a-d), the collagen fibrils display yet another distinct set of

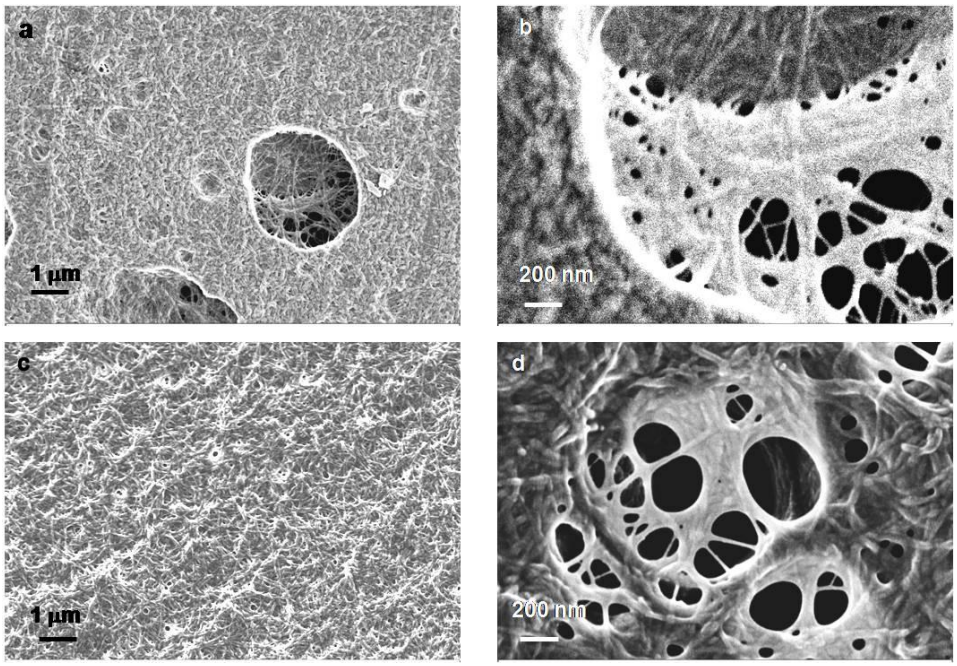

Figure 3.18 SEM images of collagen spin deposited on PET a) and b) 3 layers of collagen and c) and d) 5 layers of collagen

morphologies. A 3 layer collagen film (figure 3.18a) nearly fully spans the holes in the PET membrane – which is quite remarkable, given that the holes are nearly ten times as large as those on PC. The film appears somewhat dissimilar between supported and unsupported regions. On the PET itself, the collagen is clearly aggregated into nodular, truncated structures about 50 nm in diameter. These are clearly quite different from the few micron long, 10 nm wide, normal-looking fibrils which span the holes (figure 3.18b), suggesting the possibility of an unusual arrangement of monomers within the aggregates at submicron scales. Overall, the film is visibly more close-packed on PET than on PC. This is particularly pronounced in supported areas, but true even over the holes. On the other hand, pores in the collagen film are both larger and of a broader size distribution than on PC. Pores sizes range from 200 nm down to about 10 nm. The holes do not appear to be especially concentrated in the center or at the edges, unlike both the PC and nitride systems. In

this system, fibrils appear to span the holes in an irregular weave. The reason for this behavior is unknown.

The 5 layer collagen film on PET (figure 3.18c) does display an improvement in hole-spanning over the 3 layer film, as would naively be expected. On supported areas, the collagen aggregates appear to be far more similar to the hole-spanning fibrils than in the 3 layer sample. The fibril packing patterns were similar to the 3 layer sample: close-packed away from the holes, and an irregular weave spanning the holes. The relationship between pore size and the number of collagen layers is unclear. Over large areas of perhaps 10 microns square, no pores larger than 200 nm were clearly visible. However, at higher magnifications (figure 3.18d), pores with a large range of sizes, up to about 300 nm were observed. The physics underlying this unusual behavior is uncertain. More certain is that this film is likely to be of little value for filtration.

To summarize, CPD-dried collagen films on both PC and PET substrates exhibited significantly less tearing than the air-dried films on silicon nitride. Unfortunately, some holes larger than 100 nm remained, raising concerns about whether a small, narrow MWCO was achievable. On both PC and PET, the correlation between pore sizes and the amount of collagen deposited was not straightforward. This unpredictable behavior casts doubt on the suitability of either membrane as a substrate for collagen.

Another difficulty was encountered with these substrates, which might be solvable in an industrial environment, but proved problematic given the limited equipment available at Cornell. Without CPD, the collagen films were unstable on both substrates under all conditions tested. However, the cell culture inserts were physically too tall to fit into the available CPD tool. Thus, any membranes requiring CPD needed to be removed from the insert for processing. Reattachment of the

membrane was difficult, negating the advantage of automatic integration which had motivated the original choice of the PC and PET systems. Given the proper CPD equipment, the commercial availability of PC and PET cell culture inserts could make the further development of their composite collagen membranes attractive. Such composite systems might prove particularly useful for experiments in which cells are cultured on one side of the membrane, and other molecules selectively diffused to or collected from the cells on the other. However, keeping in mind the existing equipment limitations, the search for a suitable substrate began anew.

3.11 Commercial Anodically Etched Alumina as a Substrate

CPD was somewhat successful at stabilizing collagen films on both PC and PET. Yet a few problems remained: the continued presence of pores above 100 nm in diameter, and difficulties with combining CPD and integration. Even if these issues were resolved, both PET and PC would still have relatively low porosities (albeit at the upper end of the range available in the nanofabricated silicon nitride system). All of these issues were considered during the selection of another commercially available porous substrate – namely, anodically etched alumina.

Porous alumina is sold as a 60 μm thick disk (figure 3.19a), which is flat

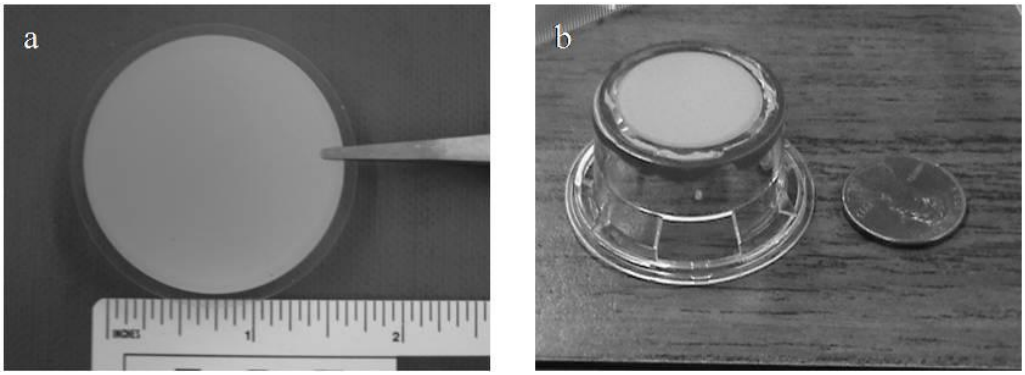

Figure 3.19 Porous alumina Whatman disk a) as sold and b) integrated into filtration setup

enough to fit into the available CPD equipment. Luckily, some disks are available in the same diameter as some commercially produced PC cell culture inserts. The original PC membranes can easily be cut from the insert with a razor blade, and the alumina membrane glued in its place. Thus, collagen could be spin cast and processed on the alumina substrate alone, and only after the CPD step, adhered to the insert with the collagen facing inward, as shown in figure 3.19b. Nail polish (L'oreal, red #430), was chosen as the adhesive to ensure a watertight seal.

Having solved the integration problem, the issues of pore diameter and density could now be considered. Fortunately, both are addressed by the method of making alumina. Alumina is created by electrochemically etching an aluminum thin film in an oxidizing acid. The etched holes initially nucleate at random positions all over the aluminum surface, allowing an estimated 25-50% of the surface [66] to be converted into open pores (figure 3.20a). The electric field causes the etch to proceed preferentially in the downward direction. As a consequence, the channels through the alumina are highly oriented, perpendicular to the surface of the substrate, as can be seen in a cleaved cross section (figure 3.20b). This geometry avoids the complications

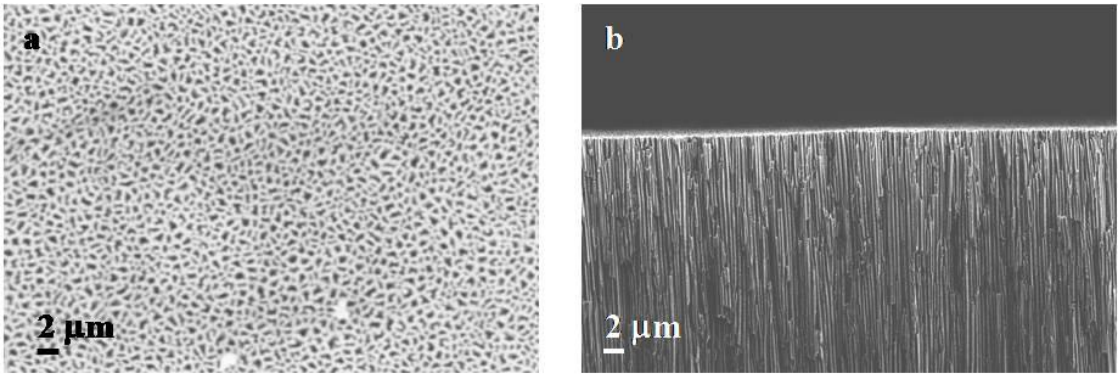

Figure 3.20 SEM of commercial alumina substrates. a) Nominal pore sizes in the initial alumina surface are 20 nm. Scale bar represents 100 nm. b) Cleaved cross-section of an alumina substrate.

of a tortuous path present in many membrane systems, and greatly simplifies attempts to theoretically model diffusion through the substrate.[67]

Unfortunately, when collagen was spun onto untreated alumina surfaces, following procedures identical to those described in figure 3.16b-d for the deposition of collagen on PC and PET, the films observed in the SEM showed poor coverage, as can be seen in figure 3.21 below. On an alumina disk manufactured with a nominal

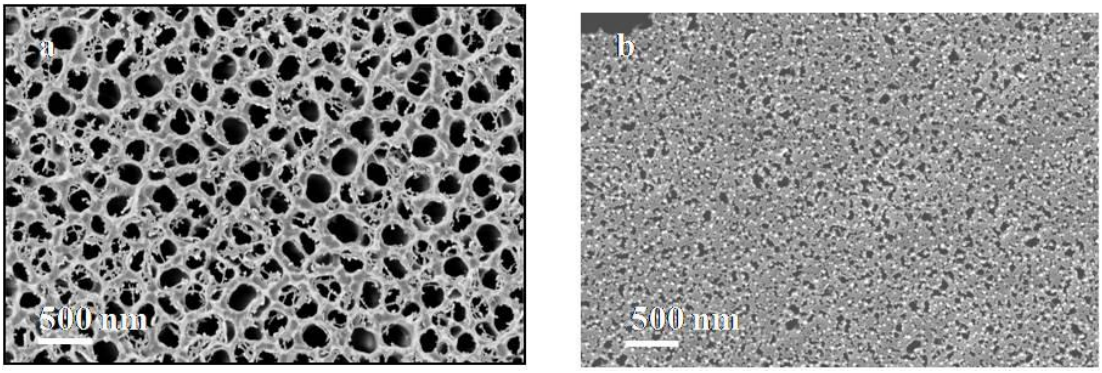

Figure 3.21 Collagen deposition on untreated alumina. Three layers of collagen spin cast on untreated alumina substrates. Nominal hole sizes in the initial alumina surface were a) 200 nm and b) 20 nm, respectively.

hole size of 200 nm, and 3 layers of collagen spin deposited, some scattered fibrils were visible on the surface, but nowhere were the holes spanned. The situation improved somewhat on an alumina substrate with 20 nm holes (figure 3.221b). The collagen film fully spanned some holes, but was entirely absent over others. Although decreasing the average hole size improved collagen adhesion, this strategy alone could never be sufficient to create a stable collagen film on alumina. Membranes with through-etched holes of less than 20 nm diameter are not commercially available. Therefore an alternate method of improving adhesion was necessary. Just as glutaraldehyde vapor priming had improved collagen adhesion on PC and PET, it was hoped that some form of surface treatment could improve adhesion on alumina.

No specific information was found in the literature about the adhesion of collagen on alumina – with or without surface treatments. It was unknown whether glutaraldehyde itself would bond to alumina as it had to PC and PET – but it was already known to bond to collagen. Therefore, it seemed logical to try glutaraldehyde

vapor priming first. The exact same procedure as in figure 3.16 was applied to alumina substrates. An SEM image of the resulting film is shown in figure 3.22.

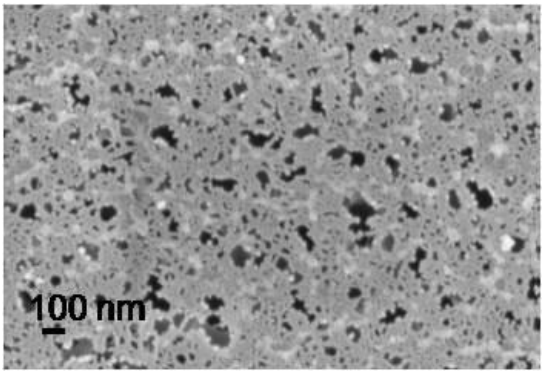

Figure 3.22 Three layer collagen film, CPD dried, on glutaraldehyde vapor primed alumina

The adhesion of collagen improved considerably over untreated alumina, with most of the holes in the alumina spanned. However, a wide distribution of pores sizes remained in the collagen film, with many of the larger pores between 100-200 nm. These pores are most likely too big to effectively filter small molecules. On the other hand, this result did support the concept of using surface chemical modification to improve collagen adhesion – only a more effective modifier was required.

In general, collagen typically adheres well to hydrophilic substrates. On hydrophobic substrates such as PET, oxidation of the surface is known to improve collagen adhesion.[12,14,18,23] This is likely because the numerous hydroxyproline residues of the collagen are able to form hydrogen bonds with carbonyl and hydroxyl groups generated on the substrate surface by the oxidant. Alumina is also known to react with oxidizing acids, even in the absence of an electric field.[68] Thus, it seemed a reasonable conjecture that treating the alumina surface with sulfuric acid might create a surface termination more amenable to collagen adhesion.[69]

Accordingly, the alumina substrates were heated in 95% sulfuric acid (Baker) at 55^{o}C. In the earliest experiments, this reaction was carried out for 1 hour. However, such harsh treatment made the alumina disks extremely fragile. An outright

majority of such substrates broke during subsequent processing, making them far too fragile for practical use. Therefore, the reaction time was decreased to 15 minutes. Once this treatment had been demonstrated to produce stable collagen films on sufficiently robust alumina disks, further optimization of the procedure was not attempted. Thus, whether or not shorter etch times, lower temperatures, and/or lower acid concentrations would provide superior surface modification of the alumina, is beyond the scope of the present work.

After a 15 minute sulfonation, the surface was indeed modified, as can be seen by comparing SEM images taken before (figure 3.23a) and after (figure 3.23b) the

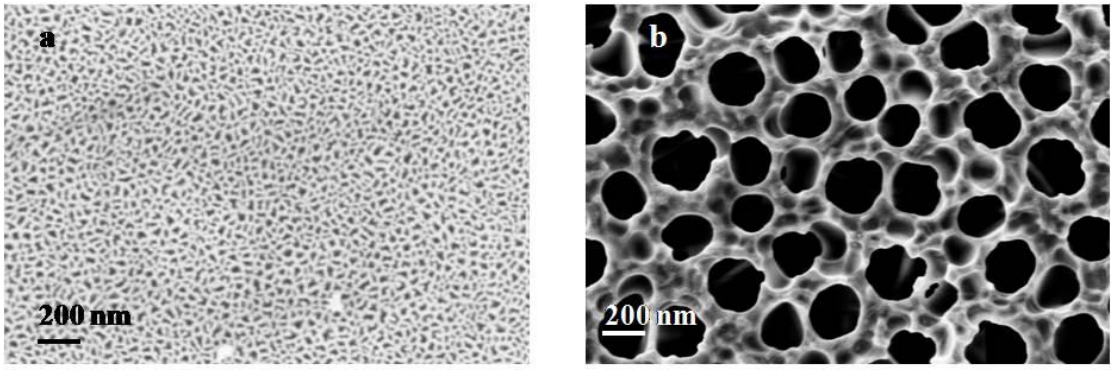

Figure 3.23 Effect of sulfuric acid on alumina substrates. a) Untreated commercial alumina substrate, with pores nominally 20 nm. b) Alumina substrate after 15 min treatment in concentrated sulfuric acid at 55^{o}C.

sulfuric acid treatment. The substrates initially had a nominal pore size of 20 nm. After the sulfonation, the pores had widened to nearly 200 nm. The treated surface was also considerably rougher than the initial surface. None of this is particularly surprising, as sulfuric acid is known to etch alumina.

The change in surface topography following sulfonation is dramatic, and is in itself likely to affect collagen adhesion to the surface. Given that this change followed a chemical reaction, chemical change to the surface termination will, for the present, also be assumed as plausible. Data in support of this assumption will be presented in the next chapter. It is not entirely certain whether the either the topographic or the

chemical changes are sufficient alone, or if the combination of both is required, to generate a stable collagen film. However, there are some tantalizing clues, which shall be discussed at length in chapter 4.

Following sulfonation, the membranes were rinsed in deionized water and allowed to air dry. The substrates could be used immediately, or stored for up to one week prior to collagen deposition. The procedures for spin depositing collagen, dehydrating the film, and CPD were identical to those described in section 3.9 for PC and PET substrates. The entire process is depicted schematically in figure 3.24.

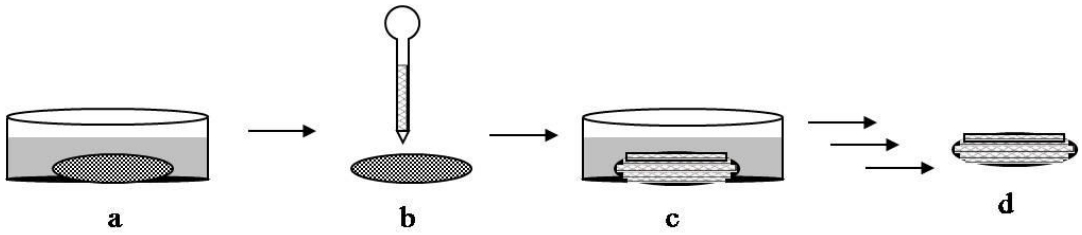

Figure 3.24 Preparation of collagen films on alumina substrates. A) Porous alumina Whatman disk heated in H_2SO_4, 55^oC, 15 min b) Saturated collagen solution spun onto sulfonated porous alumina c) Crosslink collagen in 4% glutaraldehyde in acetate buffer d) Gradually desalinate in diluted acetate buffers and dehydrate into pure ethanol for critical point drying

By following this protocol, stable collagen films were at last created on sulfonated alumina. The first film produced in the manner, with 3 layers of collagen, is shown in figure 3.25. For the first time on alumina, nearly all holes in the substrate

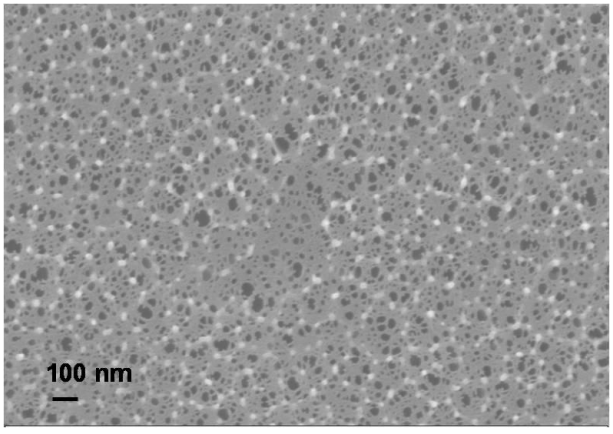

Figure 3.25 Three layer collagen film, CPD dried, on alumina sulfonated for 1 hour.

appear to be fully coated by collagen. No fibril structures are visible, suggesting that the collagen remains in monomeric form. But most interestingly, the pores in the collagen itself have a very narrow distribution of sizes, with nearly all between 10-30 nm. This is a nearly ideal size range and distribution to attempt separations of molecules of low MW (less than 1000). At last, a suitable substrate and preparation protocol had been developed for the collagen films.

3.12 Conclusions

Several materials were evaluated as possible support substrates for collagen films according to the criteria of ease of processing, microfluidic integrability, substrate porosity, and the ability of collagen to simultaneously adhere to the surface while spanning holes. A comparison of the four substrates on the test criteria is summarized in table 3.1. Silicon nitride, PC, PET, and alumina all met the first two

Table 3.1 Summary of collagen substrate properties

	ease of processing	microfluidic integrability	substrate porosity	collagen adhesion
silicon nitride	fair	poor	fair-good	good
PC	good	good	good	good
PET	good	good	fair	good
alumina	good	fair	excellent	excellent

criteria, to varying extents. However, on the latter two criteria, alumina clearly outperformed the other three substrates. Thus, alumina was selected as the substrate for further characterization of composite collagen films, as shall be seen in chapter 4.

REFERENCES:

[1] Penners, G., Priel, Z., Silberberg, A.. J Coll. Interface Sci., **80 (2)**, 437–44, 1981

[2] Mertig, M., Thiele, U., Bradt, J., Leibiger, G., Pompe, W., and Wendrock, H.. Surf. Interface Anal. **25** (**7-8)**, 514-521**,** 1997

[3] Denis, F.A., Hanarp, P., Sutherland, D.S., Gold, J., Mustin, C., Rouxhet, P.G., and Dufrene, Y. F.. Langmuir, **18**, 819-828, 2002

[4] Elliott, J.T., Woodward, J.T., Umarji, A., Mei,Y., and Tona, A. Biomat., **28,** 576-585, 2007

[5] Li, M., He, P., Zhang, Y., and Hu, N.. Biochimica et Biophysica Acta, **1749,** 43–51, 2005

[6] Chen, Q.B., Xu, S.T., Li, R., Liang, X.D., Liu, H.L.. J. Coll. Interface Sci.**, 316 (1),** 1-9, 2007

[7] Mertig, M., Thiele, U., Bradt, J., Klemm, D., and Pompe, W.. Appl. Phys. A-Mat. Sci. & Processing, 66, Part 1 Suppl. S, S565-S568, 1998

[8] Thiele, U., Mertig, M., and Pompe, W.. Phys. Rev. Lett., 80 **(**13), 2869-2872, 1998

[9] Scharnweber, D., Born, R., Flade, K., Roessler, S., Stoelzel, M., and Worch, H.. **Biomat., 25 (12), 2371-2380, 2004**

[10] Sun, M., Stetco, A. and Merschrod S., E.F.. Langmuir**, 24**, 5418-5421, 2008

[11] Dupont-Gillain, C.C., Pamula, E., Denis, F.A., De Cupere, V.M., Dufrene, Y. F., and Rouxhet, P. G.. J. Mater. Sci.- Mater. M., **15,** 347-353, 2004

[12] Dufrene, Y.F., Marchal, T.G,. and Rouxhet, P.G.. Langmuir**, 15**, 2871-2878, 1999

[13] De Cupere, V.M., Van Wetter, J., and Rouxhet, P.G.. Langmuir, **19 (17)**, 6957-6967, 2003

[14] De Cupere, V.M., and Rouxhet, P.G.. Surf. Sci., **491** (**3)**, 395-404, 2001

[15] Jacquemart, I., Pamula, E., De Cupere, V.M., Rouxhet, P,, Dupont-Gillain, C.C.. J. Coll. Interface Sci., **278** (**1)**, 63-70, 2004

[16] Gurdak, E., Rouxhet, P.G., Dupont-Gillain, C.C.. Coll. Surf. B-Biointerfaces, **52** (**1)**, 76-88, 2006

[17] Gurdak, E., Booth, J., Roberts, C.J., Rouxhet, P.G., and Dupont-Gillain, C.C.. J.Coll. Interface Sci., **302 (2),** 475-484, 2006

[18] Dupont-Gillain, C.C., and Rouxhet, P.G. Langmuir, **17** (**23)**, 7261-7266, 2001

[19] Dupont-Gillain, C.C., Nysten, B., and Rouxhet, P.G**..** Polymer Intl.**, 48 (4),** 271-276, 1999

[20] Dewez, J.L., Berger, V., Schneider, Y.J., and Rouxhet, P.G.. J. Coll. Interface Sci., **191 (1)**, 1-10, 1997

[21] Stevens, P.V., Nyström, M., Ehsani, N.. Biotechnol. Bioeng., **57,** 26-34, 1998

[22] Woodcock, S.E., Johnson, W.C., Chen, Z.. J. Coll. Interface Sci., **292** (**1),** 99-107, 2005

[23] Pamula, E., De Cupere, V., Dufrene, Y.F., and Rouxhet, P.G.. J. Coll. Interface Sci., **271 (1)**, 80–91, 2004

[24] Denis, F.A, Pallandre, A., Nysten, B., Jonas, A.M., and Dupont-Gillain, C.C.. Small, 1 (10), 984-991, 2005

[25] Xu, S.H., Liu, A.P., Chen, Q.B., Lv, M.Y., Yonese, M., and Liu, H.L.. Colloids And Surfaces B-Biointerfaces, **70 (1)**, 124-131, 2009

[26] Lv, M.Y., Chen, Q.B., Yonese, M., Xu, S.H, and Liu, H.L.. Colloids And Surfaces B-Biointerfaces, **61 (2)**, 282-289, 2008

[27] Nuxoll, E.E., Hillmyer, M.A., Wang, R.F., Leighton, C., and Siegel, R.A.. ACS App. Mat. Int., **1 (4)**, 888-893, 2009

[28] Lopez, C.A., Fleischman, A.J., Roy, S., and Desai, T.A.. Biomat., **27 (16)**, 3075-3083, 2006

[29] Alaerts, J.A., De Cupere, V.M., Moser, S., de Aguilar, P.V.B., and Rouxhet, P.G.. Biomat., **22 (12)**, 1635-1642, 2001

[30] Kuiper, S., van Rijn, C.J.M., Nijdam ,W., and Elwenspoek, M.C.. J. Membr. Sci., **150 (1)**, 1-8, 1998

[31] Nabe, A, Staude, E., Belfort, G.. J. Membr. Sci., **133**, 57–72, 1997

[32] Yang, Q., Xu, Z.-K., Dai, Z.-W., Wang, J.-L., and Ulbricht, M.. Chem. Mater., **17,** 3050–3058, 2005

[33] Wavhal, D.S., and Fisher, E.R.. Desalination, **172 (2)**, 189-205, 2005

[34] Wavhal, D.S., and Fisher, E.R.. Langmuir, **19 (1)**, 79-85, 2003

[35] Wavhal, D.S., and Fisher, E.R.. J. Membr Sci., **209 (1)**, 255-269, 2002

[36] Wang, P., Tan, K.L., Kang, E.T., and Neoh, K.G.. J. Membr. Sci., **195 (1)**, 103-114, 2002

[37] Xu, Z.-K., Wang, J.-L., Shen, L.-Q., Men, D.-F., and Xu, Y.-Y.. J. Membr. Sci., **196,** 221–229, 2002

[38] Miller, J.R., and Koros, W.J.. Sep. Sci. Technol., **25,** 1257–1280, 1990

[39] Kim, K.S., Lee, K.H., Cho, K., and Park, C.E.. J. Membr Sci., **199**, 135–145, 2002

[40] Winkler, B.H., and Baltus, R.E.. J. Membr. Sci., **226,** 75-84, 2003

[41] Lee, S.W., Shang, H., Haasch, R.T., Petrova, V., and Lee, G.U.. Nanotechnology**,** **16**, 1335–1340, 2005

[42] Barbani, N., Giusti, P., Lazzeri, L., Polacco, G., and Pizzirani, G.. J. Biomat. Sci.-Polymer Ed. **7** (**6)**, 461-469, 1995

[43] Barbani, N., Cascone, M.G., Giusti, P., Lazzeri, L., Polacco, G., and Pizzirani, G.. J. Biomat. Sci.-Polymer Ed., **7** (**6),** 471-484, 1995

[44] Bhangale, H.R.. *Investigation of Filtration Properties of Collagen on Silicon Wafer* (Cornell University, 2001)

[45] Norman, J., and Desai, T.. Ann. Biomed. Eng.**, 34** (**1),** 89-101**,** 2006

[46] Mata, A., Boehm, C., Fleischman, A.J., Muschler, G.F., and Roy, S.. Intl. J. Nanomed., **2 (3)**, 389-406, 2007

[47] Nagata F.. J. Electron Micro. **42 (6)**, 371-377, 1993

[48] http://www.2spi.com/catalog/grids/silicon-nitride.php

[49] Turner, J. N., Szarowski, D. H., Shain, W., Buttle, K., Tivol, W. F., Bagle, H.[sic], Spence, A. J., Retterer, S., Lapek, L.[sic], Richards, T., Isaacson, M., and Spencer, M.. Microsc. Microanal., **8,** 1118-1119, 2002

[50] Lepak, L.A., Richards, T., Guillen, N., Caggana, M., Turner, J.N. and Spencer, M.G.. Proc. Mater. Res. Soc., **752,** 321-326, 2002

[51] Russo, A.P., Retterer, S.T., Spence, A.J., Isaacson, M.S, Lepak, L.A., Spencer, M.G., Martin, D.L., MacColl, R. and Turner, J.N.. Sep. Sci. Tech. **39 (11)**, 2515–2530, 2004

[52] Mohamed, H., Russo, A. P., Szarowski, D. H., McDonnell, E., Lepak, L. A., Spencer, M. G., Martin, D. L., Caggana, M., and Turner, J. N.. Sep. Sci. Technol., **42,** 25 – 41, 2007

[53] Duffy, D.C., McDonald, J.C., Schueller, O.J.A., and Whitesides, G.M.. Anal. Chem., **70 (23)**, 4974-4984, 1998

[54] http://www.bdbiosciences.com/ptProduct.jsp?prodId=363079

[55] Fleischer, R.L., Alter, H.W., Walker, R.M., Furman, S.C., and Price, P.B.. Science **178 (4058)**, 255-263, 1972

[56] Apel, P.. Radiation Meas., **34 (1-6)**, 559-566, 2001

[57] Apel, P.Y., Blonskaya, I.V., Dmitriev, S.N., Orelovitch, O.L., and Sartowska, B.. J. Membr. Sci., **282 (1-2)**, 393-400, 2006

[58] http://www.bdbiosciences.com/external_files/dl/doc/manuals/live/web_enabled/BDFalconCellCultureInserts_pug.pdf

[59] http://catalog2.corning.com/Lifesciences/media/pdf/transwell_guide.pdf, 5

[60] Kim, K.J., and Stevens, P.V.. J. Membr. Sci., **123 (2)**, 303-314, 1997

[61] Sidhu, P.S., and Cussler, E.L.. J. Membr. Sci., **182 (1-2)**, 91-101, 2001

[62] Yaroshchuk, A., Boiko, Y., and Makovetskiy, A.. Langmuir, **25 (16)**, 9605-9614, 2009

[63] Sistiabudi, R., and Ivanisevic, A.. J. Phys. Chem. C, **111 (31)**, 11676-11681, 2007

[64] Baker, H.R., Merschrod, E.F., and Poduska, K.M.. Langmuir **24,** 2970-2972, 2008

[65] Monkawa ,A., Ikoma, T., Yunoki, S., Ohta, K., and Tanaka, J.. Mat. Lett.**, 60** (**29-30),** 3647-3650, 2006

[66] http://www.whatman.com/PRODAnoporeInorganicMembranes.aspx

[67] Hernandez, A., Martinez, F., Martin, A., and Pradanos, P.. J. Coll. Interface Sci., **173,** 284-296, 1995

[68] Jessensky, O., Muller, F., and Gosele, U.. Appl. Phys. Lett., **72**, 1173–1175, 1998

[69] J.N. Turner, personal communication

Chapter 4: Characterization of Collagen Thin Films on Anodically Etched Alumina

4.1 Introduction

Chapter 3 discussed the search for an appropriate support substrate for collagen thin films for molecular filtration applications. Among the substrates tested, only alumina met the preliminary criteria to merit further consideration. To evaluate the potential of the collagen-on-alumina system for commercial filtration applications, we characterized several physical, chemical, and filtration performance properties of the membranes.[1] The physical structure of the surface was determined by SEM and AFM; the surface chemistry by FTIR and zeta potential determination; wettability by contact angle measurements; and filtration performance by pressure-driven pure water flux and permeability. Each of these measurements was performed at collagen depositions ranging from one to nine layers. As coverage was increased, changes in membrane structure were monitored and correlated with changes in filtration performance.

4.2 Experimental Procedures

4.2.1 FTIR

FTIR spectroscopy was employed to identify the chemical functional groups present at the surface of the membranes. An ATR-FTIR spectrometer (Bruker Vertex 80v) was used, with a detector cooled by liquid nitrogen to reduce baseline noise. Membrane pieces were mounted on the ATR diamond crystal, and the sample chamber pumped down to a base pressure of 2.30 hPa to eliminate absorbances from water vapor and CO_2 in the air. All spectra were referenced against that of untreated alumina, which was automatically subtracted. Each spectrum is the average of 256 IR

scans, taken at a resolution of 4 cm^{-1} with an incident angle of 45°. This angle of incidence corresponds to an IR penetration depth of 2.0-4.36 μm.

4.2.2 SEM

The surface topography and cross sectional morphology of the unmodified and modified membranes were obtained at various magnifications by SEM (Zeiss/Leo 1550). To obtain cross-sections, the membranes were cracked at the edges, and the cracks were carefully propagated across the diameter of the membrane. Prior to imaging, the samples were sputter-coated (edge-on, in the case of the cross-sectional images) with a gold-palladium alloy to an approximate thickness of 5 nm. A low beam voltage (2 keV) was used to minimize damage to the samples.

4.2.3 AFM

AFM images were obtained in air with a PicoPlus Microscope (Molecular Imaging, Inc.). Silicon cantilevers (model AC160TS, Asylum Research, Inc.) with a nominal resonance frequency of 300 kHz and a force constant of 42 N/m were used in ACAFM mode. Image processing and statistical analysis (in particular, RMS surface roughness) was performed using the open-source shareware Gwyddion 2.1 (http://gwyddion.net/). At least 3 different areas were imaged on each sample, and typical values were reported.

4.2.4 Contact Angle

The water contact angle was measured on each sample, to quantify its hydrophilic vs. hydrophobic behavior. A Phoenix 150 goniometer, (Surface & Electro-Optics Corporation, South Korea, supplied by Scientific Gear LLC, VA) was used. This instrument is equipped with a sample stage, a syringe holder, and a CCD camera.

Measurements were done by the sessile drop method, using a static air/water contact angle.[2] Images of the drops were captured, and both the left- and right- side angles were measured by the software. When necessary, the 'tangential method for low angles' was used. At least 4 measurements were averaged for each sample.

4.2.5 Zeta potential

The ζ potential of the membranes was measured using an electro kinetic analyzer (EKA, Brookhaven Instruments, Holtsville, NY). In an asymmetric clamping cell (Anton Paar, Graz, Austria), the test membrane was held tightly between a grooved poly(methyl methacrylate) (PMMA) spacer and a back plate, with the active side facing the spacer. 1mM KCl, whose pH is about 5.5±0.2, was used as the electrolyte solution driven across the membrane. A pressure difference, ΔP, was applied across the membrane at zero current, while ΔE, the electrical potential difference, was measured between two Ag/AgCl electrodes at opposite ends of the clamping cell. The streaming potential, ν, was then calculated using the equation,

$$\upsilon = \frac{\Delta E}{\Delta P}$$

Finally, the ζ potential was calculated using the Fairbrother-Mastin equation. However, due to the configuration of the experimental system, this value was actually the combined zeta potential of the sample and the PMMA grooved spacer. To correct for this, the zeta potential of the sample membrane was calculated using an equation derived from Helmholtz-Smoluchowski equation (equation 2), where ζ_{Test} is the ζ potential of the sample membrane, ζ_{Avg} is the effective ζ potential measured with the membrane pressed against the spacer, and ζ_{Spacer} is the ζ potential of the PMMA spacer surface.[3]

$$\zeta_{Test} = 2\zeta_{Avg} - \zeta_{Spacer}$$

The reported values are the average of the ζ potentials determined in both flow directions with at least two membranes.

4.2.6 Pure Water Flux and Permeability

To quantify one aspect of actual filtration performance, the pressure-driven flux and permeability of water through the membrane was measured. A dead-end stirred cell setup was used, which consisted of a filtration cell (model 8050, Millipore Corp., Bedford, MA) with a total cell volume of 50 ml and an effective membrane area of 13.4 cm^2. The stirred cell was connected to a 20 L stainless reservoir containing ultra pure water. The stainless steel reservoir was pressurized with dry nitrogen. The membranes were hydraulically compacted by applying a pressure of 40 psi for at least one hour prior to flux measurements, to ensure that the system had reached steady state. After measuring the pure water flux at 40 psi, the applied pressure was reduced, and the fluxes were again measured at 30, 20 and 10 psi. The permeability was calculated by dividing the flux by the change in applied pressure with the following formula.[4]

$$L_p = \frac{J_v}{\Delta P}$$

where, L_p is the water permeability, J_v volumetric flux and ΔP change in transmembrane pressure. L_p is expressed in $(m^3/m^2.s)/kPa$ (or) m/s/kPa. The pure water flux measured at 10 psi was defined to be J_w.

4.3 Discussion

4.3.1 FTIR

The IR spectra of sulfonated alumina samples with 0, 1, 3, 6, and 9 layers of collagen are displayed together for easy comparison in figure 4.1, with each spectrum

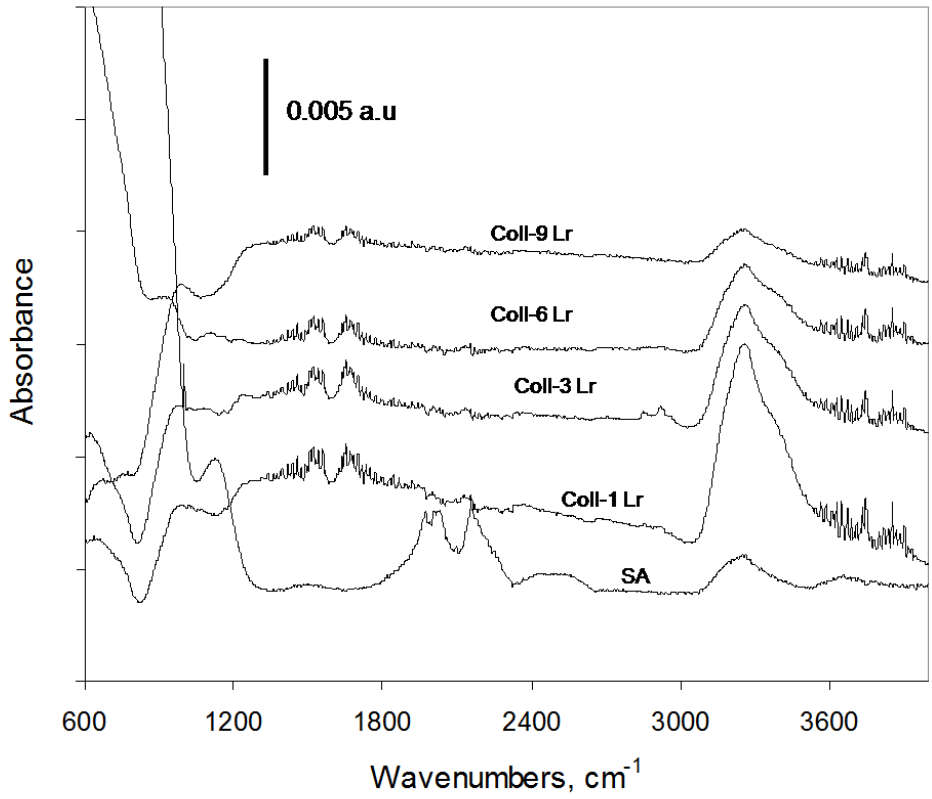

Figure 4.1 Infrared spectra of collagen films on sulfonated alumina.

offset along the y-axis for improved clarity. In the sulfonated alumina sample, the prominent peak near 1000-1200 cm^{-1} is in the expected range for sulfone groups, signaling the incorporation of $–SO_3$ groups into the alumina surface. The broad peak near 3100 cm^{-1} indicates increased hydroxylation of the surface, relative to untreated alumina. Both peaks remain stable for approximately one week after sulfonation, and gradually decay to baseline values at 2-3 weeks. This suggests that the surface chemical modification slowly deteriorates over time. As a consequence, sulfonated alumina membranes were never again stored for longer than one week prior to the deposition of collagen. Yet during the first week following sulfonation, both of these chemical changes herald a more hydrophilic surface, and thus the possibility of an improved affinity for collagen.

This is collagen affinity is confirmed by an analysis of the spectra of the collagen-spun samples.[2,5,6] All the collagen containing membranes have qualitatively similar spectra. Amide absorbances, which appear at ~1560 cm^{-1} and ~1664 cm^{-1}, are characteristic of peptide bonds, confirming the presence of protein. The lysine-glutarladehyde crosslinks within fibrils would also be expected to absorb in this wavelength range. However, being much fewer in number than the peptide bonds, they do not contribute significantly to the intensity. The broad hydroxyl absorbances in the 3000-3200 cm^{-1} range are indicative of the hydroxyproline. The intensity trends may at first seem paradoxical; as collagen is added, the amide absorbances do not change appreciably, while the hydroxyl peaks actually become less prominent. Both trends are consistent with the incorporation of the monomers into fibrils at increased collagen coverage (see sections 4.3.2 and 4.3.3, below). Most hydroxyl groups in the interior of a fibril are hydrogen bonded to other hydroxyls on adjacent monomers, decreasing their infrared absorption relative to unbonded hydroxyls at the fibril surface. As more layers of collagen are added and fibrils grow larger, fibril volume grows faster than surface area. Thus, a larger fraction of the hydroxyls become confined in hydrogen bonded, weakly absorbing states, reducing the overall absorbance at 3000-3200 cm^{-1}. In contrast, the rearrangement of monomers into fibrils has much less effect on the geometric arrangement of the peptide bonds; either way, the entire surface of the sample is covered in peptide bonds. Therefore, the amide peak intensities change very little as collagen layers are added.

4.3.2 SEM

FTIR provides insights into the chemical functionalization of a surface independent of its topography. SEM, on the other hand, can image the topography of

a surface from millimeter down to nanometer scales,[2] free of complications from probe-surface chemical interactions.

In section 3.11, and in particular figure 3.20, the surface structure of the alumina substrates themselves, prior to the deposition of collagen was discussed. Figure 4.2 illustrates, both in cross-section and viewed from above, the changes that the membrane surface undergoes as successive layers of collagen are spun on. In fact, when the first layer of collagen is added, the surface appears strikingly featureless relative to the sulfonated alumina. Nearly all of the holes in the substrate have been spanned. As can be seen from the scale bar, those that remain (black spots) are far smaller than the 200 nm diameter typical of the sulfonated alumina; they appear, coincidentally, to be similar in size to the holes in the untreated alumina. The previously highest points on the sulfonated alumina surface appear to rise above the collagen film (white spots). This suggests that the collagen film is preferentially settling into the topographic valleys and avoiding the peaks on the rough substrate surface. It also suggests that the collagen film must be very thin – or, at least, have a thickness on the order of the typical peak-to-valley height of the sulfonated alumina surface. This was confirmed by imaging the collagen film edge-on and measuring the thickness of the cross section at just over 35 nm. This is equivalent to 15-20 stacked monolayers of collagen monomers. Although this suggests that the collagen is abundant, the featurelessness of the images provides evidence that there has been little, if any, aggregation into fibrils.

At three layers of collagen deposition, some structure begins to appear in the collagen films. Short nanofibrils, most of them less than 200 nm long and 20 nm wide, are scattered across the surface, against a background that appears to still primarily consist of monomers. These nanofibrils appear to dominate the topographic landscape, such that the white ‘peaks’ from the substrate are no longer clearly visible.

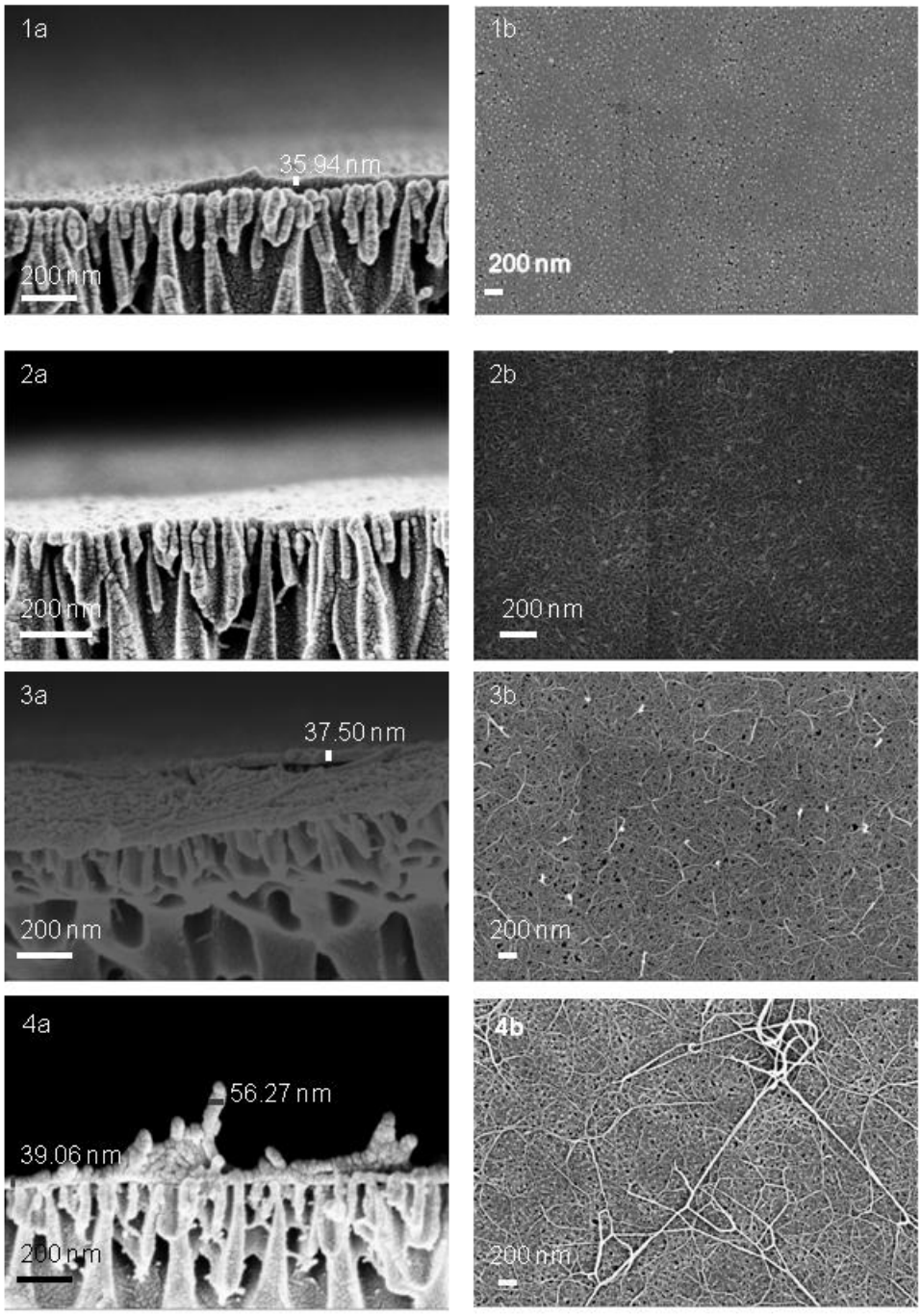

Figure 4.2 SEM images of collagen films on sulfonated alumina. The collagen coverages are 1 layer (1a,b), 3 layers (2a,b), 6 layers (3a,b) or 9 layers (4a,b). Both cross-sections (1a, 2a, 3a, and 4a) and top views (1b, 2b, 3b, and 4b) are shown at each coverage.

The overall thickness of the collagen layer has not significantly changed, however. There is essentially no visible difference between the cross sections of the 1- and 3-layer samples.

At six layers, fibrils become even more prominent on the surface – longer, thicker, and more numerous, against what still appears to be a largely monomeric background. A handful of short, thick structures may be intersections of or small aggregates of fibrils. Most fibrils, however, appear to be approximately 1 micron in length, and on average are spaced 1-2 microns apart. The diameter of these small fibrils can be estimated from the cross-section, where several are visible on the top surface, near the cleaved edge. These fibrils appear to have a diameter roughly half of the thickness of the film – around 15-20 nm. At 37.5 nm, the thickness of the collagen film itself is essentially unchanged from that of the 1- and 3- layer samples. Any additional collagen which is being incorporated into the film is being packed tightly into fibrils instead of randomly 'hairball' packing as monomers. The denser packing allows more collagen to be incorporated into the film without significantly changing its thickness.

The nine layer samples continue the trend toward longer and thicker fibrils. Fibrils over ten microns long crisscross the surface, intersect, and branch into smaller fibrils. Fibrils comprise a much larger fraction of the total surface area than in previous samples, although they still appear to be superimposed on a monomer or nanofibril background. On average, the fibrils are much wider as well; from the cross section, their diameter was directly measured to be 56 nm – nearly double the thickness of the film, and three to four times the diameter of the fibrils on the 6-layer film. As before, the thickness of the collagen film barely changed at all – edging up by about the thickness of one monolayer of monomers, to 39 nm. This clearly continues the trend of the additional collagen being incorporated into larger fibrils,

changing the surface structure rather than the thickness of the film. This could be quite useful in cell culture applications, as a collagen film of a given thickness could be tailored with a surface structure favorable to a given cell type.

It should also be noted that the cross sections of all samples, regardless of coverage, show no evidence of collagen coating the walls of the alumina pores themselves. All of the collagen modification is acting at the surface of the membrane. Thus, from a theoretical perspective, if no changes were observed in the filtration behavior of the combined collagen-on-alumina system, this would provide strong evidence that bulk mechanisms dominate the filtration process in alumina, whether or not collagen is present. If changes are observed, these must be explainable by surface filtration mechanisms. From a practical perspective, the absence of collagen from the pores has two positive consequences for the membrane performance. First, had collagen deposited in the pores, it would have physically narrowed them, reducing the flux and increasing the likelihood of fouling. Second, the ability to tailor surface properties independently from bulk properties allows an engineer to achieve a broader range of possible performance specifications, potentially making the collagen-on-alumina system useful for a wider array of applications.

4.3.3 AFM and Surface Roughness

Over distance scales of tens of microns or greater, SEM is the best means to observe topography. But over smaller areas, of only a few square microns, AFM provides higher resolution images of topography than SEM. The heights of surface features can be directly measured with atomic resolution in z, while the lateral size of features can easily be resolved to a few tens of nanometers in xy. In the last 20 years, many applications of AFM have been developed to study problems in filtration.[7]

AFM has even been used in a fluid ambient to observe the assembly of collagen into fibril films in real time.[8]

In the present work, AFM images are used for quantitative analysis, to determine the root mean square (RMS) roughness of a surface over areas of a few square microns. This is a useful both in terms of an improved theoretical understanding of the behavior of the system and for practical applications, as this surface area is comparable to both the contact area of a water droplet used to measure the contact angle, and to the size of a typical mammalian culture cell.

Unfortunately, straightforward comparisons of RMS roughness are only possible among samples with varying levels of collagen deposited on the surface. It is not possible to quantify the RMS roughness of either an unmodified alumina surface, or a sulfonated alumina surface, in a manner that would make the values directly comparable either to collagen-coated samples or to each other. Since the pores in the alumina substrate go essentially straight down into the substrate, the z piezos will extend the tip as deep into the holes as it can stretch – essentially, the total fraction of the surface occupied by pores would appear as a 'bottomless pit'. This imaging artifact will be amplified on the sulfonated alumina surface, where the pores are much larger – leading both to a larger fraction of the surface actually being 'bottomless pits', and to wider pits allowing the AFM tip to penetrate deeper into the surface, making the 'bottomless pits' artificially appear deeper. If the 'bottomless pits' are averaged in with heights on the actual alumina surface, the numbers will suggest that the surface is far rougher than any collagen molecule approaching the surface would actually experience. On the other hand, if these pixels are excluded, the actual surface area being averaged over will be much less than in a collagen-coated sample with the same lateral scan dimensions – again, making a direct comparison difficult.

Fortunately, as can be seen in figure 4.3, even at a one layer of collagen, the

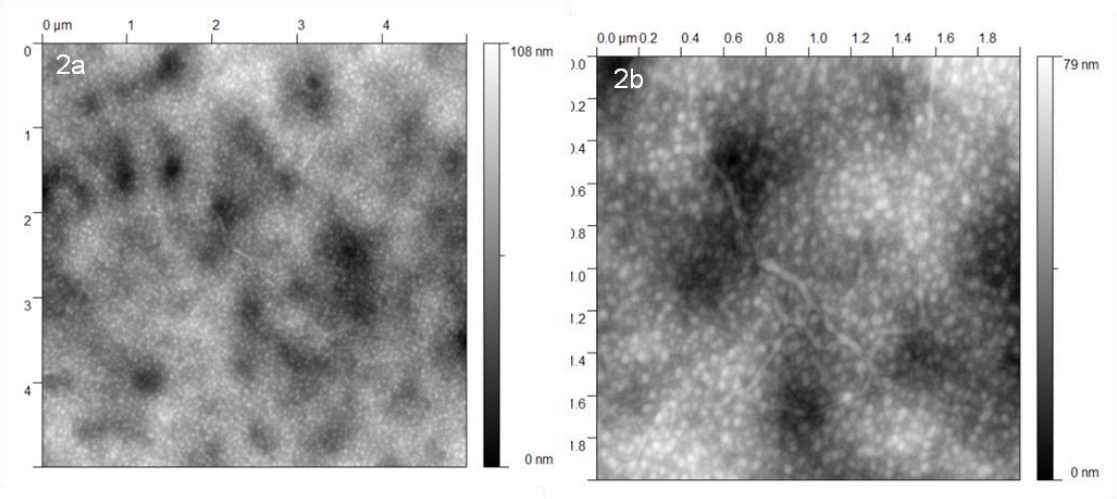

Figure 4.3 AFM image of one layer of collagen on sulfonated alumina

holes in the alumina are spanned. Few, if any, truly bottomless pits remain. Quite a bit of the alumina surface is visible, protruding through the collagen film as white dots. Thus, at least in terms of RMS roughness, the one layer film may represent a good approximation to that of the sulfonated alumina surface. At this low coverage, nearly all collagen appears to be in the form of monomers. As one steps up in coverage to the three layer film (figure 4.4), the increase in RMS roughness is quite

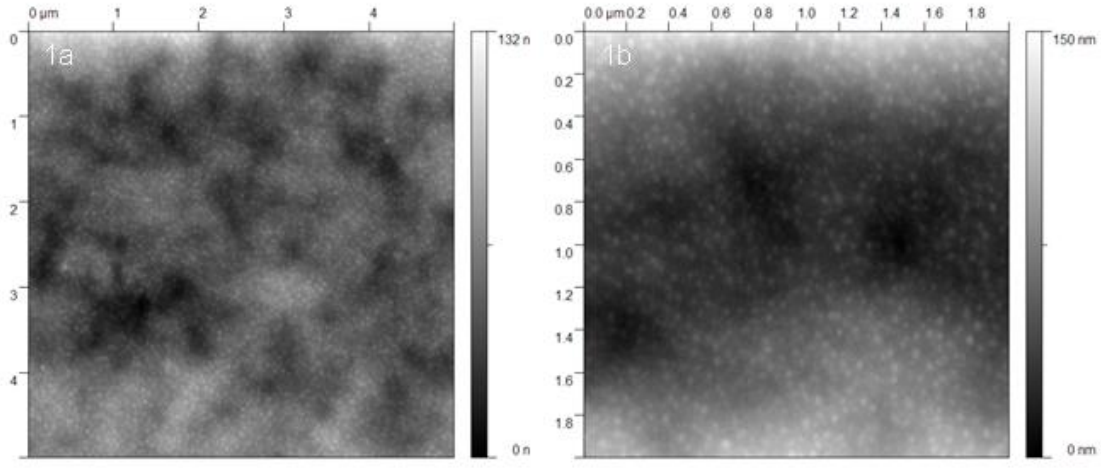

Figure 4.4 AFM image of three layers of collagen on sulfonated alumina

small. By eye, the images also appear to be very similar to a single layer, with the landscape dominated by monomers. Yet a few minor differences have begun to creep in; a few scattered nanofibrils, perhaps a micron long, are visible in both the two and five micron square images.

More dramatic changes are in store as one proceeds to the 6 layer sample. In the two micron image, nanofibrils are beginning to be quite numerous, and are enmeshed in a fine network. Over five microns, a large aggregate of fibrils is, for the first time, visible in the lower left corner. This pattern was typical at several points on the sample surface; it was still easy to find two micron areas of the surface free of large fibril aggregates, but quite difficult to find five micron areas without at least one cluster. These trends can clearly be seen in figure 4.5.

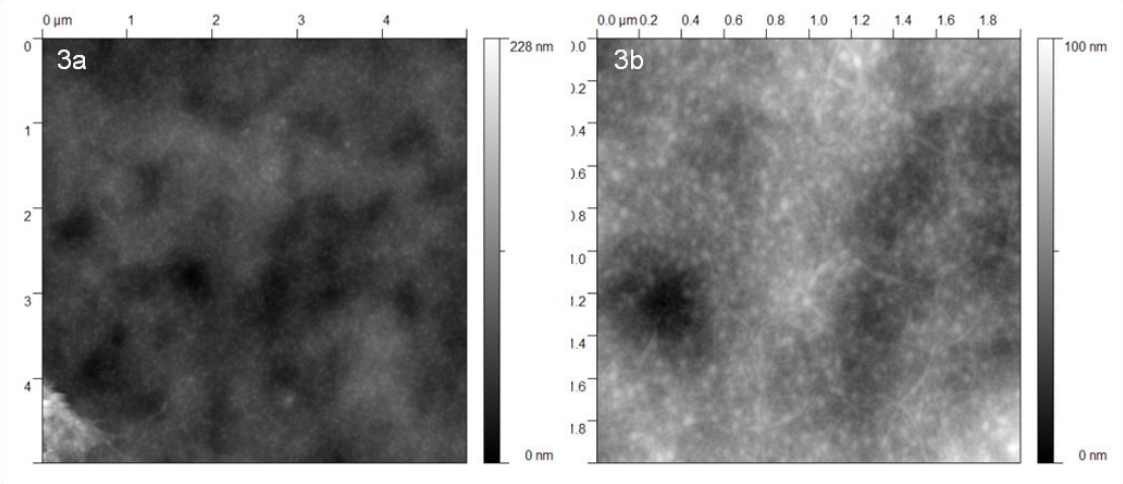

Figure 4.5 AFM image of 6 layers of collagen on sulfonated alumina

Finally, in figure 4.6, in the 9 layer sample, one sees the full progression to a surface dominated by nanofibrils even at a scale of two microns. Further, it is all but impossible to find a two micron square, much less a five micron area, which does not contain at least one larger fibril aggregate. Large fibril aggregates become much morerprominent in the topography over larger length scales, with networks of nanofibrils clearly visible in between.

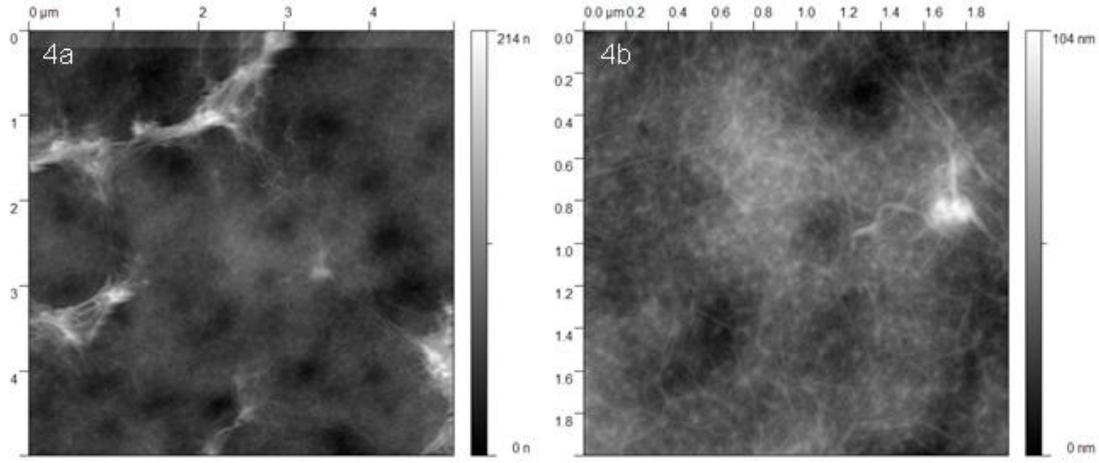

Figure 4.6 AFM image of 9 layers of collagen on sulfonated alumina

These qualitative trends are borne out quantitatively in the measurements of RMS roughness (table 4.1). Over a large surface area, five microns square, the RMS

Table 4.1 RMS roughness of collagen films at varying coverages

	RMS Roughness (nm)	
number of layers	2 x 2 um	5 x 5 um
1	9.99	11.34
3	12.07	12.29
6	10.5	15.4
9	9.86	22.7

roughness is nearly constant at low coverage, with a clear trend emerging toward increasing RMS roughness at higher collagen coverage. At 3 layers and below, the films consist primarily of monomers and thin nanofibrils. Beyond 3 layers, as collagen continues to be added, longer and thicker aggregates of fibrils become more and more prominent in the film structure, and they begin to dominate the topography. At shorter length scales, the RMS roughness is dominated by nanofibrils, which have similar structures and size distributions, on all collagen surfaces. There is very little difference in the RMS roughness of the two micron square areas between the 1, 3, 6, and 9 layer of collagen samples, at least in regions with relatively few large fibrils.

One could thus conceptualize all the collagen samples as having a fairly constant 'background' structure, where the first few monolayers of collagen film growth on alumina are in the form of monomers and nanofibrils, while any subsequent growth of collagen-on-collagen appears as the formation of larger fibrils upon this background.

4.3.4 Contact Angle

FTIR spectroscopy probes the chemical functionality of a surface, while providing no information about its physical structure. SEM and AFM, by contrast, directly image the surface topography and roughness, but yield little chemical information. The water contact angle demonstrates the interplay of both,[9] as one directly observes how strongly an aqueous solution physically interacts with a sample surface. In terms of surface chemistry, a substrate that provides plentiful opportunities for hydrogen bonding – for example, a hydroxyl terminated surface – allows a drop of water to easily spread out across the surface and display a low contact angle. On substrates with a less polar termination, such as Teflon, water hydrogen bonds to itself rather than spread out on the surface, leading to a nearly spherical drop and a high contact angle. In terms of geometry, a rough surface creates additional surface area for a drop to adhere to, allowing it to "sink in" to the surface. This results in a lower contact angle than would be present on a smooth surface with similar chemistry.

As can be seen in figure 4.7, both untreated and sulfonated alumina displayed low contact angles in the range of 30^{o}-50^{o}, indicating fairly hydrophilic surfaces. This is not surprising, given that most of the chemical bonds at the surface – namely Al-O, Al-OH, and, on the sulfonated alumina, Al-O-SO_3 – are somewhat polar. The decrease in contact angle following the sulfuric acid treatment is consistent with both the increased hydroxylation and sulfonation observed in the IR, and the rougher topography observed in the SEM.

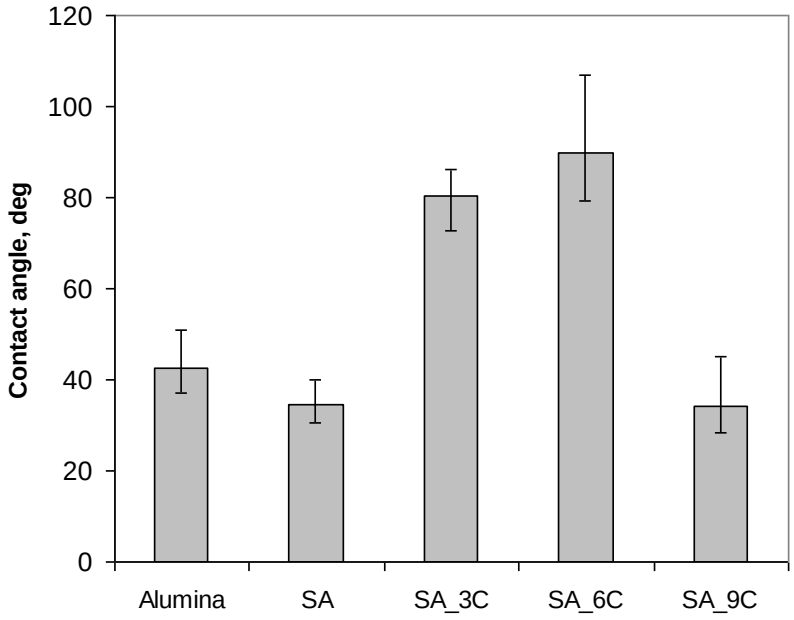

Figure 4.7 Contact angles of water droplets on alumina and collagen substrates

When 3 layers of collagen are added to the surface, the contact angle abruptly increases to near 80^{o} – barely hydrophilic at all. This is partly explained by the chemistry of collagen. Although a large fraction of the amino acid side chains are hydrophilic hydroxyprolines, a significant fraction of side chains are somewhat more hydrophobic. The surface is no longer terminated entirely with polar functional groups, so the contact angle should increase. The other part of the explanation, topography, also favors a higher contact angle. As collagen initially spans the pores in the alumina substrate, water no longer has the opportunity to partially wet the pore entrances; the surface has, in effect, become smoother.

At higher collagen coverages, the surface chemical functionalization will remain similar even as more collagen is added. Thus, differences in contact angle among different numbers of collagen layers primarily reflect changes in topography. Between 3 and 6 layers of collagen, the increase in roughness is quite small, and not surprisingly there is considerable overlap in the error bars for their respective contact

angles. In the case of the 9 layer samples, the dramatic decrease in contact angle coincides with an equally dramatic increase in the abundance of large fibrils, and consequently large increase in surface roughness.

So far, the discussion has centered on how surface topography contributes to the observed contact angle. Yet to gain a deeper understanding of how collagen films develop, it is equally instructive to invert the question: How does the water contact angle influence the subsequent development of the topography? The correlation between this contact angle data and the observed density of large fibrils is reasonably consistent with the observations of Elliott *et.al.*.[10]. In that study, large fibrils were largely absent on hydrophilic surfaces with contact angles below 63^{o}, and were observed with greatest density on surfaces with 78^{o}-87^{o} contact angles. In the present work, both untreated and sulfonated alumina surfaces had contact angles well below the 63^{o} threshold. As expected, few if any large fibrils were ever observed under SEM or AFM when a single layer of collagen was deposited on either of these surfaces. Monomers and nanofibrils dominated. Both the 3- and 6-layer surfaces, by contrast, were observed to have contact angles within the optimal range for large fibril formation. If one were to conceptualize the 6-layer sample as additional collagen deposited on a substrate with a contact angle equivalent to the 3-layer sample, and the 9-layer sample as additional collagen added to a substrate with the contact angle of a 6-layer sample, then one would expect a much greater density of large fibrils to be observed in the 6- and 9-layer samples. This is indeed the case.

4.3.5 Zeta Potential

The characterizations discussed thus far address membrane performance primarily in terms of the physical and chemical contributions to the membrane wetting behavior – considerations which apply to any filtrate, whether electrically neutral or

charged. If particles in the filtrate are charged, then electrostatic interactions between the filtrate and the membrane must also be considered. Opposite charges may cause strong enough attractions to noticeably increase fouling and shorten the useful life of the membrane.[11] Like charges may lead to repulsion between membrane and filtrate sufficient to reject passage,[12] even when an otherwise identical neutral membrane is demonstrated to pass the particle.[13]

Zeta potential is an indirect measurement of surface charge. It quantifies the surface charge-related rejection behavior of an electrically insulating membrane, and may be calculated from either electroosmotic or electrokinetic measurements. In electroosmtic flow, an electrical potential is applied across a membrane to induce an electrolyte to physically flow across, while the pressure or flow rate is measured. Electrokinetic measurements do the opposite – a known pressure is applied to drive an electrolyte across a membrane, creating a voltage (or current) which is measured. The electrokinetic approach was used in the present work.[14]

Anodically etched alumina is an amphoteric oxide, which is reported to have a positive surface charge below a pH 8.[15] As is illustrated in figure 4.8, this positive charge is confirmed by a measured streaming potential of 27±4 mV across the untreated alumina membrane. This is constistent with values observed by Winkler and Baltus. The zeta potential increases only slightly as the membrane is treated with sulfuric acid.

The deposition of collagen on the surface can be expected to significantly change the zeta potential of the alumina membranes.[16] Biological molecules often have fairly complicated charge distributions, with both positive and negative charges simultaneously present at fixed sites on the molecular surface. Many of these charges are pH-dependent, with the side chains of different amino acids having different. pkAs. This complex charge distribution makes it difficult to model the local

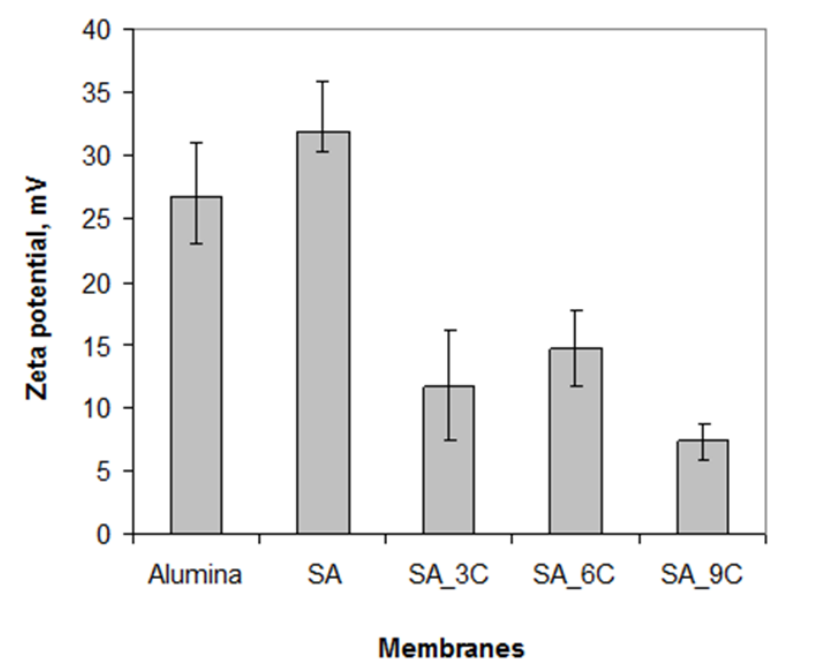

Figure 4.8 Zeta potential of alumina and collagen-coated membranes

electrostatic interactions of collagen molecules with each other, the alumina surface, or electrolytes in solution. At best, a molecular-level average of these charges may be quantified as the isoelectric point. At a solution pH above the isoelectric point, the collagen will have a net negative charge; at lower pH, it will be positively charged. Unfortunately, the isoelectric point of collagen reported in the literature varies widely, depending on species and tissue type [6,17,18].

Even in the absence of knowledge of the exact isoelectronic point of collagen, a few generalizations can be made about the effect on zeta potential of adding collagen to the alumina surface. Collagen has been demonstrated, by SEM, to form a nearly continuous film approximately 35-40 nm thick. As such, one would expect the surface charges on the underlying substrate to be somewhat masked, and the observed surface charge to reflect the electrical charges on the amino acid side chains of the collagen itself. This almost certainly would result in a change of the charge magnitude; in principle, if collagen were of the opposite charge to alumina, it could even lead to a

change of sign. Given that some fraction of the side chains are nonpolar, in contrast to the entirely polar alumina surface, one would also expect the absolute value of the charge on collagen to be smaller, whatever the sign. This is indeed observed. Referring again to figure 4.8, the surface charge decreases dramatically to 12±4 mV upon adding 3 layers of collagen. A substantial overlap of the error bars makes it unclear whether the surface charge actually changes between 3 and 6 layers, as the transition from nanofibrils to large fibrils begins. However, the trend toward a decreased surface charge clearly resumed upon reaching 9 layers, as the ζ potential to 7±1mV. Overall, as the number of layers of collagen increased, the positive surface charge decreased.

There are several possible reasons for the decreased surface charge, in addition to those already suggested. In 2005, similar observations of decreased surface charge with increased film thickness were made by Zhang *et al* [19] in the development of multi-layer composite films of collagen and hyaluronic acid. However, the explanation offered for the decreased charge in this system – overcompensation of the positive charge on collagen by the negative charge hyaluronic acid – is unlikely to be true in the collagen-on-alumina system, since no negatively charged component is intentionally incorporated into the film. Unintentional adsorption of excessive chloride ions from the KCl electrolyte is possible, and could act according to this mechanism. An alternative (or perhaps complementary) explanation involves the swelling that collagen films undergo upon hydration. The swelling of the film is likely to be greater as more layers of collagen are added, thus decreasing the charge density. The effect of swelling on thickness in the fully hydrated system is obscured in the SEM measurements, as the films are necessarily dehydrated under vacuum. Quantifying the swelling of hydrated collagen films would require lithographic patterning, followed by AFM in fluid, to definitively settle the question. Conversely, if swelling should prove

to be insignificant, yet another possible explanation for the layer-dependent reduction in zeta potential is a reconfiguration of charges exposed at the surface as the nanofibrils aggregate into large fibrils. Once again, a variation of scanned probe microscopy – either chemical force microscopy (using an AFM tip functionalized to have a charged functional group at the tip) or Kelvin probe (to make an electrical potential map of the surface) – offers the best hope of resolving the issue.

In any case, a reduced positive charge at the membrane suface should disfavor the adsorption of several important biomolecules, in particular DNA and BSA, which are negatively charged at physiological pH.[20,21] This should reduce fouling of the membrane, and prolong its useful lifetime.

4.3.6 **Pure water permeate flux and permeability**

The physical, chemical, and electrical properties of the collagen-on-alumina summarize its general behavior as a substrate. For the more specialized application of filtration, other figures of merit must be considered in addition. Among these are the flow rate of an aqueous solution across the membrane at a given applied pressure – the pure water flux – and the variation of the flow rate with pressure – the hydraulic permeability. Both of these quantities, in general, depend on both the physical pore size and the surface wettability, as has been discussed at length above. Both pure water flux and permeability have been measured for the collagen-on-alumina system.

Figure 4.9 depicts the pure water flux values measured at 30 psi. The flux of 7×10^{-4} m/s across the untreated alumina membrane is comparable to values for commercially available microfiltration membranes. It is also pleasantly high, given the extremely small average pore size. After sulfonation, the flux across the membrane nearly doubled to 14×10^{-4} m/S. This not surprising, due to the large increase in pore size. The increase in pore size by itself is likely sufficient to account for the flux

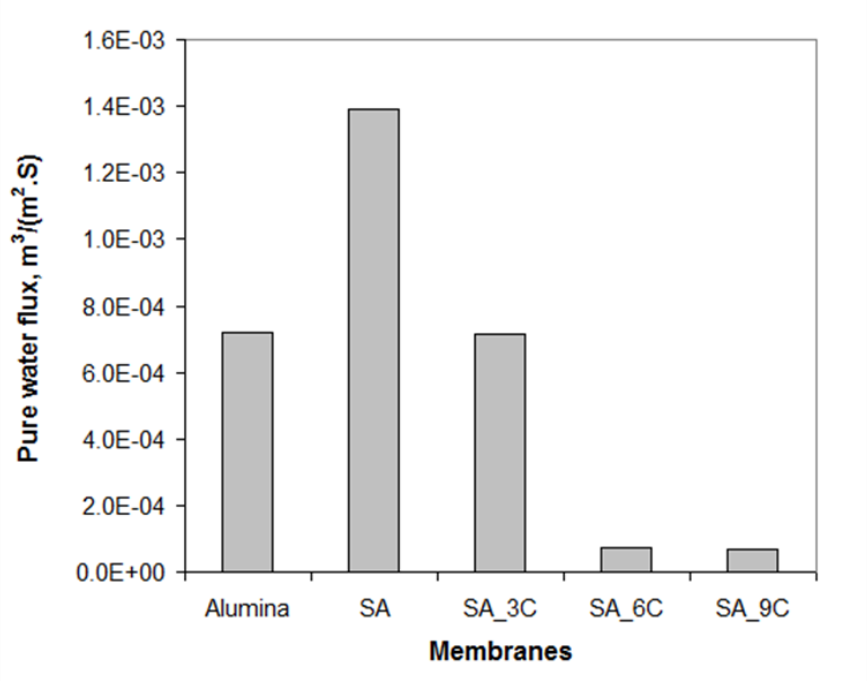

Figure 4.9 Pure water flux through alumina and collagen-coated membranes

increase, with no need to consider the change in hydrophilicity.

The effect of the addition of the initial layers of collagen upon flux would be difficult to predict *a priori*. The large extent of hydroxylation makes collagen very hydrophilic, which tends to increase the flux. Conversely, even at low coverages, the collagen partially spans most of the pores in the alumina, making them physically narrower, which should decrease the flux. In practice, the effect of the pore size dominated, as the flux decreased sharply to 7×10^{-4} m/S upon the addition of 3 layers. The observed flux was in fact quite similar to that of the unmodified alumina, and well within the microfiltration range. This similarity in flux appears in spite of the much smaller total surface area of open pores visible in the SEM in the 3 layer collagen sample. This is attributed to the greater hydrophilicity of collagen relative to untreated alumina.

Upon further deposition of collagen to 6 layers, the flux decreased by another order of magnitude to 0.7×10^{-4} m/s . The flux did not change measurably between 6

and 9 layers. One interpretation of these data builds upon the film structure postulated in the discussion of the AFM images. Between 6 and 9 fibrils, the transition from nanofibrils to large fibrils is complete; adding more collagen at this point simply increases the coverage of fibrils upon a constant monomer background. If the properties of the monomeric layer control the flux, it is likely that this is the minimum flux achievable in the collagen-on-alumina system, and will not significantly change as collagen is added beyond 6 layers. This analysis further implies that the monomer layer reaches its full development at some point between 3 and 6 layers of collagen deposition, since the flux still decreases over this range of coverage, but remains constant thereafter.

An alternate possibility is that, as with zeta potential, the observed trends in pure water flux may be partly explained by the water content of the collagen film upon hydration. Collagen films are typically modeled as semi-permeable membranes with a large water flux.[22,23] According to Free Volume Theory [24], the diffusivity is proportional to the water content of the membrane. As more layers of collagen are added, the number and size of fibrils increases, an indication that the film has become, on average, more densely crosslinked. As the crosslinking increases, the opportunities for water molecules to intercalate between monomers decreases. Thus, the overall water content of the film should go down, and the density of the film go up. The upshot will be a decrease in flux. The crosslinking density will approach some limiting value as fibrils become increasingly dominant on the surface. Thus, this model is also consistent with an asymptotic value approached by the flux at high collagen coverage. It is the model advanced by other researchers in bulk collagen and gelatin protein systems.[25,26]

Hydraulic permeability is simply defined as the pure water permeate flux normalized against pressure. In an ideal system, flux increases linearly with pressure. When this is the case, the permeability should display trends silimlar to the flux. As can be see in figure 4.10, this is indeed the case for collagen-on-alumina, at least up to

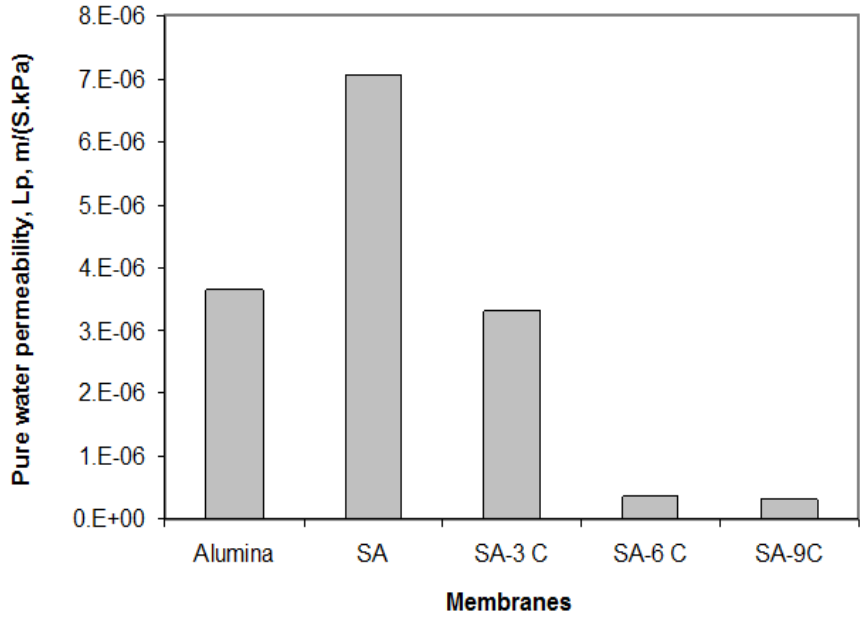

Figure 4.10 Hydraulic permeability of alumina and collagen-coated membranes working pressures of 40 psi. As with flux at 30 psi, the measured permeability of the sulfonated alumina membrane averaged over the entire range of applied pressures (7×10^{-6} m/s/kPa) was nearly twice that of the untreated alumina membrane (3.76×10^{-6} m/s/kPa). Adding collagen decreased the permeability, such that of the 3-layer collagen membrane was comparable to untreated alumina. The 6 and 9 layer collagen membranes were an order of magnitude less permeable than the 3-layer membrane.

As with flux, there are two possible explanations for this behavior. One is that the longer, wider, more densely packed fibrils in the more-layered films offered more resistance to fluid flow. The other is that the trend is really a linear decrease in flux as the monomer layer of the film reaches its peak density somewhere between 3 and 6

layers of collagen, followed by a constant permeability at higher collagen coverages, with the ever-growing mass of fibrils atop this monomeric layer not affecting the permeability. Measurements of the flux and permeability on 4- and 5- layer collagen samples would be the easiest means of distinguishing between these two scenarios.

While a theoretical understanding of the collagen-on-alumina system is ultimately needed to engineer membranes for specific applications, the performance of the membrane relative to current commecrial technologies must be considered when deciding how vigorously to pursue development of the technology. Alumina itself is somewhat fragile following sulfonation, with perhaps 20% of membranes cracking during the manual handling involved in collagen spinning and critical point drying. There is hope that this loss rate could be significantly reduced by automation in a commercial environment; in fact, nearly all surviving membranes displayed an excellent tolerance for applied hydraulic pressure over the range of 10 to 40 psi. Both the range of applied pressures and the range of resulting fluxes and permeabilities are typical of currently commercialized ultrafiltration membranes. Thus, in this respect, the collagen-on-alumina system is competitive with existing technologies.

4.4 Conclusions

The physical stucture and wetting behavior of collagen thin films on sulfonated alumina substrates was characterized. As the quantity of protein deposited on the substrate increased, the morphology of the collagen film changed from a relatively featureless film of monomers, through nanofibrils, to landscapes dominated by ever longer, wider, and more numerous fibril aggregates. While all collagen films were crosslinked with glutaraldehyde, reorientation of the monomeric collagen into fibrils only occurred at higher depositions. The surface roughness was nearly constant among low coverage (monomeric) films, but increased at higher coverages as fibrils

became more prominent. At small length scales, however, the surface roughness did remain constant in fibril-free areas. Taken together, these data suggest that the first few monolayers of collagen in intimate contact with the sulfonated alumina surface, remain monomeric regardless of collagen coverage. Only monomers several monolayers above the surface, in contact with other collagen, are free to reorient into fibrils.

In terms of surface chemistry, all collagen-containing membranes had qualitatively similar FTIR spectra, indicating similar chemical functionalities present at the surface regardless of the number of layers. The high water contact angle at lower depositions of collagen is thus more likely a consequence of surface fibril morphology than of chemistry. This morphology can be somewhat controlled, with little disruption of the filtration behavior, by controlling the amount of protein deposited. The decrease in zeta potential with increased collagen deposition could either be due to the reorientation of the surface chemical groups during fibril formation, or to charge compensation from the electrolytes in solution. In either case, the lower positive zeta potential of the collagen membranes is expected to be beneficial, by reducing fouling during biomolecular separation processes.

Following these theoretical characterizations, the observed structures were correlated with the performance of each membrane under commercially relevant conditions. Collagen-on-sulfonated alumina films displayed good stability under typical ultrafiltration pressures and excellent permeability under hydrodynamic conditions. As discussed above, the measured pure water flux and permeability could both be explained in terms of the membrane structure, in particular the pore sizes observed by SEM and AFM, and the hydrophilicity evidenced by the FTIR and the water contact angle. Varying the number of spin cast layers of collagen was, by itself, sufficient to control these parameters over a wide and experimentally useful range.

Regardless of the number of spin cast layers, the collagen films developed only on the surface of the alumina substrate, without penetration into the pores of the alumina bulk itself. By acting solely at the surface, the collagen film offered only minimal resistance to the transport of water and KCl solute across the bulk of the membrane. As a consequence, the transmembrane flux of the collagen-on-alumina system was only approximately an order of magnitude less than that of the unmodified alumina membrane – still well within a commercially useful range. The permeability of collagen-on-alumina membranes is similar to that of commercially available ultrafiltration membranes. Thus, these membranes are likely to prove suitable for biomolecular separations.

REFERENCES:

[1] Wyart, Y., Georges, G., Demie, C., Amra, C., and Moulin, P.. J. Membr. Sci., **315 (1-2)**, 82-92, 2008

[2] Yu, H.-Y., Xu, Z.-K., Yang, Q., Hu, M.-X., and Wang, S.-Y. J. Membr. Sci. **281,** 658-665, 2006

[3] Walker, S.L., Bhattacharjee, S., Hoek, E.M.V., and Elimelech, M. Langmuir **18,** 2193-2198, 2002

[4] Mehta, A., and Zydney, A.L.. J. Membr. Sci. **249,** 245-249, 2005

[5] Chen, J.-P., Chang, G.-Y., and Chen, J.-K.. Coll. Surf. A **313-314,** 183-188, 2008

[6] Baker, H.R., Merschrod, E.F., and Poduska, K.M.. Langmuir **24,** 2970-2972, 2008

[7] Hilal, N., Bowen, W.R., Alkhatib, L., and Ogunbiyi, O.. Chem. Eng. Res. Des. Special Issue In Honour of Professor Jack Richardson on the Occasion of his 85th Birthday, **84,** 282-292, 2006

[8] Goh, M.C., Paige, M.F., Gale, M.A., Yadegari, I., Edirisinghe, M., and Strzelczyk, J.. Physica A, **239**, 95-102, 1997

[9] Yasuda, T., Okuno, T., and Yasuda, H.. Langmuir, **10,** 2435-2439, 1994

[10] Elliott, J.T., Woodward, J.T., Umarji,A., Mei,Y., and Tona, A.. Biomat. **28,** 576–585, 2007

[11] Mohamed, H., Russo, A. P., Szarowski, D. H., McDonnell, E., Lepak, L. A., Spencer, M. G., Martin, D. L., Caggana, M., and Turner, J. N.. Sep. Sci. Technol., **42,** 25 – 41, 2007

[12] Stanton, B.W., Harris, J.J., Miller, M.D., and Bruening, M. L.. Langmuir, **19,** 7038-7042, 2003

[13] van Reis, R.. *Charged filtration membranes and uses therefore.* US Patent No. 7001550 B2., 2006

[14] Nyström, M., Lindstrom, M., and Matthiasson, E.. Coll. Surf., **36,** 297-312, 1989

[15] Winkler, B. H., and Baltus, R. E.. J. Membr. Sci., **226,** 75-84, 2003

[16] Zhu, J.H., Zhang, B., Fang, W.W., Lao, X.J., and Yu, H.. Coll. Surf. B-Biointerfaces, **43** (**1)**, 1-6, 2005

[17] Luescher, M., Ruegg, M., and Schindler, P.. Biopoly., **13**, 2489-2503, 1974

[18] Freudenberg, U., Behrens, S.H., Welzel, P.B., Muller, M., Grimmer, M., Salchert, K., Taeger, T., Schmidt, K. ,Pompe, W. , and Werner C.. Biophys. J., **92** (6), 2108-2119, 2007

[19] Zhang, J., Senger, B., Vautier, D., Picart, C., Schaaf, P., Voegel, J.-C., and Lavalle, P.. Biomat. **26,** 3353-3361, 2005

[20] Ku, J.R., and Stroeve, P.. Langmuir, **20**, 2030–2032, 2004

[21] Jordan, D.O.. "The physical properties of nucleic acids", in: Chargaff, E., and Davidson, J.N. (Eds.). *The Nucleic Acids*, Academic Press, New York, 1955.

[22] Higley, W. S.. *Collagen membranes for reverse osmosis desalination*, 1972

[23] Suzuki, F., Kimura, H., and Shibue, T.. J. Membr. Sci. **165,** 169-175, 2000

[24] Yasuda, H., and Lamaze, C. E.. J. Macromol. Sci. Part B Phys. **B 5,** 111-134, 1971

[25] Stevens, P. V., Nyström, M., and Ehsani, N.. Biotechnol. Bioeng. **57,** 26-34, 1998

[26] Kanamori, T., Habu, T., Shinbo, T., and Sakai, K.. Mater. Sci. Eng. C **13,** 85-89, 2000

Chapter 5: Conclusions

5.1 Future Work: Goals Revisited

The major goals of this project were outlined in chapter 1. Toward the development of bioMEMS applications, collagen thin films were investigated as a potential interface between semiconductor devices and biological material under test. To serve as a suitable interface, the collagen film should be porous for selective transport of material, integrable into standard semiconductor fabrication processes, lithographically patternable, and biocompatible. Significant progress was made toward achieving each of these goals. However, as shall be examined in this chapter, many avenues remain to extend these advances.

5.1.1 Porosity: Filtration and MWCO

In the previous chapter, stable, porous collagen membranes were ultimately created on commercially produced alumina disks. Through a series of FTIR, SEM, AFM, contact angle, and zeta potential characterizations, some fundamental insights were gained into the chemistry and physics of collagen film formation. Many physical and structural properties of the films can be controlled simply by varying the amount of collagen deposited. It is quite likely, however, that many additional variables affect the structure of collagen films. For example, in the analogous system of spin cast cellulose, both membrane structure and MWCO were found to vary with cellulose concentration, spin speed, temperature, and quenching solvent.[1] In the collagen system, this would translate into variables such as collagen concentration, pH of the buffer, spin speed, and crosslinking conditions such as chemicals, times, and temperatures. If manipulation of these variables proved inadequate to tailor the membrane properties for a particular application, one could try to incorporate one of

the various collagen structures aside from type-I-monomer-based fibrils. Collagen of other types, collagen from other source tissues or species, or composites with other ECM materials such as fibronectin, elastin, and hydroxyapatite, and even composites with a variety of synthetic polymers could be explored as necessary.[2-6] Now that one set of variables which creates a useful collagen membrane has been identified, these other system parameters can be varied one by one to demonstrate their effects upon collagen film structure.

In addition to membrane structure, some preliminary characterizations of membrane performance – flux and permeability – were carried out under industrially relevant conditions. Another crucial figure of merit, the MWCO of the collagen films as a function of the number of spin cast layers, has yet to be determined.[7] The diffusion coefficients of several small molecules across uncoated alumina films have already been determined by Jiang *et al*,[8] and could serve as a baseline for the diffusion behavior of the composite films. Following the efforts by Jiang *et al* on the alumina system [8] and by Russo *et al* [9] and Mohammed *et al* [10] on the cellulose-on-silicon-nitride system, UV/visible spectroscopy would be used to measure the simultaneous diffusion of multiple dye species across the collagen membrane. Each dye, selected over a broad range of MW, would have a unique color, allowing the MWCO to be quickly identified. Once determined, both the MWCO of each film, and the diffusion coefficient of each species across it, could be correlated with other known structural and performance properties of the film to gain a deeper theoretical understanding of the system.[11-14]

At a more applied level, the collagen membranes have an average pore size likely to make them effective for either protein-protein [15,16] or DNA-protein separations.[17,18] Separations of this kind may be worth attempting even at the current level of membrane development. One separation of particular interest is the

purification of DNA from whole blood. Blood is a very complex chemical mixture. One component is the protein hemoglobin, which includes the prosthetic group heme. Heme contains an Fe atom which binds not only molecular oxygen, but the phosphate oxygens of DNA. Heme-bound DNA is unable to participate in PCR.[19] Thus, separating heme from DNA prior to testing removes a significant inhibitor, making the process far more efficient.[20-22] The DNA-heme separation has been somewhat successfully perfomed by cellulose membranes on PC under electric field-driven diffusion.[23] It would be interesting to directly compare the filtration performance of the collagen membranes with the more fully characterized cellulose technology.

5.1.2 Integration: Collagen-on-Alumina-on-Silicon

The integration of collagen film coatings was attempted onto several substrates commonly used in either the semiconductor industry (silicon, silicion nitride, and alumina) or biotechnology industry (PC and PET). On the polymeric substrates, hole-spanning collagen films were eventually created, but the variations in the film structures with respect to the number of deposited layers proved somewhat difficult to explain. Armed with the theoretical insights gained from the collagen-on-alumina studies, the PC and PET systems are worth revisiting. By applying the protocols which have proven successful on alumina substrates, it is hoped that collagen films with more predictable properties may be developed on these polymer substrates. In particular, standardizing the size of the holes on the PC and PET substrates, ideally at the 200 nm diameter used on alumina, would make the data far easier to interpret. At a minimum, these experiments could confirm whether there is a genuine basis for the confusing variations in the collagen film structure with the number of spin cast layers, on the polymeric substrates. On the inorganic substrates, the collagen film structures developed far more predictably as the number of deposited layers was varied. On

alumina, the collagen films were primarily monomeric at low coverages (3 layers or less), with more and larger fibrils gradually dominating the surface at higher coverage.

On alumina, PC, and PET, CPD proved essential to stabilize the unsupported portions of the collagen film spanning the holes in the substrate. To date, CPD has not been attempted for collagen films on silicon nitride substrates. Since the silicon nitride fabrication process is well developed and easily integrated with other semiconductor device processes, it is worth investigating whether CPD can resolve the issue of torn films. If so, the full battery of tests applied to the collagen-on-alumina system could be applied to collagen-on-silicon nitride. Aside from the issue of the tearing of the collagen film, the SEM structural data obtained thus far on silicon nitride substrates are consistent with the data on alumina. Up to four layers of deposited collagen, the films appeared to be largely monomeric. However, only by examining the full range of depositions – including 6 and 9 layers – could one truly be certain whether or not collagen is behaving similarly on the two surfaces.

Perhaps most interestingly, several groups,[24-28] among them Jiang *et al*.,[15] have proposed procedures to integrate the production of alumina substrates with standard silicon processing, which may easily be adapted to incorporate collagen. The Jiang *et al*. fabrication process, which is outlined in figure 5.1, is very similar to

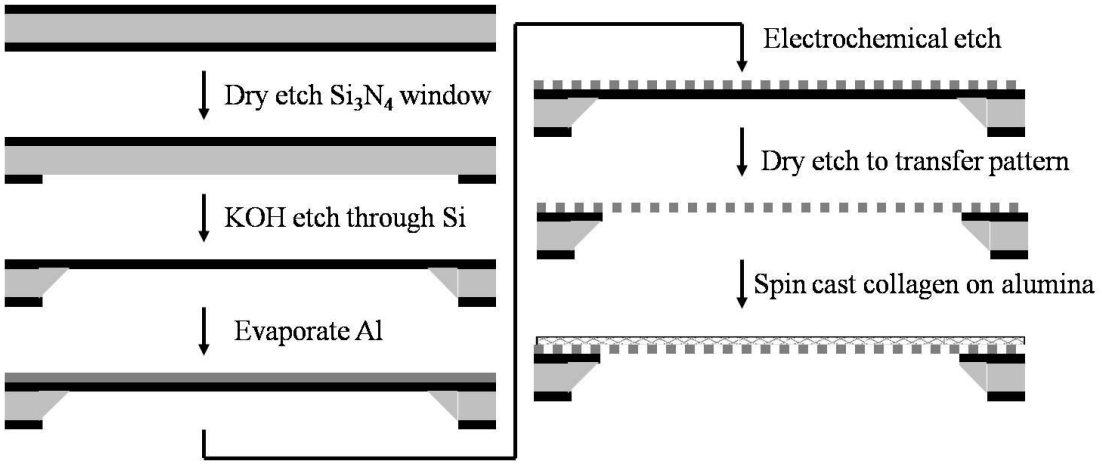

Figure 5.1 Fabrication of fully integrated collagen-on-alumina-on-silicon

the process for the creation of the silicon nitride membranes described in section 3.1. Initially, silicon nitride is LPCVD deposited on silicon. Then, instead of patterning small holes on the top side of the substrate, the large windows are lithographically patterned and plasma etched on the back side. The exposed silicon is etched away in 40% KOH to create the suspended, unpatterned silicon nitride membranes as before. At this point, aluminum is deposited on the top surface, either by thermal evaporation, electron beam evaporation, or sputtering. The aluminum is electrochemically etched in an oxidizing acid (typically either phosphoric, sulfuric, or oxalic),[29-31] to generate the through holes in the alumina film. Finally, the remaining exposed silicon nitride in the window area is removed by plasma etching. The result is an exposed porous alumina film, fully integrated onto a silicon wafer, which is ready to be spin-coated by collagen.

This process includes several adjustable parameters with the potential to impact the structure and function of the composite membrane. For instance, the average thickness of the deposited aluminum can be varied.[28,32,33] In general, however, the thickness of the aluminum is likely to be many times that of the collagen; thus, in a diffusion-driven system, aluminum thickness will control the transmembrane flux rate. Even at a consistent thickness, the technique used to deposit the aluminum may affect the RMS surface roughness of the deposited film. In an atomically rough film, 'pits' even a few nanometers deep may serve to nucleate the formation of holes during the etch. Deeper pits experience a more concentrated local electric field, increasing the etch rate within pits relative to atop peaks. Over the course of the etch, this effect amplifies the initial surface roughness. Additionally, during the etch itself, varying the choice of acid, its concentration, and the applied voltage will also affect the ultimate size and spacing of the holes through the alumina. All of these variations

in the structure of the alumina substrate are likely to affect the adhesion and structure of the deposited collagen film, as previously discussed in chapter 4.

5.1.3 Lithography: Complex Patterns Emerge

A new method of lithographically patterning porous materials – direct liftoff – was developed. Direct liftoff occurs when a porous material is deposited onto a soluble sacrificial material, and then exposed to the appropriate solvent. The solvent penetrates through the pores to dissolve the sacrificial layer and release the porous film. This technique was applied to collagen thin films in two related applications. In one, the sacrificial layer was continuous, allowing a 'thin skin' tens of nanometers thick and several square centimeters in area to be released from the substrate intact. In the other, the sacrificial layer was lithographically patterned prior to the liftoff, releasing the collagen only where the sacrificial material remained. Wherever collagen directly contacted the silicon substrate, square features as small as 25 μm consistently remained behind.

Both applications were attempted only under the conditions offering the greatest chance of success – using single layer, non-crosslinked collagen films. To be practical, both techniques must be tested under conditions similar to those of the films characterized on alumina – crosslinked, multilayer films. If successful, the patterned liftoff should additionally be applied for a variety of non-square shaped features. In particular, shapes not easily attainable by other standard patterning methods – such as gridlines which are inaccessible with parylene liftoff, too wide for dip pen lithography, and too small for microcontact printing – could prove immediately useful for certain tissue engineering applications.

For both applications, the development of biocompatible, aqueous-based sacrificial materials, such as salt, could prove beneficial. To prevent the aqueous

collagen solution itself from dissolving the sacrificial layer prematurely, presaturation of the collagen solution will likely be necessary. AFM, SEM, and TEM studies would all be required to ascertain whether the added material incorporates into, or otherwise affects film structure. To generate unbroken collagen films, it will be necessary to control the RMS surface roughness of the sacrificial film, most likely via control of the average grain size.

In the case of collagen 'thin skins', it remains to be seen whether it is possible to isolate such films on any arbitrary substrate, such as silicon nitride or PC. However, attempts to capture the 'thin skin' on standard gold-coated TEM grids failed, with the collagen flaking off as it dried. The two most likely causes point to two different remedies. On the one hand, the delamination may have resulted from the film shrinkage and tearing during air-drying, originally observed on the silicon nitride substrates. If so, drying the captured films by CPD may prevent damage. Conversely, the adhesion between the film and the substrate may have been poor even when fully hydrated. Adhesion might be improved by reacting the initial gold surface with an alkanethiol SAM to create a hydrophilic termination.[34] If this strategy proves successful, then chlorosilanes with a similar hydrophilic termination could be used to improve collagen adhesion to silicon.[35] Improved adhesion may extend the capability of direct liftoff to reliably generate patterned features smaller than 25 μm.

Finally, both lithographic procedures open up new possibilities for cell culture applications. It is well known that cells respond to both chemical and topographic cues to direct their growth.[36] Thus, patterned collagen films may prove useful for directing the growth of collagen-sensitive cell lines, particularly if direct liftoff can be extended down to feature sizes closer to cellular dimensions. Conversely, unpatterned 'thin skin' films could be useful for several applications where unique information could be obtained by optical and electron microscopy imaging in three dimensions,

unobstructed by a substrate. For example, in an unsupported thin collagen film, one could directly image the mineralization of hydroxyapatite throughout the pores in the collagen matrix, to investigate the process of bone formation.[37] In other applications, culture cells could grow freely on a lifted off 'thin skin' without the constraint of a substrate, in a manner approximating growth in vivo within the ECM. With a collagen film less than 100 nm thick, the morphology of the culture cells, including the extent of their penetration into the film, could be easily assessed.[38]

5.1.4 Biocompatibility: Patterned Growth and Filtered Intercellular Signaling

Relatively little study was done on biocompatibility for the present work. As a proof of concept, two cell types were cultured on collagen films spin cast on silicon under limited conditions. However, these conditions did not entirely coincide with those employed in later experiments to generate collagen-on-alumina films suitable for filtration. Two differences in preparation conditions are particularly likely to affect the growth of cell cultures: the concentration of glutaraldehyde, and the use of ethanol. A study of the response of cells to ethanol-treated collagen is most essential. All collagen films employed in the experiments proposed in this chapter - whether subjected to CPD for use in filtration, directly lifted off of an ethanol-soluble sacrificial layer, or both – will be exposed to absolute ethanol. Ethanol dehydrates the collagen films, thereby potentially altering the film structure in a manner that could adversely affect culture cells.

Collagen films treated with low levels of glutaraldehyde (.02%) did support live cell growth.[39] However, the collagen-on-alumina films which were characterized for filtration, were crosslinked with a much more concentrated (4%) glutaraldehyde solution. This could potentially affect cell growth, both directly and indirectly. At high concentrations, glutaraldehyde is used as a fixative for the long-

term preservation of biological material, partly because it is known to be toxic to microbes. Although the substrates are rinsed many times following crosslinking, it is conceivable that sufficient residue could remain to inhibit cell growth. Aside from directly poisoning culture cells, glutaraldehyde also increases the extent of crosslinking of the collagen, stabilizing fibril formation. The likely differences in film structure may in turn affect the ability of the collagen film to support cell growth. Astrocytes should be cultured on films produced under the collagen-on-alumina conditions, to verify their survival. If the cells show signs of stress, other crosslinking agents should be investigated, as the use of different crosslinkers has been reported to result in differences in biocompatibility.[40] In the broadest sense, some crosslinking is very likely necessary to make collagen scaffolds sturdy enough for most advanced applications in tissue engineering.

Perhaps the most powerful potential applications of collagen-on-alumina membranes may link biocompatibility with filtration. Several inorganic membranes have demonstrated initial promise for protein-protein and protein-DNA separations; [41-44] however, generally speaking, such untreated substrates have inferior biocompatibility relative to substrates coated with collagen. Experiments of this nature are likely to parallel to those of Graber *et al.*.[23] In this application, cells were cultured on cellulose-on-PC, which had a very low MWCO of approximately 350 daltons. The cellulose film blocked large proteins such as cytokines from reaching the cells, while permitting small molecules such as nitric oxide to pass through. In this manner, nitric oxide alone was proven sufficient to stimulate an inflammatory response in the cells. Similar experiments could be done to investigate chemical signal transduction among collagen-sensitive cell types, if collagen films of suitable MWCOs can be engineered.

5.2 Conclusions

To summarize, collagen was extensively investigated as a coating for the semiconductor- biological interface in bioMEMS applications. Collagen films were examined for biocompatibility, lithographic patternability, integrability with commercially available substrates, and porosity and permeability for filtration applications.

As a proof of concept for biocompatibility, both astrocytes and endothelial cells were grown on supported collagen films in an attempt to model the blood-brain barrier. A new lithographic technique which is generally applicable to porous films, direct liftoff, was developed to pattern collagen-on-silicon. Surface-bound features as small as 25 μm, and free-standing lifted off films 50 nm thick and several square centimeters in area, were created using this technique.

The integration of collagen films was investigated on several commercially available materials commonly used in the biotechnology and semiconductor industries – silicon nitride, PC, PET, and alumina. Since alumina showed the most promise, the physical, chemical, and performance properties of collagen-on-alumina films were more extensively characterized. On all these points, much work remains open for further investigation. Yet by all the forementioned criteria, collagen thin films have proven to be a very promising technology for nanofiltration.

REFERENCES:

[1] Mohamed, H., Russo, A. P., Szarowski, D. H., McDonnell, E., Lepak, L. A., Spencer, M. G., Martin, D. L., Caggana, M., and Turner, J. N.. J. Chromatogr. A, 18th Intl. Sym. on MicroScale Bioseparations, **1111,** 214-219, 2006

[2] Thomas, V., Dean, D.R., and Vohra, Y.K.. Current Nanosci., **2 (3)**, 155-177, 2006

[3] Tan, W., Krishnaraj, R., and Desai, T.A.. Tissue Eng., 7 **(**2), 203-210, 2001

[4] Salchert, K., Oswald, J., Streller, U., Grimmer, M., Herold, N., and Werner, C.. J. Mat. Sci.-Mat. Med., **16 (6)**, 581-585, 2005

[5] Chen, G.P., Sato, T., Ohgushi, H., Ushida, T., Tateishi, T., and Tanaka, J.. Biomat., **26 (15)**, 2559-2566, 2005

[6] Murugan R, Ramakrishna S.. Appl. Phys. Lett., **88 (19)**, 193124, 2006

[7] Malaisamy, R., Lepak, L., Spencer, M., and Jones, K.L., J. Membr. Sci., submitted

[8] Jiang,X., Mishra,N., Turner, J.N., and Spencer, M.G.. Microfluid Nanofluid **5**, 695–701, 2008

[9] Russo, A.P., Martin, D., Shain, W., and Turner, J.N.. Bioinformatics, Proteomics, and Functional Genomics Conference Proceedings. AIChE Annual Meeting, Indianapolis, IN, November 3–8, 2002, 171–180, 2002

[10] Mohamed, H., Russo, A. P., Szarowski, D. H., McDonnell, E., Lepak, L. A., Spencer, M. G., Martin, D. L., Caggana, M., and Turner, J. N.. Sep. Sci. Technol., **42,** 25 – 41, 2007

[11] Nakao S.. J. Membr. Sci., **96 (1-2)**, 131-165, 1994

[12] Gumi, T., Valiente, M., Khulbe, K.C., Palet, C., and Matsuura, T.. J. Membr. Sci., **212 (1-2)**, 123-134, 2003

[13] Bellona, C., Drewes, J.E., Xu, P., and Amy, G.. Water Res., **38 (12)**, 2795-2809, 2004

[14] Boussu, K., Vandecasteele, C., and Van der Bruggen, B.. J. Membr. Sci., **310 (1-2)**, 51-65, 2008

[15] Ghosh, R.. J. Chromatogr. A, **952 (1-2)**, 13-27, 2002

[16] Saxena, A., Tripathi, B.P., Kumar, M., and Shahi, V.K.. Adv. Coll. Int. Sci., **145 (1-2)**, 1-22, 2009

[17] Fu, J.P., Schoch, R.B., Stevens, A.L., Tannenbaum, S.R., and Han, J.Y.. Nature Nanotech., **2 (2)**, 121-128, 2007

[18] Ke, X.B., Shao, R.F., Zhu, H.Y., Yuan, Y., Yang, D.J., Ratinac, K.R., and Gao, X.P.. Chemical Communications, **10**, 1264-1266, 2009

[19] Akane, A., Matsubara, K., Nakamura, H., Takahashi, S., and Kimura, K.. J. Forensic Sci. **39 (2),** 362–372, 1994

[20] Al-Soud,W.A. and Radstrom, P.. J. Clin. Microbiol., **39 (2)**, 485–493, 2001

[21] Radstrom, P., Knutsson, R., Wolffs, P., Lovenklev, M., and Lofstrom, C.. Molec. Biotech., **26 (2)**, 133-146, 2004

[22] Zhang, C.S., Xu, J.L., Ma, W.L., and Zheng, W.L.. Biotech. Adv., **24 (3)**, 243-284, 2006

[23] Graber, D.J, Snyder-Keller, A., Lawrence, D.A., Shain, W., Szarowski, D.H., Al-Kofani, K.A., Roysam, B., and Turner, J.N.. J. Neuroimmunol., submitted.

[24] Das, B.. J. Electrochem. Soc., **151 (6)**, D46-D50, 2004

[25] Toh, C.S., Kayes, B.M., Nemanick, E.J., and Lewis, N.S.. Nano Lett., **4 (5)**, 767-770, 2004

[26] Kokonou, M., Giannakopoulos, K.P., and Nassiopoulou, A.G.. Thin Solid Films, **515 (7-8)**, 3602-3606, 2007

[27] Jiang, X., Mishra, N., Turner, J.N., and Spencer, M.G.. IEEE Trans. On Nanotech., **6 (3)** 328-333, 2007

[28] Sainiemi, L., Grigoras, K., and Franssila, S.. Nanotech., 20 **(**7), 075306, 2009

[29] Masuda, H. and Fukuda, K.. Science, **268**, 1466–1468, 1995

[30] Jessensky, O., Muller, F., and Gosele, U.. Appl. Phys. Lett., **72**, 1173–1175, 1998

[31] Li, A. P., Muller, F., Birner, A., Nielsch, K., and Gosele, U.. J. Appl. Phys., **84**, 6023–6026, 1998

[32] Kokonou, M., Nassiopoulou, A.G., and Giannakopoulos, K.P.. Nanotech., **16 (1)**, 103-106, 2005

[33] Rabin, O., Herz, P.R., Lin, Y.M., Akinwande, A.I., Cronin, S.B., and Dresselhaus, M.S.. Adv. Func. Mat., **13 (8)**, 631-638, 2003

[34] Hulteen, J.C., Jirage, K.B., and Martin, C.R.. J. Am. Chem. Soc., **120 (26)**, 6603-6604, 1998

[35] Urmenyi, A.M., Philipse, A.P., Lammertink, R.G.H., and Wessling, M.. Langmuir, **22 (12)**, 5459-5468, 2006

[36] Rebollar, E., Frischauf, I., Olbrich, M., Peterbauer ,T., Hering, S., Preiner, J., Hinterdorfer, P., Romanin, C., and Heitz, J.. Biomat., **29 (12)**, 1796-1806, 2008

[37] Toroian, D. , Lim, J.E. , and Price, P.A.. J. Biol. Chem., **282 (31)**, 22437-22447, 2007

[38] Brown, B., Lindberg, K., Reing, J., Stolz, D.B., and Badylak, S.F.. Tissue Eng., **12 (3)**, 519-526, 2006

[39] Ma, S.H., Lepak, L.A., Hussain, R.J., Shain, W., and Shuler, M.L.. Lab on a Chip, **5** (**1**), 74-85, 2005

[40] Wissink, M.J.B., van Luyn, M.J.A., Beernink, R., Dijk, F., Poot ,A.A., Engbers, G.H.M., Beugeling, T., van Aken, W.G., and Feijen, J.. Thrombosis And Haemostasis, **84 (2)**, 325-+, 2000

[41] Sano, T., Iguchi, N., Iida, K., Sakamoto, T., Baba, M., and Kawaura, H.. Appl. Phys. Lett**., 83 (21)**, 4438-4440, 2003

[42] Striemer, C.C., Gaborski, T.R., McGrath, J.L., and Fauchet, P.M.. Nature, 445 **(**7129), 749-753, 2007

[43] Osmanbeyoglu, H.U., Hur, T.B., Kim, H.K.. J. Membr. Sci., **343 (1-2),** 1-6, 2009

[44] Vlassiouk, I. , Apel, P.Y., Dmitriev, S.N., Healy, K., and Siwy, Z.S... Proc. Natl. Acad. Sci. USA, **106 (50)**, 21039-21044, 2009